Title
Structure and dynamics of networks with dyadic and higher order interactions

Author
Salova, Anastasiya

Publication Date
2021

Peer reviewed|Thesis/dissertation

Structure and dynamics of networks with dyadic and higher order interactions

By

ANASTASIYA SALOVA

DISSERTATION

Submitted in partial satisfaction of the requirements for the degree of

DOCTOR OF PHILOSOPHY

in

Physics

in the

OFFICE OF GRADUATE STUDIES

of the

UNIVERSITY OF CALIFORNIA

DAVIS

Approved:

Raissa M. D'Souza, Chair

James P. Crutchfield

John Rundle

Committee in Charge

2021

To my parents Oksana and Vladimir.

Contents

Structure and dynamics of networks with dyadic and higher order interactions

Abstract

The interplay between the structure of a networked system and the dynamics of its constituent elements, including their interactions, leads to non-trivial emergent behaviors. These behaviors can be essential to the function of the system as a whole, and thus mathematical frameworks that allow careful analysis of such behaviors are valuable. The contribution of this dissertation is to use the ideas of symmetries and balanced equivalence relations to show how network structure can be used to find the admissible patterns of synchronization (e.g., cluster synchronization states), track their dynamics, perform their linear stability analysis, and finally to retrieve the dynamics from data. An additional contribution is extending these principles to the analysis of cluster synchronization on hypergraphs. Hypergraphs allow capturing higher order interactions beyond the pairwise interactions captured in strictly dyadic network systems.

Symmetries are ubiquitous in nature. A networked dynamical system can have symmetries in its coupling structure, the dynamics of its constituent elements, or both. The first contribution of this dissertation is demonstrating how such symmetries present themselves in the structure and spectral properties of the Koopman operator, which is a linear infinite dimensional operator that exactly reproduces the dynamics of the system in the space of observables. This can be put into practice as the Koopman operator can be approximated via data driven methods. We demonstrate how the knowledge of the symmetries can be incorporated into such approximations to speed up the analysis and make it more accurate.

Cluster synchronization is a type of synchronization that is characterized by a subset of nodes in the system having fully synchronized trajectories (i.e., forming a cluster), while following a distinct trajectory from all the other clusters. Such behavior arises when all the nodes in the same cluster receive the same dynamical input from all the other nodes in the system. Therefore, symmetries as well as equitable partitions are useful tools to find the admissible cluster synchronization states for a given system. The second contribution of this dissertation is generalizing the results related to cluster synchronization in systems of coupled oscillators to study intricate patterns of synchronization, such as the family of states where cluster synchronization and splay states coexist. In

such states, due to the interaction between the nodal dynamics and network structure, groups of oscillators become effectively decoupled despite the existence of physical coupling between them.

Networks capture pairwise (dyadic) interactions between elements, yet some systems are inherently higher order. For instance, a 3-species chemical reaction or a publication with three coauthors involve triadic interactions. The final contribution of this dissertation is to advancing the methodology of studying dynamics on systems with higher order interactions (e.g., triadic). Since such interactions can not be represented as a sum of dyadic interactions, their analysis requires new tools. Up to now, full synchronization on hypergraphs (which encode higher order interactions) has been the main focus of in the literature, since the dyadic projection of the adjacency tensor can be sufficient in stability calculations. We show that this approach is not sufficient for more intricate dynamics such as cluster synchronization with respect to determining admissible states and performing stability calculations. To address that, we introduce a formalism based on node and edge clusters, and demonstrate how to apply it to admissibility and stability analysis. This formalism provides a principled way to organize the analysis of dynamics on hypergraphs and serves as a tool to investigate the role of higher order interactions in stabilizing and destabilizing different states.

Acknowledgments

I am very thankful to everyone who made my path through graduate school possible. First, I want to thank my advisor Prof. Raissa D'Souza for being a role model and a mentor, as well as for her constant support, patience, valuable feedback, and commitment to my professional growth throughout the years. I am also lucky to have met other research group members Jeff, Jordan, Márton, Weiran, Martin, Guga, and others. They helped me become a better researcher and contributed to making my six years in Davis enjoyable.

I thank my awesome parents Oksana Salova and Vladimir Salov, as well as my wonderful sister Natalya, for always being there for me despite being almost 10,000 km away. I am deeply indebted to my family's selflessness, commitment to education, encouragement, and support that made my journey possible.

I am very fortunate to have received guidance from Yelena Kosheleva, Aleksey Koshelev, Mariana Kosheleva, and the whole VREAC family. Their invaluable help and support has been instrumental to me being where I am now, and their commitment to helping me and others uncover their full potential is a source of inspiration.

I am thankful to my Davis friends from my cohort and beyond, including Victoria, Ariadna, Jessie, James, Chase, Jenna, Chris, Cameron, Rose, Imran, Geoff, and others. They made my graduate school years meaningful and enjoyable, and I am not convinced I would have been able to get through the challenges of classwork and research without their support. Last but not least, I thank Adam Rupe and his friendly cats Tycho and Kepler for patiently supporting me during grad school's most challenging moments, and also for all the exciting adventures and great memories we made.

CHAPTER 1

Introduction

A recurring theme of this dissertation is how the interplay between the structure and the dynamics in networked systems can lead to intricate patterns of collective behavior. To make progress in analyzing such non-trivial patterns, we focused on systems with some degree of dynamical homogeneity. Because of this homogeneity, it is possible to relate the network structure (captured in the form of an adjacency matrix, incidence matrix, or adjacency tensor) to its effective dynamics while remaining agnostic to the details of the dynamics. Additionally, the analysis can be advanced by making use of symmetries of the systems dynamics that are not contained in the structural representation or by setting specific restrictions on the coupling functions. In the rest of this section, I explain my dissertation work in more detail by describing our progress in analyzing systems with symmetries using data-driven methods, formalizing the phenomenon of dynamical decoupling in Stuart-Landau oscillators and beyond, and generalizing the analysis of cluster synchronization to systems with higher order interactions.

Data-driven methods have gained popularity in recent years. One reason is that scientists and practitioners often have to operate in the regime of abundance of data, but limited knowledge of the system's underlying dynamics. Additionally, sometimes the dynamics of the systems are known, but do not provide enough intuition about the system's emergent behaviors. One of the most promising frameworks relating dynamical systems and data-driven methods is the operator perspective [**86**]. For instance, representing the dynamics via the Koopman operator offers a trade-off between tracking the finite-dimensional nonlinear dynamics evolving the state of the system in phase space and tracking the linear infinite-dimensional Koopman operator acting in the function space [**29**,**76**]. The linearity of this operator is appealing, since linear systems are significantly better understood than general nonlinear systems. In practice, the infinite dimensionality of the operator poses a challenge, and instead it is typically approximated by a finite dimensional operator acting on a finite number of basis functions. These methods are related to dynamic mode decomposition (DMD) introduced

in Ref. [**132**] and extended dynamic mode decomposition (EDMD) introduced in Ref. [**157**], which rely on approximating the optimal linear operator evolving nonlinear observables. Methods such as DMD have been very useful in application areas such as fluid dynamics [**84**]. Chapter 2 of this dissertation focuses on how the knowledge of the networked system's discrete symmetries can be incorporated into data driven methods by relating the symmetries of the dynamics to those of the Koopman operator. Our findings inform the choice of basis functions in EDMD and lead to dimensionality reduction compared to the original problem.

Networked dynamical systems are often capable of synchronization, which is a general phenomenon characterized by weakly coupled dynamical elements adjusting their rhythms [**117**]. Examples of synchronization in engineered and natural systems range from power grids, where synchronization is central to the system's function [**104**], to fireflies lighting up in unison [**103**] or neural synchronization in the brain [**55**]. While complete synchronization is an important dynamical state to analyze, other patterns of synchronization often appear as well. For instance, chimera states are characterized by coexistence of synchronous and asynchronous domains in systems of coupled oscillators [**1**], and are hypothesized to be linked to phenomena such as epileptic seizures [**5**]. Another intriguing example of symmetry breaking is remote synchronization, a type of synchronization where two or more nodes in a dynamical network synchronize even in the absence of direct link among them [**46**]. Some useful frameworks that can be applied to analyzing the states beyond complete synchronization in systems of identical or nearly identical coupled elements are equivariant dynamical systems theory [**50**] and cluster synchronization [**114**]. We apply these frameworks and develop new tools for studying complex symmetry breaking states in systems with dyadic and higher order interactions in Chapters 3 to 5.

Chapter 3 focuses on a specific continuum of states, referred to as *decoupled states*, that can arise in systems of coupled oscillators with phase-shift symmetries and diverse coupling topologies. The states can be analyzed using the concept of equitable partitions, while taking into account the rotational symmetries of the nodal and coupling dynamics. In such decoupled states, the nodes can be partitioned into *fully synchronized clusters*, with groups of fully synchronized clusters forming *splay clusters*. Furthermore, different splay clusters are separated by an arbitrary phase difference, thus forming a continuum of decoupled states. This interesting phenomenon leads to an

effective decoupling between distinct splay clusters and has been recently observed experimentally [**43**, **97**]. We show how to analyze the admissibility and stability of such states using concepts from equivariant bifurcation theory and cluster synchronization research.

The results introduced so far were obtained for systems with purely dyadic interactions. However, some systems are better modeled using a combination of dyadic and higher-order (e.g., triadic, quartic, etc.) couplings between the interacting elements [**17**]. These higher order interactions require new methods, and developing these methods is the main focus of Chapters 4 and 5.

Projections of the adjacency tensor are useful for analyzing full synchronization in dynamical systems on hypergraphs [**30**, **37**, **45**, **93**]. In Chapter 4, we demonstrate that the projected hypergraphs are insufficient for analyzing cluster synchronization on undirected hypergraphs. The first reason we highlight is the fact that it is not always possible to reconstruct the hypergraph from its projection up to an isomorphism, potentially resulting in distinct cluster synchronization dynamics. The second reason comes from symmetry analysis and the fact that some of the admissible cluster synchronization states of the projected hypergraph are not admissible on the original higher order system. Additionally, we show that the structure of the Jacobian can not be represented by the projected adjacency matrices and node cluster assignments alone, unlike in systems with dyadic interactions. Finally, to enable this analysis we introduce a formalism based on node and edge clusters that allows us to state the admissibility and linear stability criteria for cluster synchronization in systems with higher order interactions.

Laplacian (diffusive) coupling is a common choice for a coupling function in systems with dyadic interactions [**139**,**162**]. In Chapter 5, we analyze cluster synchronization on undirected hypergraphs with Laplacian-like coupling in detail. First, we show how to determine the admissibility of different cluster synchronization patterns from the node clusters and the edge clusters, which are induced by the node clusters. We take into account that the edges containing the nodes from a unique cluster do not contribute to the system's dynamics under Laplacian-like coupling. Additionally, we demonstrate that the building blocks of the Jacobian structure are the projected Laplacian matrices corresponding to each *edge cluster* and each order of interaction as well as diagonal indicator matrices corresponding to *node clusters*. This set of matrices can then be used to block diagonalize the Jacobian, leading to a dimensionality reduction of the stability calculation.

Overall, this dissertation offers new insight into the interplay of structure and dynamics of complex networked systems, and sets the ground work for further investigations. Future directions for the work linking the structure of the Koopman operator and network symmetries include analyzing continuous symmetries, possibly connecting the work presented here to equivariant machine learning literature [**75**, **150**]. Future developments in our investigation of decoupled states could include relaxing some of the conditions on the dynamics and relating our results to systems with adaptive coupling [**20**], which will allow us to apply our admissibility results to a wider range of systems with a more direct connection to applications in, for instance, neuronal networks. Additionally, the decoupled state admissibility and stability analysis can be extended to higher order interactions. Finally, some future directions in analyzing cluster synchronization in systems with higher order interactions are investigating the role of parameter heterogeneity, analyzing the complex interplay between dyadic and higher order coupling and its role on stability, and extending our cluster synchronization analysis to directed hypergraphs or simplicial complexes with dynamics on hyperedges [**101**].

CHAPTER 2

Koopman Operator and its Approximations for Systems With Symmetries

Published as Salova, A., Emenheiser, J., Rupe, A., Crutchfield, J. P., & D'Souza, R. M. (2019). Koopman operator and its approximations for systems with symmetries. Chaos: An Interdisciplinary Journal of Nonlinear Science, 29(9), 093128.

Many natural and engineered dynamical systems — power grid networks and biological regulatory networks, to mention two — exhibit symmetries in their connectivity structure and in their internal dynamics. Some have time-reversal symmetry, others rotational and spatial translation invariance, and others still, combinations. These symmetries are often key for understanding the behavior of systems. For instance, the interplay between system behavior and structural symmetries arises in locomotion, where observed symmetries in animal gaits impose certain constraints the structure of the neural circuits that generate them. For network systems in particular, symmetries in the connectivity structure are of fundamental importance. For instance, the structural symmetries of a network of identical oscillators can determine its admissible patterns of symmetry-breaking. That said, additional information beyond knowledge of the network structure is often required to address more detailed questions about a system's dynamics, such as whether a particular configuration is stable in a given parameter regime. In these cases, the system's linearization near the steady state can be combined with interconnection symmetry to provide the answer. However, these linearization methods are only valid on a local subset of the state space and therefore are not sufficient for global characteristics of nonlinear dynamical systems, such as their attractors, basins, and transients. The Koopman operator, in contrast, is a linear infinite-dimensional operator that

evolves the functions on the state space which is valid on the entire state space. We show how to combine symmetry considerations with the Koopman analysis to study nonlinear dynamical systems with symmetries. We use representation theory to determine the effect of symmetries on the Koopman operator and its approximations, drawing out how local dynamical symmetries interact with symmetries arising from the connectivity of system variables. This, in turn, allows us to modify data-driven Koopman approximation algorithms to make them more efficient when applied to dynamical systems with symmetries. We illustrate our findings in a simple network of coupled Duffing oscillators with symmetries in individual oscillator dynamics and in their physical couplings.

2.1. Introduction

Symmetries of dynamical systems manifest themselves in asymptotic dynamics, bifurcations, and attractor basin structure. Symmetries play a crucial role in guiding the emergence of synchronization and pattern formation, which are behaviors broadly observed in natural and engineered systems. Methods from group theory, representation theory, and equivariant bifurcation theory provide useful tools to study the common features of systems with symmetries [**50**, **52**, **54**].

Dynamical elements organized into a network are an important class of dynamical systems that often exhibit these behaviors, especially when symmetries appear in both network structure and the dynamics of the individual nodes. Studying the effect of symmetries in network topology of synthetic and real-life systems using computational group theory is an active area of research [**96**, **114**, **115**]. Those symmetries lead to phenomena such as full synchronization, cluster synchronization, and formation of exotic steady states such as chimeras [**31**, **42**, **97**, **139**]. Moreover, topological symmetries underlying cluster synchronization of coupled identical elements assist in analyzing the stability of these fully synchronous cluster states [**62**, **114**]. For networks of identical coupled oscillators, the form of their limit cycle solutions and the form of their bifurcations can be derived from symmetry considerations [**10**]. Symmetries are also key in determining network controllability and observability. For example, Refs. [**40**, **125**] explored the effect of explicit network symmetries for linear time-independent and time-dependent networks. Similarly, Refs. [**88**, **155**]

considered nonlinear network motifs with symmetries and studied how the presence of different types of structural symmetries affect the observability and controllability of the system. Ref. [**100**], similar to our approach, uses the Koopman operator formalism (discussed below). They provide analytic results that link the presence of permutational symmetries in dynamical systems to their observability properties.

Many dynamical systems of current interest are high dimensional and nonlinear. For instance, this is the case for many complex networks, such as power grids and biological networks. Complexity there arises from the interaction between network interconnectivity structure and the nonlinearities in the node and edge dynamics. And, this often leads to multistability. Linearization methods can provide insight near the system's attractors, but they poorly approximate the dynamics on the rest of the state space. In contrast, operator-based methods give access to the global characteristics of nonlinear systems. And, they do so in a linear setting and are therefore more well-suited, for instance, to characterize the attractor basin structure of multistable dynamical systems or the design of control interventions. The Perron-Frobenius and Koopman operator are adjoint linear infinite-dimensional operators whose spectra can provide global information about the system. Their approximations using data-driven approaches make operator methods potentially applicable when there is no prior knowledge of the system.

The Perron-Frobenius operator evolves densities on state space. It has been used extensively to assess global behavior of nonlinear dynamical systems [**86**, **149**]. There are several well developed approaches for obtaining its numerical approximations, such as Ulam's method that relies on the discretization of state space to obtain an approximation of the Perron-Frobenius operator [**152**]. Since the Koopman operator is adjoint to the Perron-Frobenius operator, numerical approximations of the Koopman operators can be obtained using these methods as well [**73**].

The Koopman operator is an infinite dimensional linear operator that describes the evolution of *observables* (functions of the state space) [**73**,**77**,**86**]. Its definition and properties in the context of dynamical systems are provided, for instance, in Ref. [**29**], which also summarizes its applicability to model reduction, coherency analysis, and ergodic theory. Methods based on the Koopman operator decomposition have proved useful for applications such as model reduction and control

of fluid flows [**13**], power system analysis [**148**], and extracting spatio-temporal patterns of neural data [**27**].

Data driven methods to approximate the Koopman operator rely upon snapshot pairs of measurements of the system state at consecutive time steps. Reconstructing the operator from these snapshot pairs requires that a set of functions (called a dictionary of observables) be chosen. The first data driven method introduced, dynamic mode decomposition (DMD), implicitly uses linear monomials as a dictionary and thus is most applicable to systems where the Koopman eigenfunctions are well represented by this basis set [**132**]. A more recent method called extended DMD (EDMD) introduced in Ref. [**157**] can be more powerful than the standard DMD when applied to nonlinear systems as it allows the choice of more complicated sets of dictionary functions. Applying the EDMD is most computationally feasible if the number of the dictionary functions does not exceed the total number of the snapshot pairs used. That is not necessarily the case if a rich function dictionary (e.g., a dictionary of high order polynomials) is chosen. A modification of EDMD called kernel DMD introduced in Ref. [**158**] addresses this issue by providing a way to efficiently calculate the Koopman operator approximation in a case when the number of dictionary functions exceeds the number of measurements. Yet, the principled choice of an underlying dictionary that leads to an accurate approximation of the eigenspectrum corresponding to the leading Koopman modes using EDMD or kernel DMD remains an outstanding challenge. That problem is confronted, for instance, in Ref. [**89**], where an iterative EDMD dictionary learning method is presented. Although the optimal choice of dictionary functions is often unknown, there are some common choices that are known to produce accurate results for certain classes of systems [**157**].

Here we study nonlinear dynamical systems with discrete symmetries combining operator-based approaches and linear representation theory. Recently, related methods have been applied to dynamical systems with symmetries. On the one hand, Ref. [**98**] addresses symmetries of the Perron-Frobenius operator in relation to the admissible symmetry properties of attractors. On the other, Ref. [**133**] links the spatiotemporal symmetries of the Navier-Stokes equation to the spatial and temporal Koopman operator. Additionally, Ref. [**28**] noted that symmetry considerations play an important role in discovering governing equations. And, Ref. [**68**] shows how conservation laws

can be detected with Koopman operator approximations and then used to control Hamiltonian systems.

In contrast, our focus is on dynamical systems with symmetries described by a finite group. We show how the properties of the associated Koopman operator spectrum can be linked to the properties of the spectrum of the finite dimensional approximations of the Koopman operator obtained from finite data. We further show how the analytic properties of the Koopman operator decomposition can inform the choice of dictionary functions that can be used in the Koopman operator approximations. This gives a practical way to reduce the dimensionality of the approximation problem.

Our development builds as follows. section 2.2 defines the Koopman operator, introduces approximation methods (EDMD and kernel DMD), and defines equivariant dynamical systems as well as useful concepts from group theory and representation theory. section 2.3 draws out the implications of dynamical system symmetries for the structure of the Koopman operator and its eigendecomposition. section 2.4 connects the properties of the Koopman operator and the structure of its EDMD approximation for symmetric systems. This then allows modifying the EDMD method to exploit the underlying symmetries, resulting in a block-diagonal Koopman operator approximation matrix. We also provide numerical examples, showing how using particular dictionary structures speeds up the algorithm. Finally, section 4.7 summarizes our findings and outlines directions for future work.

2.2. Preliminaries

2.2.1. Koopman operator. In this section, we provide some background in operator theoretic approaches to dynamical systems, in particular, the Koopman operator and its adjoint Perron-Frobenius operator. Since in this manuscript we address the approximations of the Koopman operator where the input is discrete time data, we focus on their definition in the discretized setting. The continuous time definitions are similar [**29**]. Our results regarding the degeneracy of Koopman operator eigenvalues and the properties of its corresponding eigenfunctions presented in section 2.3 hold in both discrete and continuous time settings.

Suppose we are given a continuous time autonomous dynamical systems defined as:

$$\dot{x} = g_c(x). \tag{2.1}$$

Here, $x \in \mathbb{R}^n$, $g_c : \mathbb{R}^n \to \mathbb{R}^n$. Let $\Phi(x(t), \Delta t)$ be a flow map mapping the initial condition $x(t)$ to the solution at time $t + \Delta t$. It is defined in the following way:

$$\Phi(x(t), \Delta t) = x(t) + \int_t^{t+\Delta t} g_c(x(\tau))d\tau. \tag{2.2}$$

The system can be discretized with a finite time step Δt_{step}, so that $x_{i+1} = \Phi(x_i, \Delta t_{\text{step}})$. We denote the function evolving the dynamics of this discretized system by g:

$$x_{i+1} = g(x_i). \tag{2.3}$$

The Koopman operator is a *linear infinite dimensional* operator that evolves the functions (referred to as observables) of state space variables $f : \mathbb{R}^n \to \mathbb{C}$. The action of the Koopman operator $\mathcal{K}$ on an observable function f for discrete time systems is defined as:

$$(\mathcal{K}f)(x) = f(g(x)). \tag{2.4}$$

Since we consider data-driven Koopman operator approximation methods in this manuscript, the discrete time version of the definition is most applicable.

Pairs of eigenvalues λ and eigenfunctions ϕ of the Koopman operator $\mathcal{K}$ are defined as:

$$(\mathcal{K}\phi)(x) = \lambda\phi(x). \tag{2.5}$$

Of particular interest are the Koopman modes that can be used in model reduction and coherency estimation [**124**, **147**]. The Koopman modes v_i^f of the observable $f(x)$ are defined by:

$$f(x) = \sum_i v_i^f \phi_i(x), \tag{2.6}$$

and are projections of the observable onto the span of the eigenfunctions of the Koopman operator $\mathcal{K}$. A particularly useful set of modes is that of the full state observable $f(x) = x$, defined as:

$$x = \sum_i v_i \phi_i(x). \tag{2.7}$$

In general, parts of the Koopman operator spectrum can be continuous [**29**, **79**]. For instance, this can be the case for chaotic systems. However, we focus on the case of a discrete spectrum since the methods we refer to in the following sections (EDMD, kernel DMD) are only applicable for that case. Our results regarding the symmetry properties of the discrete parts of the Koopman operator spectrum are analogous to those related to the continuous part of the spectrum. Numerical methods related to continuous Koopman operator spectra are considered, for instance, in Ref. [**95**].

The other candidate for studying dynamical systems using an operator based approach is the Perron-Frobenius operator $\mathcal{P}$ defined as follows for deterministic dynamical systems:

$$\int_A \mathcal{P}\rho(x)dx = \int_{g^{-1}(A)} \rho(x)dx. \tag{2.8}$$

Here, $\rho(x)$ is a density on state space, and $A \subseteq \mathbb{R}^n$ is a subset of the state space, and g, defined in eq. (2.3), evolves the state of the system. The Perron-Frobenius operator is the adjoint to the Koopman operator [**86**], so an approximation of one of them provides an approximation of the other [**73**].

2.2.2. Koopman operator approximation methods. Extended dynamic mode decomposition (EDMD) introduced in Ref. [**157**] is a data-driven method of approximating the Koopman operator for discretized systems that requires an explicit choice of a dictionary of functions referred to as *observables*. How to optimally choose those functions remains an open problem for many systems, especially if the form of differential equations describing the governing dynamical system is not known in advance and only finite data on the behavior of the system is available. The method can be very accurate in capturing the dynamics of the system, but its accuracy depends strongly on the choice of an appropriate dictionary of observables. The method's convergence properties are studied in Ref. [**78**], and its relation to the Perron-Frobenius operator approximation methods is discussed in Ref. [**73**]. Here, we summarize the EDMD and its relation to the Koopman operator.

The first requirement for the method is a set of pairs of consecutive snapshots $x = [x_1, x_2, ..., x_M]$ and $y = [y_1, y_2, ..., y_M]$, where the measurements x_i and y_i are performed with a small constant time interval Δt: $y_i = \Phi(x_i, \Delta t)$, where Φ is the flow map defined in eq. (2.2). Typically, the set of snapshots contains measurements from different trajectories in state space. We define a dictionary of linearly independent observables $\mathcal{D} = \{\psi_1, ..., \psi_N\}$ and form vectors of observations Ψ_x and Ψ_y. Here, $\Psi_x \in \mathbb{R}^{M \times N}$, where N is the number of dictionary functions used in the approximation, and M is the number of data snapshots. The elements of Ψ_x are obtained from $(\Psi_x)_{ij} = \psi_j(x_i)$. We also use the notation $\Psi(x_m) = (\psi_1(x_m), ..., \psi_N(x_m))$ for the dictionary functions evaluated at a particular point on the trajectory.

A finite dimensional approximation of the Koopman operator $\mathcal{K}$ that we denote as K can be obtained using:

$$K = \Psi_x^+ \Psi_y. \tag{2.9}$$

Here, Ψ_x^+ denotes the pseudoinverse of Ψ_x. We focus on the case of the Moore-Penrose pseudoinverse for the rest of the manuscript [**116**].

If the number of snapshots is much higher than the dimensionality of the function dictionary ($M \gg N$), it is more practical instead to define the square matrices G and A as shown below and obtain the approximation in the following way:

$$K = G^+ A, \text{ where } G = \sum_m \Psi(x_m)^* \Psi(x_m), \; A = \sum_m \Psi(x_m)^* \Psi(y_m). \tag{2.10}$$

Here, * represents the complex conjugate transpose. If the only observables are the states of the system $x_1, x_2, ..., x_n$, EDMD reduces to DMD [**73**, **157**].

The eigendecomposition of K provides the Koopman eigenvalues, eigenfunctions, and modes that allow an approximate linear representation of the underlying system dynamics. Let λ_j and u_j be the jth eigenvalue and eigenvector of K. Then the corresponding Koopman eigenfunction can be approximated by:

$$\phi_j(x) = \Psi(x) u_j. \tag{2.11}$$

Let b_i be the vectors defined by $g(x)_i = \Psi b_i$, where $g(x)_i = e_i^* x$ denotes the elements the full state observable discussed in Ref. [**157**], and $B = (b_1 \ ... \ b_n)$. The Koopman eigenmodes can then be obtained as:

$$v_i = (w_i^* B)^T. \tag{2.12}$$

Here, w_i denotes the ith left eigenvector of K.

A modification of EDMD named kernel DMD [**158**] is better suited for systems with a low number of measurements and a high number of observables (e.g., the full state observable for fluid dynamical systems is very high dimensional, so defining a polynomial dictionary of the full state observable is very computationally expensive), i.e. $M \ll N$. The method relies on evaluating the kernel function:

$$k(x_i, y_i) = \Psi(x_i)\Psi(y_i)^*. \tag{2.13}$$

That allows efficient computation of $M \times M$ matrices $\hat{G}$, $\hat{A}$, and $\hat{K}$, where M is the number of trajectory time steps. The eigendecomposition of $\hat{K}$ then can be used to obtain the approximations of the Koopman eigenvalues, eigenfunctions, and modes.

In the main body of the manuscript, we focus on the case where the number of measurements is relatively high for each degree of freedom ($M \gg N$), and obtain a way to reduce the dimensionality of the EDMD approximation of the Koopman operator for systems with symmetries in section 2.4. A similar modification of the kernel DMD is discussed in section 2.6.5.

2.2.3. Discrete symmetries. In this section, we define the concepts useful to study the structure of the Koopman operator $\mathcal{K}$ and its approximations K for systems with symmetries. Throughout this section and the rest of the manuscript, we use an example of a small network of Duffing oscillators to illustrate the definitions and algorithms.

In this manuscript, we consider dynamical systems (as defined in eqs. (2.1) and (2.3)) that respect discrete symmetries. These systems are called equivariant with respect to the symmetry group Γ. We define groups by their *presentations* in a form $\langle S|R\rangle$, where S is a set of generators of

the group, and R is a set of relations among these generators that define that group. Every element of the group can be written as a product of powers of some of these generators.

For instance, the cyclic group Z_n is presented by $\langle r|r^n = 1\rangle$. An example of a realization of that group is a set of rotational symmetries of a regular n-gon.

To study dynamical systems with symmetries, we need to define the specific actions of the group on a vector space in addition to an abstract presentation of a group Γ. Let $X \subset \mathbb{R}^n$ be a vector space with elements $x \in X$. We denote the actions γ_ρ on a vector space X by $\gamma_\rho x$ if the set of these actions Γ_ρ is isomorphic to Γ. A shorthand $\gamma_\rho x = \gamma x$ is sometimes used in the literature when the action corresponding to the subscript ρ is clear from the context (for instance, it is defined by a permutation matrix of the same degree as the state space of the system), however, we use the γ_ρ notation to avoid ambiguity, since the precise definition of group action in particular cases is important in this manuscript, as shown, for instance, in example 2.2.1 and example 2.2.2.

Finally, we define what it means for a dynamical system to be symmetric. Let $\dot{x} = g_c(x)$ be a continuous time system of differential equations. Here, $x \in \mathbb{R}^n$, and $g_c : \mathbb{R}^n \to \mathbb{R}^n$. The system is Γ-equivariant with respect to the actions of Γ_ρ if for all $x \in X$ and $\gamma_\rho \in \Gamma_\rho$:

$$g_c(\gamma_\rho x(t)) = \gamma_\rho g_c(x(t)). \tag{2.14}$$

As discussed in section 2.2, data comes in discretized form, so a discrete form of that definition is useful. For discrete time systems defined by $x_{i+1} = g(x_i)$, equivariance is defined in a similar manner:

$$g(\gamma_\rho x_i) = \gamma_\rho g(x_i). \tag{2.15}$$

We note that if a continuous time system is Γ-equivariant, so is its discretization. Moreover, the set of trajectories of a γ-equivariant system in state space also respects the symmetries of the system. For discretized systems, it means that if $\{x_0, x_1, ...x_n\}$ form a trajectory in state space, then $\{\gamma_\rho x_0, \gamma_\rho x_1, ...\gamma_\rho x_n\}$ form a trajectory as well.

An important example of equivariant dynamical systems that many of the recent works have focused on (such as Refs. [**62**, **97**, **114**, **139**]) is a system of coupled identical oscillators. In that case, the set (or a subset) of actions under which the system is equivariant is defined by the set

of permutational matrices P that commute with the adjacency matrix (a matrix that describes connectivity between the nodes of the network) of that oscillator network. In this case, the action of the group is linear, however, that does not always have to be the case.

We also need to define the action of the group in function space, where $f \in \mathcal{F}$ are functions $f : X \to \mathbb{C}$ as:

$$(\gamma_\rho \circ f)(x) \equiv f(\gamma_\rho^{-1} x). \tag{2.16}$$

Note that the group action is inverted to satisfy the group action axioms (so that actions on functions form the same group structure as the actions on states). This definition will be useful since the Koopman operator acts on functions (i.e. observables).

Another concept useful for our work is a linear group *representation* T, which is a mapping from group elements $\gamma \in \Gamma$ to the elements of the general linear group (a group of matrices of degree n with the operation of matrix multiplication denoted by $\mathrm{GL}(n, V)$) on a vector space V (in this case, we are interested in $V = \mathbb{C}^n$). The characters $\chi_i(\gamma)$ of a group representation $T_i(\gamma)$ are defined as $\chi_i(\gamma) = \mathrm{Tr}(T_i(\gamma))$.

A representation is called irreducible if it has no nontrivial invariant subspaces (meaning that the representation matrices corresponding to the group elements can not be simultaneously non-trivially block diagonalized into the same block form). For each Γ we can obtain all of its irreducible matrix representations. We denote their elements mapping $\gamma \in \Gamma$ to $p \times p$-dimensional matrices as $R_i(\gamma)$, where the index i corresponds to the ith irreducible representation. Irreducible representations are defined up to an isomorphism. For the purposes of this manuscript, it is useful to make use of either the unitary irreducible representations or their characters.

A vector space, e.g. the space of square integrable functions $\mathcal{F}$, can be uniquely decomposed into components that transform like the ith irreducible representation of Γ under the actions of Γ_ρ. These components are called *isotypic components* [**50**]. We denote these components by $\mathcal{F}_i$. An *isotypic decomposition* of the square integrable function space with respect to Γ_ρ is then defined as $\mathcal{F} = \bigoplus_i \mathcal{F}_i$, where the $\bigoplus$ symbol denotes the direct sum here and thereafter. We illustrate the construction of an isotypic decomposition using an example of a Z_2-equivariant system.

EXAMPLE 2.2.1. *Symmetries of a single Duffing oscillator dynamics and isotypic components in function space corresponding to the actions of its symmetry group.*

The unforced Duffing oscillator equation has the form:

$$\ddot{x} = -\sigma\dot{x} - x(\beta + \alpha^2 x). \tag{2.17}$$

We can rewrite the above equation as a system of differential equations to obtain:

$$\begin{aligned} \dot{x} &= y, \\ \dot{y} &= -\sigma y - x(\beta + \alpha^2 x). \end{aligned} \tag{2.18}$$

Let $\boldsymbol{x} = \begin{pmatrix} x \\ y \end{pmatrix}$*, and let the dynamics be denoted by* $\dot{\boldsymbol{x}} = g_c(\boldsymbol{x})$*. Let* $r_s = \begin{pmatrix} -1 & 0 \\ 0 & -1 \end{pmatrix} = -I_{2\times 2}$ *be the action on the state space that flips the signs of both variables. The actions* r_s *and* $e_s = I_{2\times 2}$ *form a group* Γ_s *isomorphic to* $\Gamma = Z_2 = \langle r | r^2 = e \rangle$*. Let* $\gamma_s \in \Gamma_s$*, then:*

$$\gamma_s g_c(\boldsymbol{x}) = g_c(\gamma_s \boldsymbol{x}). \tag{2.19}$$

Thus, the Duffing oscillator system is Z_2*-equivariant with respect to the actions* γ_s*.*

We now illustrate the isotypic component decomposition of Z_2 *in function space.* Z_2 *has two one-dimensional irreducible representations: the trivial representation defined by* $R_{tr}(r) = 1$ *and the sign representation defined by* $R_{sign}(r) = -1$*. Then the space of square integrable functions* $\mathcal{F}$ *can be decomposed into* $\mathcal{F} = \mathcal{F}_{tr} \oplus \mathcal{F}_{sign}$*, where* $\mathcal{F}_{tr} = \{f : r_s \circ f = f(-x,-y) = f(x,y)\}$ *and* $\mathcal{F}_{sign} = \{f : r_s \circ f = f(-x,-y) = -f(x,y)\}$*. In this case, the sets of functions* $\mathcal{F}_{tr}$ *and* $\mathcal{F}_{sign}$ *consisting of even and odd functions respectively transform like the trivial and sign irreducible representations with respect to sign flip as a group generator action.*

We now extend the example to a network of Duffing oscillators and explore additional permutation symmetries.

EXAMPLE 2.2.2. *We now consider the dynamics of a network of Duffing oscillators, as shown in fig. 2.1. Suppose the coupling is linear in* x *with a coupling coefficient assigned to every edge* η_{ij}*.*

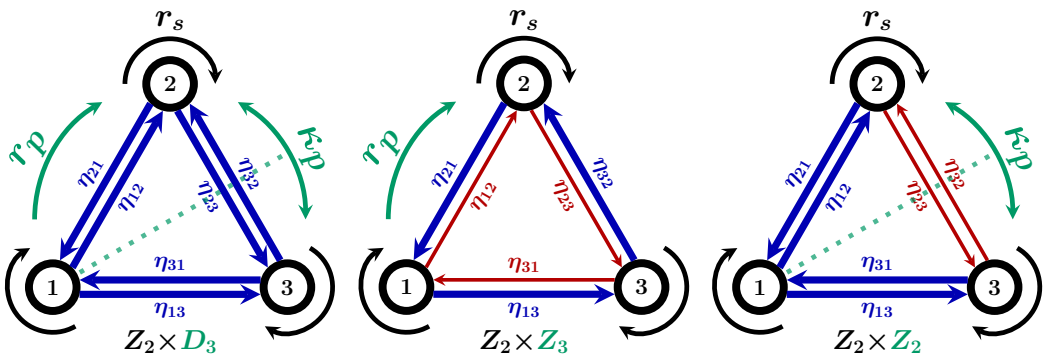

(a) Duffing oscillator network with $Z_2 \times D_3$ symmetry (b) Duffing oscillator network with $Z_2 \times Z_3$ symmetry (c) Duffing oscillator network with $Z_2 \times Z_2$ symmetry

FIGURE 2.1. Possible symmetries of a network of three identical Duffing oscillators depending on the coupling strength between the oscillators. Different coupling strengths are shown in blue and red. Green arrows correspond to permutational symmetries arising from physical coupling, black arrows correspond to the symmetries of nodal dynamics. Scenarios (a)-(c) are considered in examples 2.2.1 and 2.4.1 to 2.4.3.

Then for each node i in the network, we have the following dynamics:

$$\begin{aligned} \dot{x_i} &= y_i, \\ \dot{y_i} &= -\sigma \dot{y_i} - x_i(\beta + \alpha^2 x_i) + \sum_{ij} \eta_{ij}(x_i - x_j). \end{aligned} \tag{2.20}$$

*This general coupling scheme is used to model many systems in the literature [**114**, **139**].*

We now consider the case of a 3-node network. Depending on what the coupling terms are, the system may be Γ-equivariant with respect to different symmetry groups that act by permuting node indexes. Some examples are:

a) *If all coupling strengths η_{ij} are equal, the network has D_3 symmetry. This case is shown on fig. 2.1a. Let the state of the system be defined by $x = (x_1\ y_1\ x_2\ y_2\ x_3\ y_3)^T$. Then, the symmetry group is presented by $D_3 = \langle r, \kappa | r^3 = \kappa^2 = e, \kappa r \kappa = r^{-1} \rangle$ and generated by the actions $r_p = \begin{pmatrix} 0 & 1 & 0 \\ 0 & 0 & 1 \\ 1 & 0 & 0 \end{pmatrix} \otimes I_{2\times 2}$ and $\kappa_p = \begin{pmatrix} 1 & 0 & 0 \\ 0 & 0 & 1 \\ 0 & 1 & 0 \end{pmatrix} \otimes I_{2\times 2}$.*

b) *If the coupling strengths obey the conditions* $\eta_{ij} \neq \eta_{ji}$ *and* $\eta_{ij} = \eta_{jk}$ *for* $i \neq k$*, the network has* Z_3 *symmetry. This case is shown on fig. 2.1b. The symmetry group is presented by* $Z_3 = \langle r | r^3 = e \rangle$ *and generated by the action* r_p *defined above.*

c) *If the coupling strengths obey the conditions* $\eta_{12} = \eta_{21} = \eta_{13} = \eta_{31}$*, as well as* $\eta_{23} = \eta_{32}$*, and no other equalities hold, the network has* Z_2 *symmetry. This case is shown on fig. 2.1c. The symmetry group is presented by* $Z_2 = \langle \kappa | \kappa^2 = e \rangle$ *and generated by the action* κ_p *defined above.*

Even though in case (c) the permutation symmetry is isomorphic to the same group as the sign flip symmetry in example 2.2.1, the isotypic components in function space $\mathcal{F}$ *induced by the group action are different.* Z_2 *has two one-dimensional irreducible representations: trivial representation* $R_1(\kappa) = R_{tr}(\kappa) = 1$ *and sign representation* $R_2(\kappa) = R_{sign}(\kappa) = -1$*. Let* $\boldsymbol{x_i} = \begin{pmatrix} x_i \\ y_i \end{pmatrix}$*. The isotypic components are defined by the permutative relations* $\mathcal{F}_{tr} = \{f : \kappa_p \circ f = f(\boldsymbol{x}_1, \boldsymbol{x}_3, \boldsymbol{x}_2) = f(\boldsymbol{x}_1, \boldsymbol{x}_2, \boldsymbol{x}_3)\}$ *and* $\mathcal{F}_{sign} = \{f : \kappa_p \circ f = f(\boldsymbol{x}_1, \boldsymbol{x}_3, \boldsymbol{x}_2) = -f(\boldsymbol{x}_1, \boldsymbol{x}_2, \boldsymbol{x}_3)\}$*.*

Additionally, each node still has Z_2 *symmetry with respect to the action* r_s *which is not broken since the coupling function is odd. That symmetry is also depicted in fig. 2.1. The isotypic components of the entire symmetry group are then intersections of the isotypic components of* Z_2 *(acting by a sign flip) and the symmetry group of the network geometry (acting by a permutation, e.g.* D_3 *for case (a) of this example, also illustrated in fig. 2.3a).*

Any function can be rewritten as a sum of projections into different isotypic components. The procedure is outlined in the following section.

2.3. Properties of the Koopman operator for systems with symmetries

In this section, we consider the structure of the eigenspace of the Koopman operator of Γ-equivariant systems. We show how to obtain a particular eigenbasis of the system corresponding to the isotypic decomposition in function space and demonstrate that the isotypic decomposition induces a block diagonal structure on the matrix representation of $\mathcal{K}$.

THEOREM 2.3.1. *For a Γ-equivariant dynamical system $x_{i+1} = g(x_i)$ and an arbitrary function f, the Koopman operator commutes with the actions of the elements of Γ:*

$$\gamma_\rho \circ (\mathcal{K}f)(x) = \mathcal{K}(\gamma_\rho \circ f)(x). \tag{2.21}$$

Proof:

The commutativity follows from the definitions of the Koopman operator and the definition of the action of the group in state space and function space.

$$\gamma_\rho \circ (\mathcal{K}f)(x) = \gamma_\rho \circ f(g(x)) = f(\gamma_\rho^{-1} g(x)) = f(g(\gamma_\rho^{-1} x)) = \mathcal{K}f(\gamma_\rho^{-1} x) = \mathcal{K}(\gamma_\rho \circ f)(x) \tag{2.22}$$

*This result is similar to Theorem 3.1 in Ref. [**98**], where it is shown that the action of Perron-Frobenius operator commutes with the action of the symmetry group Γ for Γ-equivariant systems.*

COROLLARY 2.3.1. *The space of eigenfunctions of the Koopman operator $\mathcal{K}$ with eigenvalue λ for a Γ-equivariant system is Γ-invariant.*

Proof:

Let S_λ be the set of eigenfunctions of $\mathcal{K}$ with eigenvalue λ. Let $\phi \in S_\lambda$. Then, using the commutativity of $\mathcal{K}$ and Γ_ρ, we can show that $\forall \gamma_\rho \in \Gamma_\rho$:

$$\mathcal{K}(\gamma_\rho \circ \phi(x)) = \gamma_\rho \circ (\mathcal{K}\phi)(x) = \lambda \gamma_\rho \circ \phi(x). \tag{2.23}$$

Thus, $\phi_{\gamma,\rho} \in S_\lambda$, where $\phi_{\gamma,\rho}$ is also an eigenfunction with an eigenvalue λ defined as $\phi_{\gamma,\rho}(x) = \gamma_\rho \circ \phi(x)$.

We now consider a particular form of the eigenbasis of the Koopman operator that induces block diagonal structure of the matrix representation of the action of the Koopman operator $\mathcal{K}$. The result quoted below is useful for that purpose.

THEOREM 2.3.2. *(Theorem 3.5 in Chapter XII of Ref. [**54**]).*

Let Γ be a compact Lie group acting on the vector space V decomposed into isotypic components $V = W_1 \bigoplus ... \bigoplus W_t$. Let $A : V \to V$ be a linear mapping commuting with Γ. Then $A(W_k) \subset W_k$.

This result is applicable to finite symmetry groups. Isotypic components of $\mathcal{F}$ with respect to Γ induce block diagonal structure of the matrix representation of the Koopman operator. Since $\mathcal{K}$ and Γ commute, $\mathcal{K}(\mathcal{F}_k) \subset \mathcal{F}_k$. This block structure can be exploited in finding the Koopman operator approximations, as we show in the next section. Thus, we need to be able to obtain an isotypic component basis from an arbitrary function dictionary. This is a well defined procedure [**33**], outlined below. Functions obtained via isotypic decomposition are useful to perform calculations in many areas of physics, for instance, they can simplify finding approximate solutions to Schrodinger equation, or in studying crystallographic point groups [**33**, **143**]. The construction is also widely applied to dynamical systems, for instance, to study states and their stability using equivariant bifurcation theory.

Suppose we start from an arbitrary basis function dictionary $\mathcal{D}_\psi = \{\psi_i\}$. Each of those functions can be expanded in the isotypic component basis with at least one nonzero coefficient α^p_{mn}:

$$\psi = \sum_p \sum_{m,n=1}^{d_p} \alpha^p_{mn} \xi^p_{mn}. \tag{2.24}$$

Here, ξ^p_{mn} is a basis function in the pth isotypic component of $\mathcal{F}$ with respect to the actions of the symmetry group Γ, and d_p is the dimension of that isotypic component. Alternatively, it can be thought of as a sum over all inequivalent (non-isomorphic) irreducible representations of Γ, where ξ^p_{mn} transforms as the (m,n)th element of the pth irreducible representation of Γ [**33**]. We define a projection operator and form a new function basis consisting of functions $\{\xi^p_{mn}\}$ as outlined below.

The projection operator is defined as:

$$\mathcal{P}^p_{mn} = \frac{d_p}{|\Gamma|} \sum_{\gamma \in \Gamma} [R_p(\gamma)]^*_{mn} \gamma_\rho. \tag{2.25}$$

Here, $[R_p(\gamma)]_{mn}$ denotes the element in nth row and mth column of the ith unitary irreducible representation of $\gamma \in \Gamma$, and γ_ρ is the group action. We can form an orthonormal basis $\mathcal{D}_\xi = \{\xi_i\}$ using the projection operator as follows:

$$\xi^p_{mn}(x) = \frac{1}{c_{np}} \mathcal{P}^p_{mn} \circ \psi(x). \tag{2.26}$$

Here, $c_{np} = \langle \mathcal{P}^p_{nn}\psi, \mathcal{P}^p_{nn}\psi \rangle^{1/2}$, where $\langle , \rangle$ denotes the inner product, which can be omitted for our purposes since the scaling of basis functions does not affect the EDMD results (namely, the approximation matrix K, along with its eigenvalues and eigenvectors). Similarly, the overall factor $\frac{d_p}{|\Gamma|}$ of the projection operator in eq. (2.27) only affects the scaling of the basis functions and therefore can be eliminated.

Equivalently, due to orthogonality relations of characters of irreducible representations, the projection operator can be obtained using the following expression:

$$\mathcal{P}^p = \frac{d_p}{|\Gamma|} \sum_{\gamma \in \Gamma} \chi_p(\gamma)^* \gamma_\rho. \tag{2.27}$$

Here, $\chi_p(\gamma)$ is a character of the pth irreducible representation of Γ. If this formula is used, each irreducible representation of degree d_p provides a basis function, and $d_p^2 - 1$ other basis functions can be formed using the Gram-Schmidt orthogonalization process [**33**, **114**, **143**].

Once an isotypic component basis is obtained, the action of the Koopman operator on function space can be presented in the form of a block diagonal matrix. Each irreducible unitary representation of dimension d_p in this case corresponds to a number d_p of $d_p \times d_p$ sized blocks in that matrix $\mathcal{K}$. Similar analysis applies to the Koopman operator approximation K. The reason why this additional decomposition works can be found in section 2.6.1.

2.4. Implications for EDMD

2.4.1. Constructing a basis for systems with known symmetries. In this section we show that the approximation of K obtained using EDMD can be reduced to the block diagonal structure similar to $\mathcal{K}$ under certain assumption on the data. We provide some examples of constructing an isotypic component basis from a given function dictionary. We highlight that the basis depends on both the structure of Γ and the definition of its actions Γ_ρ.

First, we establish that the Koopman operator approximation K commutes with the actions γ_ρ of Γ if the data used in the calculation respects the symmetry, meaning the set of pairs of data points satisfies the condition:

$$\{(\gamma_\rho x_i, \gamma_\rho y_i)\} = \{(x_i, y_i)\}. \tag{2.28}$$

In other words, the set of trajectories is closed under the action of the symmetry group of the underlying dynamical system. This condition on trajectories can be achieved by averaging over a symmetry group, which has been used in literature related to other data-driven methods, for instance, the proper orthogonal decomposition [**12**]. We note that this requirement can sometimes be relaxed, as discussed in section 2.6.3.

In order to perform further simplifications, we pick a particular order of group elements $\{\gamma_1, ..., \gamma_{|\Gamma|}\}$ and create the vectors Ψ_x (and analogously Ψ_y) according to that ordering:

$$\Psi(x) = \begin{pmatrix} \gamma_1 \circ \Psi(x) & ... & \gamma_{|\Gamma|} \circ \Psi(x) \end{pmatrix},$$

$$\Psi_x = \begin{pmatrix} \Psi_1(x_1) & ... & \Psi_{N/|\Gamma|}(x_1) \\ \vdots & \ddots & \vdots \\ \Psi_1(x_M) & ... & \Psi_{N/|\Gamma|}(x_M) \end{pmatrix}. \tag{2.29}$$

Given the ordering of the group elements, we can also construct the permutation representation of the group such that:

$$P_{\gamma_k}(\gamma_1, ..., \gamma_{|\Gamma|})^T = (\gamma_k\gamma_1, ..., \gamma_k\gamma_{|\Gamma|})^T. \tag{2.30}$$

By Cayley's theorem, such permutations form a group isomorphic to Γ. Determining the actions P_{γ_k} of the group generators is sufficient to find the actions of all group elements. Let $\boldsymbol{P}_{\gamma_k} = P_{\gamma_k} \otimes I_{n\times n}$. We note that $(\boldsymbol{P}_{\gamma_k})^* = (\boldsymbol{P}_{\gamma_k})^{-1}$. It can be shown that:

$$\boldsymbol{P}_{\gamma_k} G = G\boldsymbol{P}_{\gamma_k},\ \boldsymbol{P}_{\gamma_k} A = A\boldsymbol{P}_{\gamma_k}. \tag{2.31}$$

By definition, $A = \Psi_x^*\Psi_y$. We note that for symmetric trajectories satisfying eq. (2.28):

$$((\Psi_x\boldsymbol{P}_{\gamma_k})^*\Psi_y\boldsymbol{P}_{\gamma_k})_{ij} = \sum_m \psi_i^*(\gamma_k^{-1}x_m)\psi_j(\gamma_k^{-1}x_m) = \sum_m \psi_i^*(x_m)\psi_j(x_m) = (\Psi_x^*\Psi_y)_{ij}\,. \tag{2.32}$$

Therefore,

$$(\Psi_x\boldsymbol{P}_{\gamma_k})^*\Psi_y\boldsymbol{P}_{\gamma_k} = \Psi_x^*\Psi_y. \tag{2.33}$$

Thus, A and G (for analogous reasons) commute with the action of the symmetry group.

If G is invertible and G commutes with γ_ρ, G^{-1} commutes with γ_ρ as well. Then:

$$\boldsymbol{P}_{\gamma_i} K = \boldsymbol{P}_{\gamma_i} G^{-1} A = G^{-1} A \boldsymbol{P}_{\gamma_i} = K \boldsymbol{P}_{\gamma_i}. \tag{2.34}$$

If G is not invertible, the commutativity result still holds for G^+. G is a normal matrix since it satisfies $GG^* = G^*G$. In section 2.6.2, we show that if G is normal, $GG^+ = G^+G$, so G commutes with its Moore-Penrose pseudoinverse, and therefore the actions of K and Γ commute.

Since K commutes with the actions of Γ, $K\mathcal{F}_i \subset \mathcal{F}_i$. This shows that K can be block-diagonalized in the same way as $\mathcal{K}$.

Suppose we start from a dictionary of observables. Since that dictionary is not necessarily an isotypic component dictionary corresponding to Γ and its action, in order to obtain a block diagonal matrix K, the dictionary needs to be modified using the procedure outlined in section 2.3. In the example below, we show explicitly how to perform this transformation into the isotypic component basis.

In order for the basis to faithfully represent the symmetries of the system we require that:

- The dictionary is closed under the action of the symmetries of the system:

$$\text{If } \psi \in \mathcal{D},\ \gamma_\rho \psi \in \text{span}(\mathcal{D}) \tag{2.35}$$

- Each isotypic component is present after the isotypic component decomposition of the original function basis:

$$\forall m, p\ \exists \psi \in \mathcal{D},\ \text{s.t. } \mathcal{P}^p_{mn} \psi \neq 0 \tag{2.36}$$

For instance, using a monomial basis for a D_3 equivariant system does not satisfy the second requirement.

If these requirements are satisfied, the change of basis does not affect the result obtained by applying the EDMD algorithm as shown in section 2.6.4. Additionally, we note that the eigenvalues of K do not typically have the same degeneracy properties as the eigenvalues of $\mathcal{K}$, but the symmetries of the underlying dynamical system are preserved in trajectory reconstructions.

EXAMPLE 2.4.1. *Constructing an isotypic component basis for a single Duffing oscillator.*

We start from a system with Z_2 symmetry described in example 2.2.1. Suppose a polynomial basis is chosen to form basis functions. For instance, $\mathcal{D}_{poly} = \{1, x_1, x_2, x_1^2, x_2^2, x_1x_2, ...\}$. Each of the dictionary items can be written as $p_{mn}(x_1, x_2) \equiv x_1^m x_2^n$. For even $m+n$, $p_{mn} \in \mathcal{F}_{tr}$, and for odd $m+n$, $p_{mn} \in \mathcal{F}_{st}$, where $\mathcal{F}_{tr}$ and $\mathcal{F}_{st}$ are the isotypic components corresponding to the trivial and standard irreducible representations of Z_2, as discussed in example 2.2.1. Thus, using $\mathcal{D}_{poly}$ results in a sparse matrix K, and K is block diagonal after reordering the basis functions.

*Another possible choice for a set of dictionary functions is a radial basis function set. This type of functions was used to find the EDMD approximation of the Koopman operator in Ref. [**157**]. We use an initial dictionary $\mathcal{D}_\psi$ of n mesh-free radial basis functions. The radial basis function centers can be obtained by either k-means clustering of the data or sampling from a predetermined distribution. As an example, we chose a specific form $\psi(c, x) = r_c log(r_c)$, where c is a 2-dimensional radial basis function center, and $r_{c,x} \equiv ||x - c||^{1/2}$.*

In this case, the individual basis functions do not generally belong to a single isotypic component. We use eq. (2.25) *to construct an isotypic component basis by obtaining the projections of the dictionary onto the isotypic components corresponding to the irreducible representations of Z_2, which are the trivial and standard representations defined in example 2.2.1. Projecting onto the trivial isotypic component leads to:*

$$\mathcal{P}^{tr} \circ \psi(c, x) = \frac{1}{2}\left([R_{tr}(e)]^* \psi(c, x) + [R_{tr}(r)]^* \psi(-c, x)\right) = \frac{1}{2}(\psi(c, x) + \psi(-c, x)) \tag{2.37}$$

Analogously, projecting onto the standard isotypic component results in:

$$\mathcal{P}^{st} \circ \psi(c, x) = \frac{1}{2}(\psi(c, x) - \psi(-c, x)) \tag{2.38}$$

We simplify the notation by denoting $\psi_i^+ \equiv \psi(c_i, x)$. In order to satisfy eq. (2.35), for each ψ_i^+, the basis should also contain $\psi_i^- \equiv \psi(-c_i, x)$. Ignoring the irrelevant multiplicative factor:

$$\begin{pmatrix} \xi_1^{tr} \\ \vdots \\ \xi_n^{tr} \\ \xi_1^{st} \\ \vdots \\ \xi_n^{st} \end{pmatrix} = T_{Z_2} \otimes I_{n\times n} \begin{pmatrix} \psi_1^+ \\ \vdots \\ \psi_n^+ \\ \psi_1^- \\ \vdots \\ \psi_n^- \end{pmatrix} = \begin{pmatrix} \psi_1^+ + \psi_1^- \\ \vdots \\ \psi_n^+ + \psi_n^- \\ \psi_1^+ - \psi_1^- \\ \vdots \\ \psi_n^+ - \psi_n^- \end{pmatrix}. \tag{2.39}$$

For functions in $\mathcal{D}_\xi$ ordered like in eq. (2.39), the approximation matrix K is block diagonal.

EXAMPLE 2.4.2. *Constructing an isotypic component basis for a network of Duffing oscillators from a given basis.*

We also consider a more complicated case of a system of Duffing oscillators with identical coupling as depicted in fig. 2.1a. In that case, the system has $Z_2 \times D_3$ symmetry. Suppose we want to construct an isotypic component basis from a given function dictionary $\mathcal{D}$. As an example, we use an initial dictionary $\mathcal{D}_\psi$ of n mesh-free radial basis functions. Analogously to example 2.4.1, each function can be presented in a form $\psi(c, x) = r_c log(r_c)$, where c is a 6-dimensional radial basis function center, and $r_{c,x} = ||x - c||^{1/2}$. In order to preserve the symmetries of the system, we need to have dictionary elements corresponding to acting on the basis functions by each $\gamma_\rho \in \Gamma_\rho$. Due to the form of these functions, $\gamma_\rho \circ \psi(c, x) = \psi(\gamma_\rho^{-1} c, x)$.

Since $\Gamma = Z_2 \times D_3$ is a direct product of two groups, we can write the projection operator in the following form:

$$\mathcal{P}_{mn}^{pq} = \frac{d_p}{|Z_2|}\frac{d_q}{|D_3|} \sum_{\gamma_i \in Z_2} \sum_{\gamma_j \in D_3} [R_{pq}(\gamma_i, \gamma_j)]_{mn}^* (\gamma_i^{flip}, \gamma_j^{perm}), \tag{2.40}$$
$$\text{where } R_{pq}(\gamma_i, \gamma_j) = R_p(\gamma_i) \otimes R_q(\gamma_j)$$

Here, $R_p(\gamma_i)$ denotes the pth irreducible representation of $\gamma_i \in Z_2$. Analogously, $R_q(\gamma_j)$ denotes the qth irreducible representation of $\gamma_j \in D_3$. Specific actions of group elements γ_i^{flip} and γ_j^{perm} are labeled by the superscripts.

The symmetry group Z_2 has 2 degree 1 irreducible representations, discussed in example 2.2.1:

- *Trivial representation*
- *Sign representation*

The symmetry group D_3 has 2 degree 1 and 1 degree 2 irreducible representations, defined by:

- *Trivial representation R_{tr}: $R_{tr}(r) = 1$, $R_{tr}(\kappa) = 1$*
- *Sign representation R_{sign}: $R_{sign}(r) = 1$, $R_{sign}(\kappa) = -1$*
- *Standard representation R_{st}: $R_{st}(r) = \begin{pmatrix} \omega & 0 \\ 0 & \omega^2 \end{pmatrix}$, $R_{st}(\kappa) = \begin{pmatrix} 0 & 1 \\ 1 & 0 \end{pmatrix}$. Here, $\omega = e^{2\pi i/3}$.*

Note that the dimensions d_i of the irreducible representations of Γ satisfy $\sum d_i^2 = |\Gamma|$ (if $\Gamma = D_3$, $|\Gamma| = 6$). Therefore, the number of isotypic component basis functions obtained from any set $\{\gamma \circ \psi_i\}_{\gamma \in D_3}$ is equal to the number of group elements, so the sizes are consistent.

Suppose we form a vector of basis functions in $\mathcal{D}_\psi$,

$$\Psi = (\psi_{1,1}\psi_{2,1}, ..., \psi_{n,1}, ..., \psi_{1,|\Gamma|}, \psi_{2,|\Gamma|}, ..., \psi_{n,|\Gamma|})^T, \tag{2.41}$$

where the first index corresponds to acting on $\psi_{1,i}$ by the j^{th} element of Γ_ρ. Using eq. (2.40), we obtain transformation matrices that we can use to get the isotypic component basis:

$$T_{D_3} = \begin{pmatrix} 1 & 1 & 1 & 1 & 1 & 1 \\ 1 & 1 & 1 & -1 & -1 & -1 \\ 1 & \omega & \omega^2 & 0 & 0 & 0 \\ 0 & 0 & 0 & 1 & \omega^2 & \omega \\ 1 & \omega^2 & \omega & 0 & 0 & 0 \\ 0 & 0 & 0 & 1 & \omega & \omega^2 \end{pmatrix}, \; T_{Z_2} = \begin{pmatrix} 1 & 1 \\ 1 & -1 \end{pmatrix}. \tag{2.42}$$

The isotypic component basis then can be obtained by modifying a set of functions in $\mathcal{D}_\psi$:

$$\Xi = T\Psi, \quad T \equiv T_{Z_2} \otimes T_{D_3} \otimes I_{n \times n}. \tag{2.43}$$

The matrix $T_{Z_2} \otimes T_{D_3}$ is a 12×12 matrix, and its dimensions are equal to the size of the underlying symmetry group $Z_2 \times D_3$. The matrix $I_{n \times n}$ ensures that every element of the original dictionary gets maps to an element of the new isotypic component dictionary.

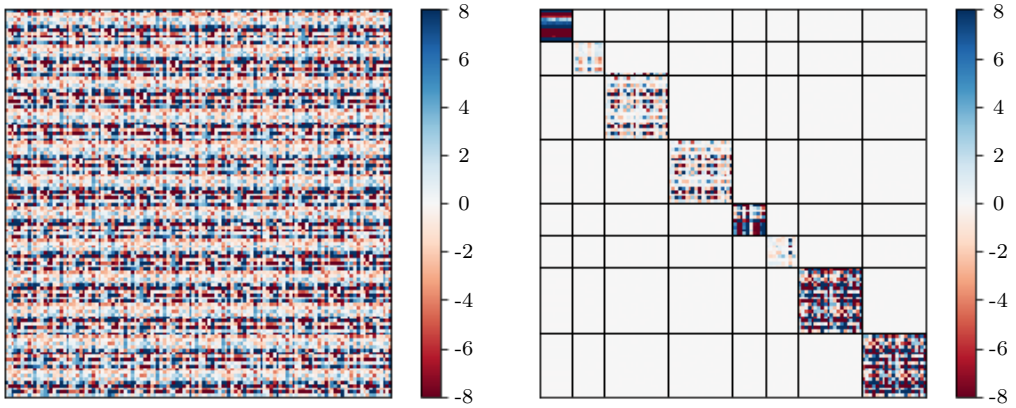

(a) K for a standard dictionary of observables

(b) K for a symmetry adapted dictionary of observables

FIGURE 2.2. Structure of K for different choices of dictionary functions

If we use Ξ as a basis, we obtain K decomposed into 8 blocks, each corresponding to an irreducible representation of $Z_2 \times D_3$.

We implement the EDMD algorithm to obtain the approximation of $\mathcal{K}$. Here, the data comes from 500 initial trajectories of length 10 that were then reflected and rotated so that the data respects the symmetries. The parameter values of $\alpha = 1$, $\beta = -1$, $\delta = 0.5$, and $\eta = 1$ were used. We plot the approximation matrix K in fig. 2.2. In this case, a dictionary of 120 radial basis functions was used. fig. 2.2a illustrates the Koopman operator approximation matrix K calculated using an initial dictionary D_ψ and requires performing matrix operations on the full 120×120 matrix. fig. 2.2b shows K obtained from the symmetry adapted basis functions. The order of calculations can be reduced significantly since it is only necessary to perform matrix operations on blocks. K calculated in the symmetry adapted basis has 4, 10×10 and 2, 20×20 unique blocks.

As shown in the examples above, we can construct a basis that block diagonalizes the Koopman operator matrix approximation K from the elements of any arbitrary basis. Since the off block-diagonal elements of the matrix are a priori known to be zero, we do not need to compute these elements explicitly. This suggests that for systems with symmetries it is more efficient to perform the EDMD algorithm for isotypic decomposition blocks. We denote the number of conjugacy classes or irreducible representations of Γ by r_Γ. In that case, instead of performing $O((mr_\Gamma)^\alpha)$ operations of matrix inversion, multiplication, and eigendecomposition, it is sufficient to perform

these operations for each of the r_Γ blocks, with operations being $O(m^\alpha)$. Here $2 < \alpha < 3$, e.g. as seen in Ref. [**74**]. Even though the algorithmic complexity only differs by a factor that scales with the size of the group that is fixed for any given system, in practice, the computation is more efficient when EDMD specific to Γ-equivariant systems is used. We also note that each d_p dimensional irreducible representation contributes d_p *equal* blocks, each one of dimension $d_p \times d_p$, to K_{symm}, which further simplifies the calculation. Moreover, in the case of networks of high dimensionality, it allows parallel eigendecomposition computation for isotypic component blocks. table 2.1 summarizes the modified EDMD algorithm for Γ-equivariant systems and highlights that the order of computations can be lowered.

Koopman eigenfunctions and eigenmodes have many applications in dimensionality reduction, finding the basins of attraction, characterizing coherency between oscillatory systems, etc. Block diagonalizing K allows the efficient computation of the Koopman eigenvalues, eigenfunctions, and modes.

The kernel DMD is closely related to the EDMD algorithm. It relies on calculating the eigentriples associated with K from a dual matrix $\hat{K}$ evaluated using a kernel trick commonly applied in machine learning [**158**]. This method can be computationally advantageous for cases when the number of basis functions exceeds the number of available measurements of the state of the system. We find that the kernel DMD can also be modified to include symmetry considerations in order to optimize the calculations. The method is provided in section 2.6.5.

2.4.2. Consequences of symmetry assumptions in the basis. Assume the data is symmetric as defined by eq. (2.28) with respect to the symmetry group Γ. A "perfect" basis is the one respecting the isotypic decomposition of Γ. Suppose the basis functions belong to isotypic components of $\Sigma \neq \Gamma$. That choice will affect the structure of K. We study that structure by evaluating the elements of A, since K and G^+ have the same structure as A.

If the system is Γ-equivariant and $\Sigma \subset \Gamma$ and the set of actions of Σ is a subset of actions of Γ, the system is also Σ-equivariant. Thus, picking a basis respecting the isotypic decomposition of Σ will have the block diagonal structure corresponding to Σ. This means that the choice of basis results in block diagonal K, but its structure does not provide any additional information about the symmetries of the system.

Standard EDMD	EDMD for Γ-equivariant systems
• Pick a dictionary of N observables • Evaluate the observables at data points x_i and y_i • Evaluate the entries of G, A: N^2 elements • Obtain G^+: $N \times N$ matrix • Find $K = G^+A$: $N \times N$ matrices • Find the eigendecomposition of K: $N \times N$ matrix	• Pick a dictionary of N observables • Identify the symmetry Γ of the system, find the irreducible representations of Γ • Change the basis to a Γ-symmetric basis using eq. (2.27) and eq. (2.26) : multiplying at most $N/\lvert\Gamma\rvert$ $\lvert\Gamma\rvert \times \lvert\Gamma\rvert$ matrices by vectors $\lvert\Gamma\rvert \times 1$. Let N_p be the number of functions obtained from applying a projection operator $\mathcal{P}^p$ corresponding to p th irreducible representation of Γ (e.g., $N_p = N/\lvert\Gamma\rvert$ for cyclic groups). • Evaluate the observables at data points x_i and y_i • To obtain the blocks K_{pq} of K (each isotypic component corresponds to d_p blocks), for each p: – Evaluate the entries of G_{p1}, A_{p1}: $(N_p/d_p)^2$ elements – Obtain G^+_{p1}: $(N_p/d_p) \times (N_p/d_p)$ matrix – Find $K_{p1} = G^+_{p1}A_{p1}$: $(N_p/d_p) \times (N_p/d_p)$ matrices – Find the eigendecomposition of K_{p1}: $(N_p/d_p) \times (N_p/d_p)$ matrix – The other K_{pq} blocks equal to K_{p1} • $K = \bigoplus_p \bigoplus_{q=1}^{d_p} K_{pq}$. Its eigenvalues are the eigenvalues of K_p, and its eigenvectors only have N_p nonzero elements. Mathematically, eigenvectors v_{kl} of K are of the form $(v_{kl})_i = \bigoplus_p \delta_{pk} v_{pl}$.

TABLE 2.1. EDMD vs modified EDMD for Γ-equivariant systems. $|\Gamma|$ is the order of Γ. The irreducible representations of Γ are indexed by p and are d_p-dimensional.

If the system is Γ-equivariant and $\Gamma \subset \Sigma$, functions belonging to particular isotypic components of Σ are not preserved by the action of K. In the case of symmetric trajectories, that can provide information on what the true symmetries of the system are.

A simple case corresponds to $\Sigma = \Sigma_0 \times \Gamma$. In this case, every action of Σ_0 commutes with every action of Γ. Each isotypic component of $\mathcal{F}$ with respect to Σ can be expressed as $\mathcal{F}_{pq} = \mathcal{F}^p_{\Sigma_0} \cap (\mathcal{F}_\Gamma)^q$, where $\mathcal{F}^p_{\Sigma_0}$ denotes the pth isotypic component of Σ_0. In this case, the off-diagonal blocks corresponding to interactions between isotypic components $\mathcal{F}_{p_1 q_1}$ and $\mathcal{F}_{p_2 q_2}$ are zero if $q_1 = q_2$, and generally nonzero otherwise. For instance, if a network of three Duffing oscillators similar to those

discussed in, e.g., example 2.4.2, but has no permutation symmetry and $\Sigma = Z_2 \times D_3$, with the action of Z_2 being a sign flip in nodal dynamics, the isotypic components corresponding to these Z_2 symmetries will not interact with each other, resulting in two blocks in K.

Next, we consider a more general case. We denote the pth isotypic component of $\mathcal{F}$ with respect to the symmetry group Σ by $\mathcal{F}^p_\Sigma$. We note that if the following conditions hold:

$$\mathcal{F}^p_\Sigma \cap \mathcal{F}^{q_1}_\Gamma \neq \varnothing, \tag{2.44}$$

$$\mathcal{F}^p_\Sigma \cap \mathcal{F}^{q_2}_\Gamma \neq \varnothing, \tag{2.45}$$

where q_1 and q_2 index different isotypic components of Γ, then the off-diagonal blocks of K corresponding to interactions between those components are generally nonzero.

The condition for $\mathcal{F}^p_\Sigma \cap \mathcal{F}^q_\Gamma \neq \varnothing$ is equivalent to:

$$\mathcal{P}^p_\Sigma \circ (\mathcal{P}^q_\Gamma \circ f) \neq 0, \tag{2.46}$$

where f is an arbitrary function, and $\mathcal{P}^p_\Sigma$ denotes the projection operator onto the pth isotypic component with respect to the symmetry group Σ.

$$\mathcal{P}^p_\Sigma \circ (\mathcal{P}^q_\Gamma \circ f) = \sum_{\sigma\in\Sigma} \chi_p(\sigma)^* \sigma_\rho \circ \sum_{\gamma\in\Gamma} \chi_q(\gamma)^* \gamma_\rho \circ f = \sum_{\sigma\in\Sigma,\gamma\in\Gamma} \chi_p(\sigma)^* \chi_q(\gamma)^* (\sigma_\rho \gamma_\rho) \circ f. \tag{2.47}$$

Let H be the set of *left cosets* of Γ in Σ (defined as $H = \Sigma/\Gamma = \{\sigma\Gamma : \sigma \in \Sigma\}$, where $\sigma\Gamma = \{\sigma\gamma : \gamma \in \Gamma\}$ [**50**]). Thus, the condition of eq. (2.46) holds if for all $h \in H$:

$$\sum_{\gamma\in\Gamma} \chi^*_p(h\gamma^{-1}) \chi^*_q(\gamma) = 0 \tag{2.48}$$

Using eq. (2.48), the structure of Γ can be determined given the structure of K and Σ used in the calculation. Characters of irreducible representations are available for small order symmetry groups, and scaling up to larger order is possible using computational group theory software. Below is an example for the subgroups of a dihedral group D_3.

EXAMPLE 2.4.3. *Coupled Duffing oscillators: $(Z_2 \times Z_2)$- or $(Z_2 \times Z_3)$-equivariant system with $Z_2 \times D_3$ basis functions.*

We consider different coupling schemes of networks of 3 Duffing oscillators shown in fig. 2.1b and 2.1c. We first note that the Z_2 symmetry generated by a sign flip is still present in the system for both cases, so two non-interacting blocks corresponding to irreducible representations of that group with respect to that action are still present. Now we focus on the structure of K within each of these non-interacting blocks.

First, let the function dictionary symmetry be $\Sigma = D_3 = \langle r, \kappa | r^3 = \kappa^2 = e, \kappa r \kappa = r^{-1} \rangle$ and the true symmetry of the system be $\Gamma = Z_3 = \langle r | r^3 = e \rangle$, where r_{D_3} and r_{Z_3} have the same action. The isotypic component decomposition of D_3 is defined in example 2.4.2 and can be written as $\mathcal{F} = \mathcal{F}_{tr,D_3} \oplus \mathcal{F}_{sign,D_3} \oplus \mathcal{F}_{st,D_3}$. The isotypic component decomposition of Z_3 is defined as $\mathcal{F} = \mathcal{F}_{tr,Z_3} \oplus \mathcal{F}_{\omega,Z_3} \oplus \mathcal{F}_{\omega^2,Z_3}$ (Z_3 has 3 1-dimensional irreducible representations with $\chi_{tr}(r) = 1$, $\chi_\omega(r) = \omega$, $\chi_{\omega^2}(r) = \omega^2$). We note that:

- $\mathcal{F}_{tr,Z_3} \cap \mathcal{F}_{tr,D_3} \neq \varnothing$

  Functions belonging to $\mathcal{F}_{tr,Z_3}$ satisfy the following condition:

  $\mathcal{F}_{tr,Z_3} = \{f : f(\boldsymbol{x}_3, \boldsymbol{x}_1, \boldsymbol{x}_2) = f(\boldsymbol{x}_1, \boldsymbol{x}_2, \boldsymbol{x}_3)\}$

  Functions belonging to $\mathcal{F}_{tr,D_3}$ satisfy the following conditions:

  $\mathcal{F}_{tr,D_3} = \{f : f(\boldsymbol{x}_3, \boldsymbol{x}_1, \boldsymbol{x}_2) = f(\boldsymbol{x}_1, \boldsymbol{x}_2, \boldsymbol{x}_3), f(\boldsymbol{x}_1, \boldsymbol{x}_3, \boldsymbol{x}_2) = f(\boldsymbol{x}_1, \boldsymbol{x}_2, \boldsymbol{x}_3)\}$

  Thus, $\mathcal{F}_{tr,Z_3} \cap \mathcal{F}_{tr,D_3} = \mathcal{F}_{tr,D_3}$
- $\mathcal{F}_{tr,Z_3} \cap \mathcal{F}_{sign,D_3} \neq \varnothing$

  This can be shown in a similar fashion.
- $(\mathcal{F}_{\omega,Z_3} \cup \mathcal{F}_{\omega^2,Z_3}) \cap \mathcal{F}_{st,D_3} = \mathcal{F}_{st,D_3}$

  Functions belonging to $\mathcal{F}_{\omega/\omega^2,Z_3}$ satisfy the following condition:

  $\mathcal{F}_{\omega,Z_3} = \{f : f(\boldsymbol{x}_3, \boldsymbol{x}_1, \boldsymbol{x}_2) = \omega f(\boldsymbol{x}_1, \boldsymbol{x}_2, \boldsymbol{x}_3)\}$

  $\mathcal{F}_{\omega^2,Z_3} = \{f : f(\boldsymbol{x}_3, \boldsymbol{x}_1, \boldsymbol{x}_2) = \omega^2 f(\boldsymbol{x}_1, \boldsymbol{x}_2, \boldsymbol{x}_3)\}$

  Functions belonging to $\mathcal{F}_{st,D_3}$ satisfy the following conditions:

  $\mathcal{F}_{st,D_3} = \{f_1, f_2 : f_1(\boldsymbol{x}_3, \boldsymbol{x}_1, \boldsymbol{x}_2) = \omega f_1(\boldsymbol{x}_1, \boldsymbol{x}_2, \boldsymbol{x}_3)$

  $f_2(\boldsymbol{x}_3, \boldsymbol{x}_1, \boldsymbol{x}_2) = \omega^2 f_2(\boldsymbol{x}_1, \boldsymbol{x}_2, \boldsymbol{x}_3)$

  $f_1(\boldsymbol{x}_1, \boldsymbol{x}_3, \boldsymbol{x}_2) = f_2(\boldsymbol{x}_1, \boldsymbol{x}_2, \boldsymbol{x}_3)$

  $f_2(\boldsymbol{x}_1, \boldsymbol{x}_3, \boldsymbol{x}_2) = f_1(\boldsymbol{x}_1, \boldsymbol{x}_2, \boldsymbol{x}_3)\}$

  Thus, $(\mathcal{F}_{\omega,Z_3} \cup \mathcal{F}_{\omega^2,Z_3}) \cap \mathcal{F}_{st,D_3} = \mathcal{F}_{st,D_3}$

Thus, the off block-diagonal structure of K is defined by:

- $K\mathcal{F}_{tr,D_3} \cap \mathcal{F}_{sign,D_3} \neq \varnothing$

  To see that is the case, we need to refer back to conditions in eq. (2.44) *and eq.* (2.45)*. Since the intersections of both $\mathcal{F}_{tr,D_3}$ and $\mathcal{F}_{sign,D_3}$ with $\mathcal{F}_{tr,Z_3}$ are nonzero, the intersection of the components produces non-zero elements in K.*

- $K\mathcal{F}_{sign,D_3} \cap \mathcal{F}_{tr,D_3} \neq \varnothing$

  This can be shown in a similar fashion.

- *other off-diagonal blocks are zeros*

  For instance, since the intersections of both $\mathcal{F}_{tr,D_3}$ and $\mathcal{F}_{st,D_3}$ with no specific isotypic component of Z_3 are ***simultaneously*** *nonzero, $K\mathcal{F}_{tr,D_3} \cap \mathcal{F}_{st,D_3} = \varnothing$ and $K\mathcal{F}_{st,D_3} \cap \mathcal{F}_{tr,D_3} = \varnothing$, thus corresponding to blocks of zeros in K.*

This structure is illustrated in fig. 2.3b and differs from that in fig. 2.3a.

Now, let $\Sigma = D_3$ and $\Gamma = Z_2$. Here, $Z_2 = \langle e, \kappa | \kappa^2 = e \rangle$, and κ_{D_3} and κ_{Z_2} have the same action. The isotypic component decomposition of Z_2 is defined as $\mathcal{F} = \mathcal{F}_{tr,Z_2} \oplus \mathcal{F}_{sign,Z_2}$.

We note that:

- $\mathcal{F}_{tr,Z_2} \cap \mathcal{F}_{tr,D_3} \neq \varnothing$
- $\mathcal{F}_{tr,Z_2} \cap \mathcal{F}_{st,D_3} \neq \varnothing$
- $\mathcal{F}_{sign,Z_2} \cap \mathcal{F}_{sign,D_3} \neq \varnothing$
- $\mathcal{F}_{sign,Z_2} \cap \mathcal{F}_{st,D_3} \neq \varnothing$

Additionally:

- $\mathcal{F}_{tr,Z_2} \cap \mathcal{F}_{sign,D_3} = \varnothing$
- $\mathcal{F}_{sign,Z_2} \cap \mathcal{F}_{tr,D_3} = \varnothing$

Thus, the off block-diagonal structure of K is defined by:

- $K\mathcal{F}_{tr,D_3} \cap \mathcal{F}_{sign,D_3} = \varnothing$
- *other off-diagonal blocks corresponding to interactions between node permutation isotypic components are generally nonzero*

This structure is illustrated on fig. 2.3c and differs from that on fig. 2.3a and fig. 2.3b.

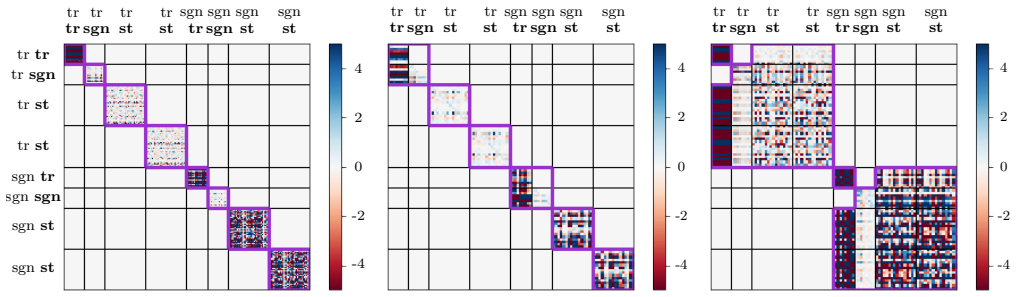

(a) K if $\Sigma = \Gamma = D_3$ (b) K if $\Sigma = D_3$, $\Gamma = Z_3$ (c) K if $\Sigma = D_3$, $\Gamma = Z_2$

FIGURE 2.3. Structure of K with basis functions belonging to the isotypic components of $\Sigma = D_3$ for different underlying symmetries of the system. The labels above and to the left correspond to the isotypic components interacting in each block. Two labels are needed to index over D_3 (**bold font**) and Z_2 (standard font).

This example shows that the structure of the approximation K with maximal symmetries assumed provided information about the actual underlying symmetries of the system. In this specific example, we can see that any off-diagonal block can be used as an indicator of whether a symmetry subgroup Z_2 or Z_3 is present, as seen in fig. 2.3b and fig. 2.3c.

In summary, the symmetries of the system can be detected from the structure of the Koopman operator approximation matrix. This allows using the same method both to detect the symmetries of dynamical systems from data and to obtain their Koopman operator approximation. However, we also note that there are multiple other methods to detect the symmetries of dynamical systems, for instance, this work can be related to symmetry detectives [**15**]. Additionally, in many cases we do not expect perfect symmetries to be present in data, as discussed in the next subsection. Thus, it would be useful to see how these imperfections affect the results in order to be able to apply the symmetry considerations in a more practical setting.

2.4.3. Towards realistic systems. In this manuscript, we provide a general approach for dimensionality reduction in the calculation of Koopman operator approximations by exploiting the underlying symmetries present in both the system's dynamics and system's structure. The exact scaling achieved by the reduction depends on the structure of the symmetry group of the dynamical system, specifically, the number of irreducible representations of the symmetry group and the dimensionality of these irreducible representations.

The results outlined in this manuscript, similar to most of the other literature related to dynamical systems with symmetries, are immediately applicable in the case of the existence of exact symmetries in nonlinear dynamics. That is the case when the system is completely deterministic and the initial conditions respect the symmetries of the system. If the symmetries of the system are known and the available trajectories are deterministic, it is always possible to reconstruct the trajectories that are related via the symmetry group of the system. Then, a full set of trajectories respecting the symmetries of the system can be used to approximate the Koopman operator and its eigendecomposition.

However, in many systems, that information is not necessarily available ahead of time and the symmetries are not present in data, even if the initial conditions are symmetric, because of the presence of noise in the system. Some of the examples of not fully symmetric data include the following cases and their combinations:

- Deterministic systems with measurement noise. DMD for systems with measurement noise and possible ways to correct for it are presented in Ref. [**36**]. It is shown in section 2.6.6 that in this case the expected values of off-diagonal elements of K computed using the EDMD are zero, so the block decomposition may still be applicable.
- Stochastic systems with symmetric initial conditions and process noise. DMD applied to the systems with process noise is studied, for instance, in Ref. [**14**].
- Systems with imperfect symmetries due to sampling and unknown underlying symmetries.
- Systems with imperfect symmetries in dynamics (e.g. slight parameter mismatch).

All these cases require separate treatment, and whether the isotypic component decomposition is still useful in computing the Koopman operator approximation will vary depending on specific characteristics of the data available from the system, such as the strength of the noise or the trajectory sampling characteristics.

2.5. Conclusion

In this manuscript, we apply tools from group theory and representation theory to study the structure of the Koopman operator for equivariant dynamical systems. This approach can be applied to systems with permutation symmetries (e.g. networks symmetric under node permutations

where the information about the symmetries is contained in the adjacency matrix), systems with intrinsic dynamical symmetries, and systems with both types of symmetries present. We find that the operator itself and its approximations can be block diagonalized using a symmetry basis that respects the isotypic component structure related to the underlying symmetry group and the actions of its elements. For the approximation matrix to be exactly block diagonal, the data must respect the symmetries of the system. That can be readily accomplished if the underlying symmetry is known ahead of time (e.g., the topology of the network is known). Symmetry considerations are applicable to both EDMD and kernel DMD, which means they become useful both in the regime when the number of observables is much larger than that of measurements and vice versa.

Moving forward, it would be possible to extend these results. For instance, a natural next step would be to investigate the effect of noise and imperfect symmetries on the Koopman operator approximations for equivariant or nearly equivariant dynamical systems in more detail. It would also be useful to apply the symmetry considerations beyond the range of applicability of EDMD. In that case, symmetry considerations can be used to study, for instance, systems with continuous Koopman spectra. Other future directions include relating our results to existing literature on equivariant bifurcation theory, stability analysis, and continuous symmetries.

2.6. Appendices

2.6.1. Block diagonalization of isotypic components obtained from d_p-dimensional irreducible representations. We show that d-dimensional irreducible representations of Γ yield identical blocks of $\mathcal{K}$ in the isotypic component basis obtained using the unitary irreducible representations of Γ.

Let the function space be decomposed into isotypic components according to the actions of the symmetry group Γ of order $|\Gamma|$, $\gamma_\rho \in \Gamma_\rho$: $\mathcal{F} = \mathcal{F}_1 \oplus ... \oplus \mathcal{F}_N$, where N is the number of irreducible representations of Γ. Let $\mathcal{F}_p$ be one of these isotypic components with a corresponding *unitary* irreducible representation with elements $R_p(\gamma)$ corresponding to $\gamma \in \Gamma$, and let d_p be the dimensionality of that representation.

The projection operator is defined as:

$$\mathcal{P}^p_{mn} = \frac{d_p}{|\Gamma|} \sum_{\gamma \in \Gamma} [R_p(\gamma)]^*_{mn} \gamma_\rho. \tag{2.49}$$

It acts on $f \in \mathcal{F}$ to produce sets of projected functions according to:

$$\xi^p_{mn} = \mathcal{P}^p_{mn} \circ f. \tag{2.50}$$

We already know that $\mathcal{K}\xi^p_{mn} = h_p$, where $h_p \in \mathcal{F}_p$. The subspace $\mathcal{F}_p$ can be decomposed into d_p components $\mathcal{F}_p = \mathcal{F}_{p,1} \oplus ... \oplus \mathcal{F}_{p,d_p}$, where $\mathcal{F}_{p,m} = \{g | g = \mathcal{P}_{mn} \circ f,\ f \in \mathcal{F}, n = 1, ..., d_p\}$. This is a well-defined decomposition since $\langle \mathcal{P}^p_{mn} f, \mathcal{P}^p_{kl} h \rangle = \langle f, \mathcal{P}^p_{nm} \mathcal{P}^p_{kl} h \rangle = \langle f, \delta_{mk} \mathcal{P}^p_{nl} h \rangle$ [**33**] can be nonzero only when $m = k$.

We want to show that $\mathcal{K}\xi^p_{mn} \in \mathcal{F}_{p,m}$ (also true for any linear operator that commutes with the action of the symmetry group). Since the operator commutes with the actions of the group:

$$\mathcal{K}\mathcal{P}^p_{mn} \circ f = \mathcal{P}^p_{mn} \mathcal{K} \circ f = \mathcal{P}^p_{mn} \circ h \in \mathcal{F}_{p,m}. \tag{2.51}$$

Here, $\mathcal{K} \circ f \equiv h$.

Let $f_\Gamma = \{\gamma \circ f | \gamma \in \Gamma\}$. Any set of linearly independent functions that span f_Γ can be transformed into a symmetry respecting basis obtained by calculating all the projections $\mathcal{P}^p_{mn} \circ f_\gamma$, where $f_\gamma \in f_\Gamma$. That corresponds to a block diagonal form of the Koopman operator.

We've already shown that K, the approximation of $\mathcal{K}$, also commutes with the actions of the elements of Γ for Γ-equivariant dynamical systems with Γ-equivariant data. Thus, we can obtain an observable dictionary that block diagonalizes K into $|\Gamma|$ blocks, where each d_p-dimensional irreducible representation results in d_p $d_p \times d_p$-dimensional blocks.

Additionally, suppose $\mathcal{K}\mathcal{P}^p_{mn} \circ f = h$, then $\mathcal{K}\mathcal{P}^p_{kn} \circ f = \mathcal{P}^p_{km}\mathcal{K}\mathcal{P}^p_{mn} \circ f = \mathcal{P}^p_{km} \circ h$. This gives us the relation between blocks in $\mathcal{K}$ corresponding to the same irreducible representation p. In context of the approximation K, it means that we get that $K_{p,i}$ (blocks corresponding to $\psi \in \mathcal{F}_{p,i}$) are equal for all i (for data respecting the symmetries of the system and a proper ordering of basis functions).

2.6.2. Commutativity of K and γ_ρ acting in function space. We show that G and G^+ ($^+$ denotes the Moore-Penrose pseudoinverse) commute. We note that G is a Hermitian matrix since:

$$G^* = \left(\sum_m \Psi^*(x_m)\Psi(x_m) \right)^* = \sum_m \Psi^*(x_m)\Psi(x_m) = G \tag{2.52}$$

Thus, G is also normal, i.e. $GG^* = G^*G$. We show that if G is normal, $GG^+ = G^+G$.

Two of the criteria that define the Moore-Penrose pseudoinverse [**116**] state that $G^+ = G^+GG^+$ and $(GG^+)^* = GG^+$. It follows that the following relation holds: $G^+ = G^+(GG^+)^* = G^+(G^+)^*G^*$. Using that relation [**19**] and commutativity of $^+$ and * operations, we obtain:

$$\begin{aligned} G^+G = G^+(G^+)^*G^*G = (G^+)^*G^+GG^* \\ = (G^+)^*G^* = (G^+(G^+)^*G^*)^*G^* = GG^+(G^+)^*G^* = GG^+. \end{aligned} \tag{2.53}$$

Since the action of γ commutes with A and G, and since G commutes with G^+, the action of γ commutes with $K = G^+A$. which is a Koopman operator approximation.

2.6.3. Requirements of symmetrizing the data set. We note that the off-diagonal blocks of the approximation matrix K are only zero if the symmetries are present in the data. The non-diagonal elements can be set to zero explicitly, making computations more efficient.

Moreover, if the symmetries are known a priori, a fully symmetrized data set is not necessary to obtain an approximation of the diagonal block elements of K. Suppose we have a dictionary of basis functions belonging to a particular isotypic component with respect to the action of the full symmetry group Γ. We label that component by p, and the corresponding unitary irreducible representation by $R_p(\gamma)$. We then define $R'_p(\gamma) \equiv R_p(\gamma) \otimes I_{n\times n}$, where n is the number of functions in the pth isotypic component. By definition of isotypic components, even for unsymmetrized data it is the case that:

$$\Xi^*(\gamma x_m)\Xi(\gamma y_m) = (\Xi(x_m)R'_p(\gamma))^*(\Xi(y_m)R'_p(\gamma)) = (R'_p(\gamma))^*\Xi^*(x_m)^*\Xi(y_m)R'_p(\gamma) \tag{2.54}$$

If $R(\gamma)$ is a diagonal matrix:

$$\Xi^*(\gamma x_m)\Xi(\gamma y_m) = \Xi^*(x_m)\Xi(y_m). \tag{2.55}$$

In case of one-dimensional irreducible representations, it is not necessary to use reflected data to produce the blocks of K. For instance, as in example 2.4.2, where one of the generators of D_3, κ, corresponds to a non-diagonal matrix $R(\kappa)$. In that case:

$$\sum_{\gamma}\sum_{m} \Xi^*(\gamma x_m)\Xi(\gamma y_m) = 3(\Xi^*(x_m)\Xi(y_m) + \Xi^*(\kappa x_m)\Xi(\kappa y_m)). \tag{2.56}$$

This demonstrates that the method is data-efficient and sets up requirements on the symmetry properties of data.

2.6.4. Change of basis and the EDMD approximation. We show that rotating the observable dictionary preserves the symmetries of the reconstructed trajectories.

Suppose we have a basis consisting of dictionary functions $\mathcal{D}_\psi$ and a dictionary $\mathcal{D}_\xi$ obtained by $\Xi = T\Psi$. Let $\Psi(t) \equiv (\psi_1(x(t))\ \psi_N(x(t)))^T$ and $\Xi(t) \equiv (\xi_1(x(t))\ \xi_N(x(t)))^T$. We show that rotating the dictionary function vector by the projection matrix T does not affect the trajectory reconstruction:

$$\Psi_{t+1} = K_\psi \Psi_t, \quad \Xi_t = T\Psi_t \quad \Xi_{t+1} = K_\psi T\Psi_t = TK_\psi\Psi_t = T\Psi_{t+1}. \tag{2.57}$$

Next, we show that the state reconstruction preserves the symmetries of the system. Let P be the action of the symmetry group on the basis functions Ψ. We aim to show that if $\Psi_{t+1} = K\Psi_t$, then $P\Psi_{t+1} = KP\Psi_t$. It follows directly from the fact that K and P commute:

$$P\Psi_{t+1} = PK\Psi_t = KP\Psi_t. \tag{2.58}$$

Thus, the trajectories of basis functions reconstructed using the EDMD approximation are Γ-equivariant, just like the original system. In particular, this is true in case of the evolution of the full state observable.

2.6.5. Applicability to kernel methods. Kernel DMD introduced in Ref. [**158**] is a variant of approximating the Koopman operator matrix most efficient when the number of measurement

points is much smaller than the number of basis functions. Kernel DMD relies on evaluating $\hat{G}$ and $\hat{A}$ using the kernel method. Their elements can be found by indirectly evaluating the inner products in the basis function space: $k(x_m, y_n) = \Psi(x_m)\Psi(y_n)^*$ (e.g., if k is a polynomial kernel, $k(x, y) = (1 + xy^T)^\alpha$). We note that $k(\gamma x, \gamma y) = k(x, y)$ due to the properties of inner products.

In kernel DMD, $\hat{G}_{ij} = k(x_i, x_j)$ and $\hat{A}_{ij} = k(x_i, y_j)$. The eigendecomposition of $\hat{G} = Q\Sigma^2 Q^T$ is then used to find the matrix $\hat{K}$ and use it in computing the eigendecomposition of the Koopman operator approximation matrix K:

$$\hat{K} = (\Sigma^+ Q^T)\hat{A}(Q\Sigma^+). \tag{2.59}$$

Again, we pick a particular order of group elements similarly to eq. (2.29):

$$\Psi_x = \begin{pmatrix} \Psi(\gamma_1 \mathbf{x}) \\ \vdots \\ \Psi(\gamma_{|\Gamma|}\mathbf{x}) \end{pmatrix}, \quad \text{where } \Psi(\mathbf{x}) = \begin{pmatrix} \Psi_1(x_1) & ... & \Psi_N(x_1) \\ \vdots & \ddots & \vdots \\ \Psi_1(x_{M/|\Gamma|}) & ... & \Psi_N(x_{M/|\Gamma|}) \end{pmatrix} \tag{2.60}$$

We also construct a permutation representation of the group with elements denoted by P_{γ_i} as defined in eq. (2.30).

By Cayley's theorem, such permutations form a group isomorphic to Γ. Determining the actions P_{γ_i} of the group generators is sufficient to find the actions of all the group elements. Let $\boldsymbol{P}_{\gamma_k} = P_{\gamma_k} \otimes I_{n\times n}$. We note that $(\boldsymbol{P}_{\gamma_k})^* = (\boldsymbol{P}_{\gamma_k})^{-1}$. It can be shown that:

$$\boldsymbol{P}_{\gamma_i}\hat{G} = \hat{G}\boldsymbol{P}_{\gamma_i}, \ \boldsymbol{P}_{\gamma_i}\hat{A} = \hat{A}\boldsymbol{P}_{\gamma_i}. \tag{2.61}$$

We do so for $\hat{A}$, and the proof for $\hat{G}$ is equivalent. We find that:

$$(\boldsymbol{P}_{\gamma_i}\hat{A})_{kl} = \hat{A}_{pl} = k(x_p, y_l), \ \gamma_p = \gamma_i\gamma_k, \quad (\hat{A}\boldsymbol{P}_{\gamma_i})_{kl} = \hat{A}_{kq} = k(x_k, y_q), \ \gamma_q = \gamma_i^{-1}\gamma_l. \tag{2.62}$$

And finally, $k(x_p, y_l) = k(\gamma_i x_k, \gamma_i y_q) = k(x_k, y_q)$.

Since the relation 2.61 holds, the same reasoning can be applied to block diagonalize the matrix $\hat{K}$. It is sufficient to apply the projection operator [**143**]:

$$\mathcal{P}^p_{mn} = \frac{d_p}{|\Gamma|}\sum_{\gamma\in\Gamma}[R_p(\gamma)]^*_{mn}P_{\gamma_i}. \tag{2.63}$$

Standard kernel DMD	Kernel DMD for Γ-equivariant systems
• Pick a dictionary of N observables • Evaluate the kernel functions at data points x_i and y_i • Evaluate the entries of $\hat{G}, \hat{A}$: M^2 elements • Obtain $\hat{G}^+$: $M \times M$ matrix • Find $\hat{K} = (\Sigma^+ Q^T)\hat{A}(Q\Sigma^+)$: $M \times M$ matrices • Find the eigendecomposition of $\hat{K}$: $M \times M$ matrix	• Pick a dictionary of N observables • Identify the symmetry Γ of the system, find the irreducible representations of Γ • Change the basis to a Γ-symmetric basis using eq. (2.30) and eq. (2.63) • Evaluate the observables at data points x_i and y_i, add trajectories to reflect the symmetries if necessary • To obtain the blocks $\hat{K}_{pq}$ of $\hat{K}$ (each isotypic component corresponds to d_p blocks), for each p: – Evaluate the entries of $\hat{G}_{p1}, \hat{A}_{p1}$: $(M_p/d_p)^2$ elements – Obtain $\hat{G}^+_{p1}$: $(M_p/d_p) \times (M_p/d_p)$ matrix – Find $\hat{K}_{p1} = \hat{G}^+_{p1}\hat{A}_{p1}$: $(M_p/d_p) \times (M_p/d_p)$ matrices – Find the eigendecomposition of $\hat{K}_{p_1}$: $(M_p/d_p) \times (M_p/d_p)$ matrix – The other $\hat{K}_{pq}$ blocks equal to $\hat{K}_{p1}$ • $\hat{K} = \bigoplus_p \bigoplus_{q=1}^{d_p} \hat{K}_{pq}$. Its eigenvalues are the eigenvalues of $\hat{K}_p$, and its eigenvectors only have M_p nonzero elements. Mathematically, eigenvectors v_{kl} of K are of the form $(v_{kl})_i = \bigoplus_p \delta_{pk} v_{pl}$.

TABLE 2.2. kernel DMD vs modified kernel DMD for Γ-equivariant systems. $|\Gamma|$ is the order of Γ. The irreducible representations of Γ are indexed by p and are d_p-dimensional. Here, M be the number of data points used by the algorithm, and $\{(x_m, y_m)\}$ respect the symmetries of the system.

This projection operator is analogous to the one introduced in equation 2.25, except the symmetry group in this case acts by permuting the group elements.

We can apply the singular value decomposition of $\mathcal{P}$ to obtain the basis for the projection subspaces of irreducible representations (isotypic components). We form the transformation matrix T by finding the singular value decomposition (SVD) and stacking its eigenvectors as rows of T such that $\boldsymbol{T} = T \otimes I_{n \times n}$.

Similarly to EDMD, the isotypic component basis simplifies calculating the approximations of $\hat{K}$.

$$\begin{aligned} \hat{A}_D = \bigoplus_p \bigoplus_q \hat{A}_{pq},\ \hat{G}_D = \bigoplus_p \bigoplus_q \hat{G}_{pq} = \bigoplus_p \bigoplus_q Q_{pq}\Sigma_{pq}^2 Q_{pq}^T, \\ \hat{K}_D = \bigoplus_p \bigoplus_q (\Sigma_{pq}^+ Q_{pq}^T)\hat{A}_{pq}(Q_{pq}\Sigma_{pq}^+). \end{aligned} \tag{2.64}$$

The modification is summarized in table 2.2.

Finally, the approximations of Koopman eigenvalues, eigenfunctions, and eigenmodes can be calculated using K_D, as shown in Ref. [**158**].

2.6.6. Deterministic systems with sensor noise. Transfer operators with process and measurement noise were also studied in Ref. [**135**]. Characterizing and correcting for the effect of sensor noise in DMD is discussed in Ref. [**36**]. We need to extend the results to EDMD to quantify the effect of sensor noise on the structure of the matrix K. The main modification that needs to be made is the consideration of the effect of the noise in measuring X and Y on Ψ_x and Ψ_y.

Let X and Y be matrices analogous to Ψ_x and Ψ_y corresponding to the full-state observable evaluated at discrete time steps. We denote the sensor noise matrices by N_x and N_y, so that the measured X_n and Y_n can be found from $X_n = X + N_x$ and $Y_n = Y + N_y$. We assume that the noise distributions respect the symmetries of the system, which might be the case, for instance, for symmetric networks. Moreover, we assume that the noise is state-independent.

We can form vectors Ψ_{xn} and Ψ_{yn} that can be used to find the approximation K using EDMD:

$$K_n = \Psi_{xn}^+ \Psi_{yn}. \tag{2.65}$$

Here, $(\Psi_{xn})_{ij} = \psi_j((X_n)_i)$, $(\Psi_{yn})_{ij} = \psi_j((Y_n)_i)$, and $N_{\Psi,x}$ and $N_{\Psi,y}$ correspond to noise matrices obtained as:

$$(N_{\Psi,x})_{ij} = \psi_j(X_i + N_{x,i}) - \psi_j(X_i). \tag{2.66}$$

We aim to show that $\mathbb{E}(PK_n) = \mathbb{E}(K_nP)$, meaning that the expected value of the Koopman operator K_n commutes with the permutation matrix corresponding to an element of the symmetry group. If that is the case, then the expected values of the off-block-diagonal elements of K_n in a

symmetry adapted basis as defined in eq. (2.27) are zero. To do that, we can express K_n as:

$$\begin{aligned} K_n = \Psi_{xn}^{+}\Psi_{yn} = (\Psi_x + N_{\Psi,x})^{+}(\Psi_y + N_{\Psi,y}) \\ = ((\Psi_x + N_{\Psi,x})^{*}(\Psi_x + N_{\Psi,x}))^{+}(\Psi_x + N_{\Psi,x})^{*}(\Psi_y + N_{\Psi,y}) \\ = (\Psi_x^{*}\Psi_x + \Psi_x^{*}N_{\Psi,x} + N_{\Psi,x}^{*}\Psi_x + N_{\Psi,x}^{*}N_{\Psi,x})^{+} \\ (\Psi_x^{*}\Psi_y + \Psi_x^{*}N_{\Psi,y} + N_{\Psi,x}^{*}\Psi_y + N_{\Psi,x}^{*}N_{\Psi,y}). \end{aligned} \tag{2.67}$$

If the inverse of the first term exists, it can be expanded into the Taylor series with terms of the form below in a weak noise limit. We need to show that:

$$\boldsymbol{P}_{\gamma_k}\mathbb{E}(M_1^{*}M_2...M_{n-1}^{*}M_n) = \mathbb{E}(M_1^{*}M_2...M_{n-1}^{*}M_n)\boldsymbol{P}_{\gamma_k} \tag{2.68}$$

Here, the matrices M_i are selected from $N_{\Psi,x/y}$ and $\Psi_{x/y}$. That follows directly from:

$$\begin{aligned} \mathbb{E}((M_1\boldsymbol{P}_{\gamma_k})^{*}(M_2\boldsymbol{P}_{\gamma_k})...(M_{n-1}\boldsymbol{P}_{\gamma_k})^{*}(M_n\boldsymbol{P}_{\gamma_k})) \\ = \boldsymbol{P}_{\gamma_k}^{-1}\mathbb{E}(M_1^{*}M_2...M_{n-1}^{*}M_n)\boldsymbol{P}_{\gamma_k} = \mathbb{E}(M_1M_2^{*}...M_{n-1}M_n^{*}) \end{aligned} \tag{2.69}$$

Thus, the expected values of the off-block-diagonal elements of K_n are zero in the isotypic component basis.

CHAPTER 3

Decoupled synchronized states in networks of linearly coupled limit cycle oscillators

Published as Salova, A., & D'Souza, R. M. (2020). Decoupled synchronized states in networks of linearly coupled limit cycle oscillators. Physical Review Research, 2(4), 043261.

Networks of limit cycle oscillators can show intricate patterns of synchronization such as splay states and cluster synchronization. Here we analyze dynamical states that display a continuum of seemingly independent splay clusters. Each splay cluster is a block splay state consisting of subclusters of fully synchronized nodes with uniform amplitudes. Phases of nodes within a splay cluster are equally spaced, but nodes in different splay clusters have an arbitrary phase difference that can be fixed or evolve linearly in time. Such coexisting splay clusters form a decoupled state in that the dynamical equations become effectively decoupled between oscillators that can be physically coupled. We provide the conditions that allow the existence of particular decoupled states by using the eigendecomposition of the coupling matrix. We also provide an alternate approach using the external equitable partition and orbital partition considerations combined with symmetry groupoid formalism to develop an algorithm to search for admissible decoupled states. Unlike previous studies, our approach is applicable when existence does not follow from symmetries alone and also illustrates the differences between adjacency and Laplacian coupling. We show that the decoupled state can be linearly stable for a substantial range of parameters using a simple eight-node cube network and its modifications as an example. We also demonstrate how the linear stability analysis of decoupled states can be simplified by taking into account the symmetries of the Jacobian matrix. Some network structures can support multiple decoupled patterns. To illustrate

that, we show the variety of qualitatively different decoupled states that can arise on two-dimensional square and hexagonal lattices.

3.1. Introduction

Networks of oscillators are pervasive in the world around us, from electric power grids to brain networks. Thus understanding the coordinated, dynamical patterns of oscillation that can spontaneously arise in such networks is of broad interest. Coupled oscillators provide a useful model to study many biological [**8**, **32**, **60**, **146**] and engineered [**112**, **122**] systems. Full synchronization, where each node in the network follows the exact same trajectory in phase space, is the most basic form and widely observed [**44**, **83**, **144**]. By considering the details of the network structure and dynamics, more intricate forms of synchronization can be predicted, such as cluster synchronization [**18**, **54**, **65**, **66**, **99**, **114**, **131**, **139**], splay states [**145**, **164**], chimera states [**1**, **7**, **31**, **161**] and fully asynchronous states. Here we focus on intriguing states of synchronization that have been largely unstudied. The states have intricate synchronization patterns of seemingly independent (but interwoven) sub-clusters that arise because the equations of motion lead to the cancelling out of terms of often physically coupled oscillators. Hence such a state was called "decoupled" when first discovered [**3**, **4**]. Such a state appears naturally in analysis of symmetric networks of phase oscillators with homogeneous parameters [**10**, **26**], and was only recently achieved in experiment for a ring of phase-amplitude oscillators [**97**], demonstrating emergent long-range order that is a consequence of decoupling. But the range of decoupled states that can be supported on any arbitrary network topology has not yet been addressed, likewise the stability properties of decoupled states are largely unexplored.

Here we focus on decoupled states in networks of linearly coupled phase shift invariant limit cycle oscillators (e.g. Stuart-Landau oscillators). Their phase shift symmetry combined with linear coupling provides an opportunity for diverse decoupled states to exist. Previously, the decoupled state has been analyzed from the symmetry perspective [**4**, **10**]. Here we show that the sufficient conditions on the network topology that allow decoupling can not be derived from the symmetries alone, echoing the results from groupoid formalism [**51**, **142**] and recent cluster synchronization literature [**131**, **134**, **139**]. This allows us to create an iterative algorithm to obtain allowed patterns

of decoupling from network structure in the distinct cases of adjacency and Laplacian coupling. We use the notions of (external) equitable partitions [**131**] and orbital partitions [**31**, **114**] which together take into account the balanced equivalence relations of the network as well as the symmetries of the associated quotient network. All nodes within each cell of the equitable partition are fully synchronized, and detailed patterns of phase shift synchronization can be obtained from the symmetries of the quotient network [**142**].

Additionally, we show how to use the eigendecomposition of the coupling matrix to check for admissibility of decoupled states of a given structure by generalizing recent analysis of partial synchronization in Stuart-Landau oscillator networks [**81**, **118**]. Finally, we provide a general outline for determining the stability of these states and show how to use symmetry considerations to simplify the stability calculations using the symmetries arising from the automorphism group of the coupling matrix [**114**] and beyond [**43**,**50**]. As an illustration, we explicitly perform stability calculations for a decoupled state consisting of two independent splay clusters that occurs in an example network of eight oscillators coupled on a cube (which corresponds to the case of decoupling that can be explained by symmetries alone) in cases of adjacency and Laplacian coupling. Additionally, we perform stability calculations for the same state for two distinct coupling topologies that are similar to the cube, but break the symmetry in ways that keeps the state admissible only for adjacency and Laplacian coupling respectively.

The rest of the manuscript is organized as follows. First we discuss decoupled states in more detail. Then, in section 4.2, we present the necessary background, including the types of dynamics and coupling matrices we consider, the formal definition of decoupling, and the notation that will be used throughout the manuscript. In section 3.4, we consider how decoupling in linearly coupled networks arises from the network topology, expanding existing results to cases when the presence of these states is not purely dictated by symmetries. To illustrate the methods, we present examples on various networks, from simple modifications of ring topology to periodic square and hexagonal lattices. We then illustrate how the stability calculation can be simplified based on symmetry considerations beyond cluster synchronization in section 3.5. Finally, we summarize our findings and point out future directions in section 3.6.

3.2. Decoupled states

A decoupled state consists of several distinct splay clusters. Each splay cluster is a block splay state, and nodes in different splay clusters have an arbitrary phase difference that can either be fixed in time, meaning the state is periodic, or evolve linearly for quasiperiodic states. Here, the term *decoupled* refers to the fact that the coupling terms responsible for intra-cluster interactions cancel out in the dynamical equations, even if physical coupling between the oscillators in different splay clusters is present. Block splay states (also referred to as twisted states or traveling wave states in the literature [**145**, **164**]) arise as a form of symmetry breaking for a variety of coupling matrix structures, for instance, rings [**42**,**97**,**156**], all-to-all coupling [**82**], and lattices of oscillators [**58**,**87**]. These states are characterized by synchronization with a nonzero winding number (meaning that for some ordering of oscillators, each pair of neighbors is separated by an equal phase difference, and the winding number is determined by how many of the differences add up to 2π). See, for instance, Fig. 3.1(b-d) which show three distinct block splay states that can exist for a ring of eight identical oscillators. Such a ring supports a decoupled state consisting of two independent splay clusters as shown in Fig. 3.1(e), with δ_{12} denoting the arbitrary phase difference between the two splay clusters. The oscillators can be simple phase oscillators or can be limit cycle oscillators, such as nanoelectromechanical oscillators [**42**, **97**] and Stuart-Landau oscillators, where further patterns including amplitude death can exist [**81**, **118**].

The phase shift invariance of the full dynamical system allows existence of decoupled states consisting of multiple splay clusters with an arbitrary winding number. However, it is possible to obtain decoupling from more relaxed conditions [**4**]. In that case, however, the admissible splay states will be restricted by specific symmetries of the individual oscillator dynamics and coupling terms.

A periodic decoupled state was first observed in an analysis of bifurcations on rings of coupled oscillators [**3**], and motivated a symmetry based analysis of decoupling phenomena in networks with more general structure [**4**]. Under the presence of symmetries in nodal dynamics and with linear coupling, these states can be present in a diverse range of systems such as oscillators coupled in rings, hypercubes, full bipartite graphs, and infinite chains [**4**]. The state appears naturally in analysis of symmetric networks of phase oscillators with homogeneous parameters [**10**, **26**] (the

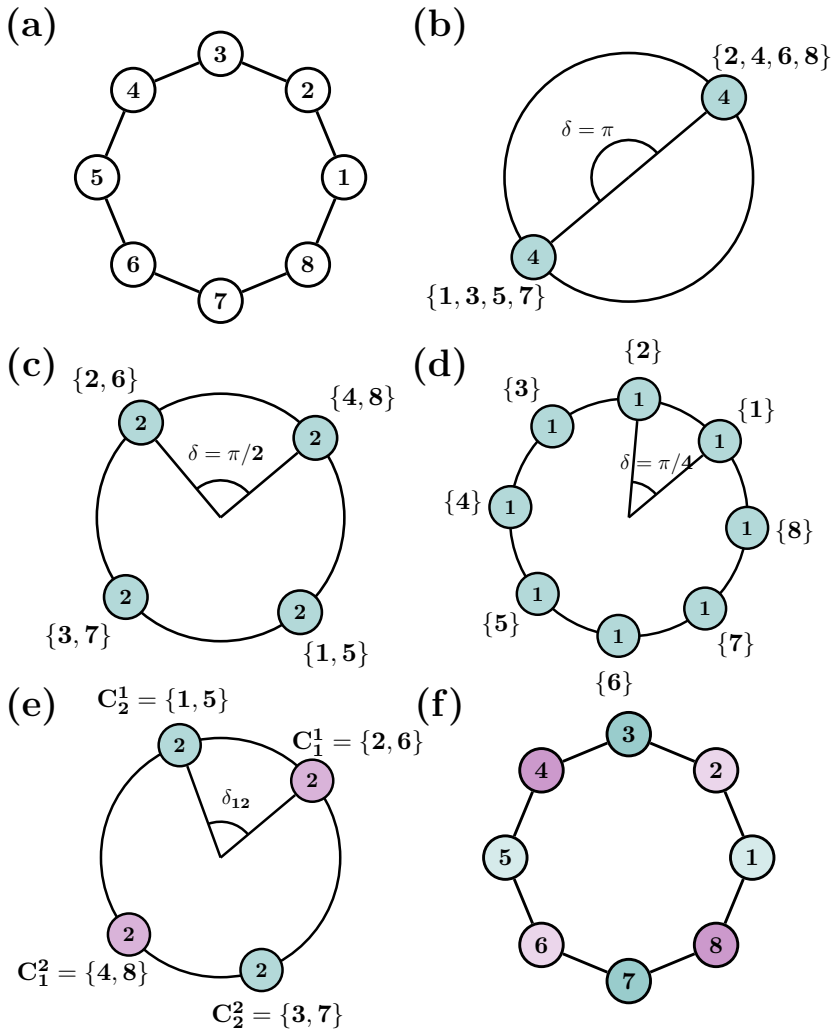

FIGURE 3.1. Illustrating splay states (b-d) and a decoupled state (e-f) in a ring network of 8 limit cycle oscillators. (a) The physical coupling and node indexes. (b-e) Each state is visualized on a ring corresponding to unit amplitude. Each small circle corresponds to the instantaneous phase of a subset of nodes, with the number of oscillators in that phase denoted by the number inside the circle, and their indexes provided next to the circle. (b) A splay state with 2 fully synchronized sub-clusters, each consisting of 4 nodes. (c) A splay state with 4 fully synchronized sub-clusters, each consisting of 2 nodes. (d) A splay state with 8 fully synchronized sub-clusters, each consisting of a single node. (e) A decoupled state consisting of two splay state clusters (violet and teal nodes) with an arbitrary phase difference δ_{12} between them. Each phase is labeled by $C_p^q = \{i, j\}$ where p denotes which *splay cluster* nodes i and j belong to, and q further partitions each splay cluster into *fully synchronized sub-clusters*, each consisting of 2 oscillators. (f) Visualizing the decoupled state (e) on a ring (a), where colors correspond to the splay clusters, and different intensities distinguish between different fully synchronized sub-clusters.

latter considers a general case of difference and product coupling), where the state is described as *partitioned rotating blocks*.

More recently, the state was predicted to occur in rings of $4n$ coupled phase-amplitude nanoelectromechanical oscillators [**42**], and, to our knowledge, experimentally observed for the first time in 2019 [**97**]. Interestingly, in ring networks, the physically coupled neighboring nodes have an arbitrary phase difference and are effectively decoupled from each other. Stability analysis of the decoupled states on $4n$-node ring networks with uniform and non-uniform natural frequencies was performed in Ref. [**43**]. There, it was shown that the amplitude degree of freedom is essential for the linear stability of that state (i.e., the state would not be linearly stable for phase only oscillators in the absence of explicit long-range, nonpairwise, or nonphase coupling). Moreover, it was demonstrated that mismatches in the natural frequencies of oscillators lead to intricate patterns of stability that show sensitive dependence on the relative frequencies of groups of oscillators in distinct splay clusters.

3.3. Formalism

In this manuscript, we consider networks of phase shift invariant limit cycle oscillators (such as Stuart-Landau oscillators) with linear coupling, with dynamical behavior governed by:

$$\dot{z}_j = f(|z_j|, \psi_j) \cdot z_j + \kappa_{jk} e^{i\beta_{jk}} \sum_k M_{jk} z_k. \tag{3.1}$$

The first term corresponds to the evolution of the state of each oscillator, denoted by, $z_j = r_j e^{i\theta_j} \in \mathbb{C}$, in absence of coupling. Without coupling, the system would evolve according to a nonlinear function $f(|z_j|, \psi_j) \cdot z_j$ (where the nonlinearity arises from the form of the function f). Specifically, we consider functions where, in absence of coupling, one of the admissible states of the system is a limit cycle with fixed amplitude r_j and linearly evolving phase θ_j. Here, ψ_j denotes the parameters of individual oscillators.

The oscillators are coupled through the coupling matrix M, and parameters κ_{jk} and β_{jk} contribute to the strength of dissipative coupling $\mathrm{Re}(\kappa_{jk} e^{i\beta_{jk}})$ and reactive coupling $\mathrm{Im}(\kappa_{jk} e^{i\beta_{jk}})$. The coupling matrix M is constrained to have binary off-diagonal entries and can either correspond to the adjacency matrix A or the graph Laplacian L, where $L = A - D$ (note the sign convention) the

diagonal matrix D is defined by $D_{ij} = \delta_{ij} \sum A_i$, and δ_{ij} is the Kronecker delta. Here, we assume the network is undirected. However, the results generalize for directed networks as well.

States of dynamical systems described by eq. (3.1) and its modifications (e.g., with added time delay) have been extensively analyzed in case of Stuart-Landau oscillators, where the individual oscillator dynamics are of the form:

$$f(|z_j|, \psi_j) \cdot z_j = (\lambda_j + i\omega_j - |z_j|^2) z_j, \tag{3.2}$$

where $\lambda_j \in \mathbb{R}$ is the bifurcation parameter, and $\omega_j \in \mathbb{R}$ is the individual oscillator frequency. Similarly, the dynamics of experimentally realized nanoelectromechanical oscillators [**97**] is well approximated by equations of the form of eq. (3.1) [**90**], with individual oscillator dynamics following:

$$f(|z_j|, \psi_j) \cdot z_j = \left(-1 + i\omega_j + 2i\alpha_j |z_j|^2 + \frac{1}{|z_j|} \right) z_j, \tag{3.3}$$

where $\omega_j \in \mathbb{R}$ is the oscillator frequency, and α_j is the Duffing nonlinearity. We will use these types of individual oscillator dynamics in our illustrative examples throughout the manuscript.

Some basic parameters are needed to define a state consisting of multiple splay clusters. We illustrate this with an example of a decoupled state in a network of nanoelectromechanical oscillators shown in fig. 3.1 (e-f) and studied in Ref. [**43**]. Let k denote the number of independent splay clusters. Let m denote the number of fully synchronized sub-clusters in the splay cluster, and let n denote the number of nodes in each sub-cluster. The number of nodes in the network is simply $N = kmn$. For fig. 3.1 (e-f), $k = 2, m = 2, n = 2$. We will also use the key notation C_p^q with $p \in 1, 2, \cdots k$ indicating the splay cluster index and $q \in 1, 2, \cdots m$ indicating the fully synchronized sub-cluster index. We provide formal details below (including the more complicated case where m and n can vary for different splay clusters).

EXAMPLE 3.3.1. *A network of eight nanoelectromechanical oscillators coupled to their nearest neighbors via Laplacian coupling on a ring (shown schematically on fig. 3.1 (a)) exhibits a variety of states that can be observed in experiment [**97**]. Assuming the parameters of the network are*

homogeneous, the equation below is a good approximation of the dynamics of the system:

$$\dot{z_j} = -z_j + i\omega z_j + 2i\alpha|z_j|^2 z_j + \frac{z_j}{|z_j|} + i\delta \sum_{k=j\pm1} A_{jk}\left(z_k - z_j\right). \tag{3.4}$$

In addition to multiple splay states, some of which shown on fig. 3.1(b-d), this system admits a decoupled state (shown in fig. 3.1 (e-f)) defined by:

$$(z_1, ..., z_8) = (z_1, z_2, -z_1, -z_2, z_1, z_2, -z_1, -z_2). \tag{3.5}$$

Here, $z_1 = e^{i\theta_1}$, $z_2 = e^{i\theta_2}$, and $\theta_2 - \theta_1$ is an arbitrary free parameter, and the oscillators are labeled by going around the ring.

Using the C_p^q notation (defined formally below in definition 3.3.2), $C_1^1 = \{1, 5\}$, $C_1^2 = \{3, 7\}$, $C_2^1 = \{2, 6\}$, $C_2^2 = \{4, 8\}$, and $C_1 = \{1, 3, 5, 7\}$, $C_2 = \{2, 4, 6, 8\}$. So the "even" nodes are decoupled from the "odd" nodes (evident from neighbors of each node being in antiphase in relation to each other), and the neighboring nodes that are physically coupled are separated by an arbitrary but fixed phase difference.

If the parameters in eq. (3.4) *are homogeneous, all the nodes (and therefore the splay clusters) move with the same frequency, resulting in the constant time-independent phase difference $\theta_2 - \theta_1$.*

We now define the (periodic or quasiperiodic) decoupled state more generally as a combination of different splay clusters, where each splay cluster can have a unique number of fully synchronized sub-clusters as well as nodes within each sub-cluster:

DEFINITION 3.3.1. *We say a set of mn nodes is in a **splay state** (with m fully synchronized clusters) if for some ordering of nodes their states are $\{z, ..., z, \omega z, ..., \omega z ..., \omega^{m-1} z, ..., \omega^{m-1} z\}$. Here, ω is the m^{th} primitive root of unity.*

DEFINITION 3.3.2. *Here we define a **decoupled state** consisting of k distinct but interleaved splay states, where each splay state is called a **splay cluster** for conceptual convenience.*

*Let the nodes of the system be labeled by indexes $I = \{1, ..., N\}$, where N is the total number of nodes. We can partition the nodes according to their phases into non-overlapping clusters C_p^q with **subscripts** indicating the **splay cluster** to which the node belongs and the **superscripts** indicating the **fully synchronized sub-cluster** within each splay cluster. Let the splay state*

clusters be indexed by p. Then m_p is the number of fully synchronized sub-clusters in splay cluster p and n_p is the number of nodes in each of the fully synchronized sub-clusters (the total number of nodes is then $N = \sum_{p=1}^{k} n_p m_p$.).

Mathematically, this is described by:

- C_p^q, $p = 1, ..., k$, $q = 1, ..., m$, *s.t. if* $i, j \in C_p^q$, $z_i = z_j$, *and* $|C_p^q| = n_p m_p$;
- $C_p = C_p^{q_1} \cup ... \cup C_p^{q_{m_p}}$, *s.t. if* $i \in C_p^{q_r}$ *and* $j \in C_p^{q_s}$, $z_i = e^{2\pi i |q_r - q_s|/m} z_j$, *and the phase difference is fixed over time;*
- *if* $i \in C_t^{q_1}$ *and* $j \in C_u^{q_1}$, $z_i = e^{i\delta_{tu}} \frac{r_i}{r_j} z_j$, *and the condition holds instantaneously, but* δ_{tu} *is allowed to evolve linearly in time.*

The partition of nodes into the cells $C_1^1, ..., C_1^{m_1}, ..., C_k^1, ..., C_k^{m_k}$ *defines the state.*

In presence of adjacency coupling, the ***decoupling*** *is manifested by the fact that the total effect of the nodes in the cluster* C_p *on each node* j *in the cluster* C_r $(p \neq r)$ *cancel out. Mathematically, the interaction terms are proportional to* $\sum_{k \in C_p} A_{jk} z_k = 0$. *In case of Laplacian coupling, the only effects of the nodes in* C_p *on each node* j *in the cluster* C_r $(p \neq r)$ *are manifested through the self-interaction terms. Mathematically, the interaction term affecting the state of the node* j *if proportional to* $\sum_{k \in C_p} A_{jk}(z_k - z_j) = -n_{pj} z_j$, *where* n_{pj} *denotes the number of edges coming into the node* j *from the cluster* p.

To further illustrate how the oscillators are organized into splay clusters and fully synchronized sub-clusters in a decoupled state, and how this corresponds to our notation, we present schematic examples of possible amplitudes and relative phases of such states in fig. 5.1 for phase-amplitude oscillators. fig. 5.1(a) corresponds to the case when the amplitudes of all the oscillators are equal. In contrast, fig. 5.1(b) shows a state where the amplitudes of oscillators in different splay clusters differ. Moreover, each splay cluster has a distinct number (2, 3, and 4) of fully synchronized sub-clusters, which leads to interesting multi-frequency oscillation behavior.

A state where both antiphase synchronization and multifrequency behavior are present, similarly to the one on fig. 5.1(b), is described in Ref. [**151**]. However, in the state presented there, clusters of oscillators of different amplitudes all either have the same or opposite phases, making it different from the decoupled state considered in our manuscript.

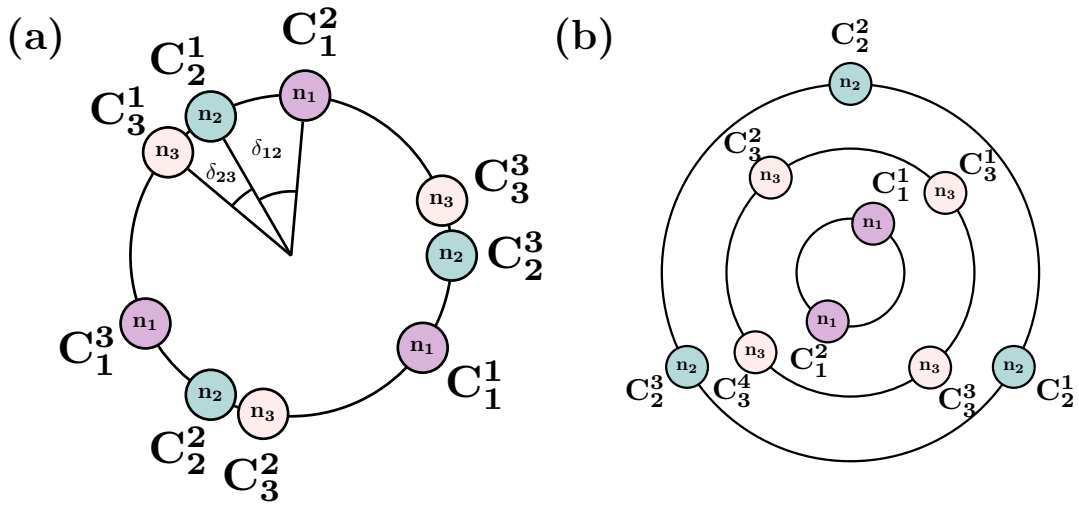

FIGURE 3.2. Schematic examples of possible phase (position on a ring) and amplitude (ring radius) configurations in decoupled states in networks of limit cycle oscillators. Different colors represent different splay clusters. C_p^q corresponds to qth fully synchronized sub-cluster in pth splay cluster. (a) Equal amplitude state with constant phase differences, $m_1 = m_2 = m_3 = 3$ (could be periodic or quasiperiodic, depending on the details of the system). (b) Quasiperiodic state with different amplitudes, $m_1 = 2,\ m_2 = 3,\ m_3 = 4$.

We note that the dynamics described by eq. (3.1) is not the only type of dynamics producing decoupled clusters. For example, the state can arise in mean field coupled networks of phase-only oscillators such as Kuramoto and Kuramoto-Sakaguchi oscillators [**10**,**26**], which can be considered as the approximation linearly coupled Stuart Landau oscillators in case of weak coupling. Such models have fewer degrees of freedom and may be easier to analyze, but do not capture the amplitude dynamics or full stability properties of the decoupled states of phase-amplitude oscillators [**43**].

In this section, we presented the general form of a decoupled state. Now, a natural question to ask is what coupling topologies admit its existence. In addition to the all-to-all case, some examples of these networks have been investigated in literature, e.g., in context of rings of Josephson junctions [**3**] and nanoelectromechanical oscillators [**97**]. More generally, in [**4**], the constraints on the topologies allowing the existence of decoupled states are formulated based on symmetry considerations for a more general class of dynamical equations with adjacency coupling. In section 3.4 of this manuscript, we demonstrate that the decoupled states do not uniquely arise from symmetries

alone, even in case of adjacency coupling. Therefore, our analysis covers cases not addressed in earlier work.

3.4. Decoupled states and network topology

In this section, we investigate what decoupled states are admissible for a given network topology and, conversely, what network topologies are allowed to form a decoupled state of a given form. Linearity of the dynamics in z allows directly predicting the form of allowed decoupled states from the eigendecomposition of the adjacency or Laplacian matrix of the network, as we show in section 3.4.1. Checking the admissibility of a given form of the decoupled state is based on these conditions is trivial. However, finding all the allowed decoupled states based on the conditions in section 3.4.1 hold can be challenging in practice, as the corresponding eigenvalues can be highly degenerate.

An alternative way to search for decoupled states is by investigating the structure of the coupling network directly. Previously, the decoupling conditions were formulated for oscillator networks with adjacency coupling and symmetries [**4**]. However, we show that decoupling is admissible for a much wider range of network topologies as well as for Laplacian coupling. We build upon work showing that cells of equitable partition of networks can synchronize [**51**, **113**, **131**, **134**], and more intricate patterns of synchrony can be inferred from the symmetries of the quotient networks [**53**, **142**]. Combining these results with adjacency and Laplacian coupling and taking the decoupling effects into account, in section 3.4.2 we formulate the conditions on decoupling that expand the set of networks previously discussed. In both cases, the network parameters can have modular structure, as discussed in section 3.4.3. section 3.4.4 demonstrates how the algorithms in section 3.4.2 can be used to reveal ways in which the decoupled state and its combination with amplitude death can appear in coupled oscillators on 2D square and hexagonal lattices.

It is worth noting that the analysis below can be extended to include the concept of amplitude death, which is a phenomenon associated with stabilization of the trivial steady state solution that can be observed in Stuart Landau oscillator networks [**102**]. For simplicity, most of the results below are presented for the state in which all the oscillators have nonzero amplitudes, and thus no partial amplitude death [**11**] is observed. However, adding nodes exhibiting amplitude death

to the adjacency coupled network in a way that keeps the dead nodes decoupled from other nodes would not change the admissibility of state of the other nodes (though it will influence its stability properties). This also extends to Laplacian coupling. Specifically, nodes that are only connected to one fully synchronized cluster can be synchronized with the rest of the cluster without destroying the decoupled state on other nodes.

3.4.1. Admissible patterns of decoupling from eigendecomposition. In this section, we discuss the conditions on admissibility of a specific decoupled state given the coupling via an adjacency/Laplacian matrix M. These conditions can be formulated in terms of the eigenvectors of M (similar to Ref. [**81**, **118**], where the concept of eigensolutions is discussed). Assuming the parameters are homogeneous throughout the network, the dynamics of the system in eq. (3.1) reduces to:

$$\dot{z} = f(|z|) \cdot z + \kappa e^{i\beta} M z. \tag{3.6}$$

The coupling matrix can be decomposed according to:

$$Mv = \eta v, \tag{3.7}$$

where η and v are its eigenvalues and eigenvectors.

First, we seek eigendecompositions that result in a *periodic* decoupled state that evolves according to:

$$z(t) = z_0 r_\eta e^{i\omega_\eta t}, \tag{3.8}$$

where z_0 is an initial condition corresponding to the decoupled state as defined in definition 3.3.2.

eq. (3.8) suggests that the conditions on the eigendecomposition of the coupling matrix M (again, $M = A$ for adjacency coupling, and $M = L = A - D$ for Laplacian coupling) that result in a periodic decoupled state with z_0 are:

- If $i, j \in C_p^q$:

$$[v_p]_i = [v_p]_j. \tag{3.9}$$

- If $i \in C_p^{q_1}$ and $j \in C_p^{q_2}$:

$$[v_p]_j = e^{2\pi i |q_1 - q_2|/m} [v_p]_i. \tag{3.10}$$

- If $i \notin C_p$:

$$[v_p]_i = 0. \tag{3.11}$$

- Consider distinct clusters C_{p_1} and C_{p_2}, with corresponding eigenvalues and eigenvectors arising from $M v_{p_1} = \eta_{p_1} v_{p_1}$ and $M v_{p_2} = \eta_{p_2} v_{p_2}$. For these clusters:

$$\eta_{p_1} = \eta_{p_2}, \tag{3.12}$$

  which results in any vector corresponding to the decoupling state $v_{\mathrm{d}} = \sum e^{i\delta_j} v_{p_j}$ being an admissible eigenvector.

To summarize, we require that any vector with the entries corresponding to an instance of a decoupled state with an arbitrary phase difference between splay clusters is an eigenvector of M.

We can now show that these conditions on the eigendecomposition lead to decoupling. Let v_d be an eigenvector. We use an ansatz $z_i = [v_d]_i z_\eta$ to obtain:

$$v_d \circ \dot{z}_\eta = \left(f(|v_d \circ z_\eta|) + \kappa e^{i\beta} M \right) v_d \circ z_\eta,$$

where $\circ$ denotes element-wise product. Using our key assumption of phase shift invariance in the full system, which is manifested in the form of eq. (3.6), we arrive to:

$$\dot{z}_\eta = \left(f(|z_\eta|) + \eta \kappa e^{i\beta} \right) z_\eta \tag{3.13}$$

The resulting solution is then of the form:

$$z(t) = r_\eta e^{i\omega_\eta t} v_d, \tag{3.14}$$

which corresponds to the evolution of a decoupled state. The amplitude r_η and the angular frequency ω_η depend on the parameters and the form of the function f.

A condition similar to eq. (3.12) (normalized $v_{p_1} + v_{p_2}$ is an eigenvector of the Laplacian) without eqs. (3.9) to (3.11) holding does not result in a decoupled state. For instance, an adjacency/Laplacian matrix for a ring of six coupled oscillators has eigenvectors corresponding to splay clusters (rotating blocks) with winding numbers 2 and 3, but these states are not decoupled. Yet, multiple decoupled states are admissible for all-to-all coupled networks of six oscillators, as shown in fig. 3.3 (c-d).

On the other hand, if all the conditions in eqs. (3.9) to (3.11) hold, but eq. (3.12) does not hold, the resulting decoupled state is quasiperiodic. That quasiperiodic state is characterized by:

$$z_j = z_{\eta,p}[v_p]_j, \quad z_{\eta,p} = r_{\eta,p} e^{i\omega_{\eta,p} t}, \tag{3.15}$$

for $j \in C_p$. This allows the oscillator amplitudes and frequencies, $r_{\eta,p}$ and $\omega_{\eta,p}$, to be different for nodes in different splay clusters, as shown in fig. 5.1 (b).

Our approach extends the analysis of eigensolutions describing the dynamics of constant amplitude states in networks of coupled Stuart-Landau oscillators, as presented in Refs. [**81**,**118**]. There, the eigendecomposition was associated with splay states and their coexistence with amplitude death (the state in which $z(t) = 0$ for some oscillators) [**102**], but decoupling was not considered. We discuss the case of Stuart Landau oscillators in more detail in section 3.7.1. For networks of Stuart Landau oscillators, the decoupled state can coexist with partial amplitude death. For instance, if the decoupled state is an admissible state, the state a set of nodes belonging to a decoupled cluster has zero amplitude is admissible as well. Additionally, eq. (3.15) demonstrates that multifrequency oscillations previously associated with coexistence with amplitude death can occur even in absence of it.

EXAMPLE 3.4.1. *As described in example 3.3.1, a decoupled state exists in an eight oscillator ring with nearest neighbor coupling, and the solution is valid both for adjacency and Laplacian coupling schemes. This is evident since the following eigenvectors that share an eigenvalue correspond to decoupling of the even and odd nodes on the ring:*

$$v_{p_1} = (1, 0, -1, 0, 1, 0, -1, 0)^T, \quad v_{p_2} = (0, 1, 0, -1, 0, 1, 0, -1)^T, \quad \eta_{p_1} = \eta_{p_2}. \tag{3.16}$$

In case of Laplacian coupling, breaking the symmetry by adding an edge between any pairs of nodes related by $i, j \in C_p^q$ does not affect these eigenvectors, and the state is still admissible. However, this does not hold for adjacency coupling.

We also note that this if the state is a result of symmetries (when the state belongs to a fixed point subspace of an isotropy subgroup of the symmetry group of the system [**54**]), these conditions become identical to the ones presented in Ref. [**4**] and could result in periodic or quasiperiodic states [**43**].

Using the approach outlined here is easy if the goal is to check whether a particular decoupled state is admissible for a coupling topology encoded in M. However, it is not always trivial to enumerate the decoupled states of larger networks based on the eigendecomposition of the coupling matrix. This method is not very easily applicable to highly regular networks, such as periodic lattices discussed in section 3.4.4, because the eigenvalues become highly degenerate, making it nontrivial to check conditions in eqs. (3.9) to (3.12) numerically. In the following section, we introduce an alternative method that can be used to address this issue and allows to make a more intuitive connection between the network structure and the decoupled state dynamics.

3.4.2. Admissible patterns of decoupling from network partitions. In this section, we provide a complementary approach of relating network structure to the existence of decoupled states. Since the admissibility of states depends on both the network structure and the coupling type, we consider Laplacian and adjacency coupling separately. Specifically, we provide an iterative algorithm that partitions the Laplacian coupled network nodes into splay clusters C_p and fully synchronized clusters C_p^q based on the concepts of equitable and orbital partitions used in cluster synchronization literature [**114**, **115**, **131**, **134**, **139**]. We also show how the adjacency coupling case is different and provide a way to search for decoupled states in that case as well.

For both coupling types, we require that the coupling between the nodes within a splay cluster admits a splay state. However, in the Laplacian case, the edges between any nodes in the same fully synchronized cluster can be ignored, whereas in case of adjacency clustering these edges also affect the admissibility of the state. Additionally, we have take into account that self-terms can

arise from Laplacian coupling between different splay clusters, which is not an issue for adjacency case.

Let the set of nodes in the network be defined by I.

DEFINITION 3.4.1. *An **equitable partition** is a partition of the indexes of network nodes into non-overlapping **cells** (collections of nodes) $I_1, ..., I_d$, where the number of edges from a node in I_i to a node in I_j is the same for any choice of individual nodes within these cells. An **external equitable partition** is a partition where these conditions hold for $i \neq j$.*

DEFINITION 3.4.2. *An **orbital partition** is a division of network nodes into non-overlapping **cells** $I_1, ..., I_d$ according to the orbits of the automorphism group of that network (the symmetry group formed by the node permutations that keep the network topology invariant). The nodes that permute among one another under the action of all symmetry group elements get assigned to the same cell.*

DEFINITION 3.4.3. *A **quotient network** associated with a particular coarse-grained version of the original network, such that each cell of the that partition becomes a new node and the weights between these new nodes are the out-degrees between the cells in the original graph.*

Now, we can define an algorithm to obtain decoupled states in networks with Laplacian coupling. (The algorithm for adjacency coupling is presented in Alg. 3.4.0.2.) In contrast with existing decoupled state literature [**4**, **10**], we consider the states that arise from more than symmetries alone.

ALGORITHM 3.4.0.1. *To find admissible decoupled states for **Laplacian** coupling, it is sufficient to:*

(1) Find an external equitable partition of the network and form an quotient network associated with that partition (it is possible that the equitable quotient is the same as the original network).

(2) Check if the resulting quotient network formed in step 1 is symmetric with respect to any symmetry group of the form $\Gamma = Z_{m_1} \times ... \times Z_{m_k}$ that acts on k non-overlapping sets of nodes, the union of which is the entire quotient network. Find an orbital partition of the

quotient network under the action of the symmetry group Γ *and form the new quotient network from the cells of this partition.*

(3) Check if the number of edges coming ***into*** *every node of the quotient network formed in step 2 is divisible by the weight of that node (the number of nodes of the quotient network in Step 2 combined into that node).*

- *If that is* ***not*** *satisfied, go back to step 2 and try a new orbital partition. In case that does not work, go to step 1 and try a new external equitable partition.*
- *If that is satisfied, then a decoupled state is obtained. The orbital partition provides the assignment into splay clusters* C_p*, and the equitable partition provides the assignment into fully synchronized clusters* C_p^q*.*

In a special case of homogeneous parameters, if $m_1 = ... = m_k$, and the weights on all self-loops and edges in an orbital quotient network are equal, the state is periodic.

We show that these conditions indeed characterize the decoupled states.

The first step is forming an equitable partition. It has been shown that equitable partitions lead to synchronization [**131**, **134**], since all the nodes in a given partition cell get the same input from all the other cells. Thus, the nodes in each cell of that partition can synchronize.

The second step is forming an orbital partition with respect to a symmetry group $Z_{m_1} \times ... \times Z_{m_k}$, where Z_{m_i} refers to the cyclic group of degree m_i. This ensures that a block splay state exists within each cluster [**48**, **49**]. We note that the symmetry of the quotient network does not necessarily translate to the symmetry of the original network.

The last step combined with the second step ensures that each of the nodes in a decoupled state is not influenced by other splay clusters in the dynamical equations.

We also note that the steps are not uniquely defined. First, there can be multiple equitable partitions of the network. In some cases, different network partitions correspond to qualitatively distinct decoupled states. For instance, in a network of 6 oscillators, two distinct decoupled states are possible, see fig. 3.3. One of them corresponds to $m = 3$ with $n_1 = n_2 = 1$, the other to $m = 2$ with $n_1 = n_2 = n_3 = 1$. Another case corresponds to finding partitions that could be further refined to produce decoupled states. In that case, the state obtained is a restriction of a decoupled state

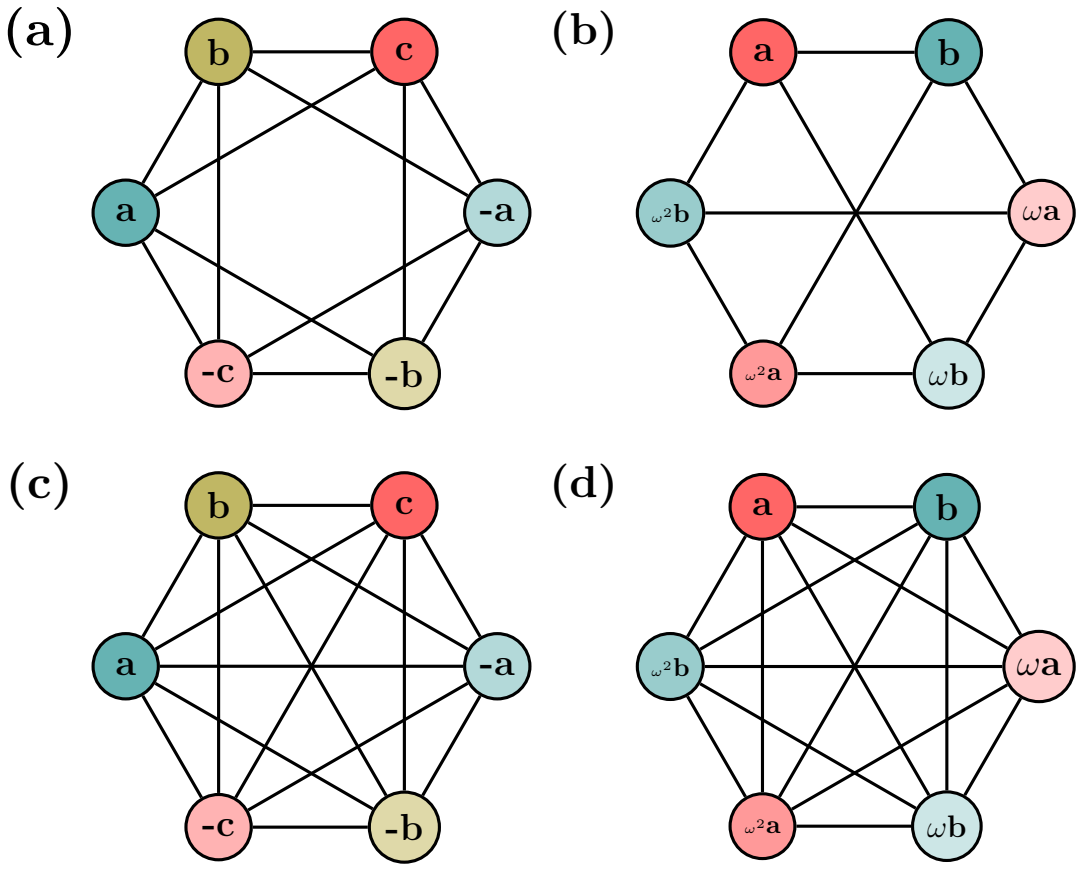

FIGURE 3.3. Examples of decoupling on a 6-node network. A decoupled state does not appear in a ring with nearest neighbor coupling. (a) Three decoupled clusters in case of next neighbor coupling. (b) Two decoupled clusters for nearest neighbor coupling with additional edges across the ring (ω stands for $e^{2\pi i/3}$). (c-d) Both of the states are admissible for all-to-all coupling.

with more clusters to a specific inter-cluster phase difference. Finally, the same quotient network structure could correspond to qualitatively different decoupled states (e.g., shown in section 3.4.4).

Below is an example of applying the algorithm:

EXAMPLE 3.4.2. *We consider a network of eight oscillators similar to the ring in example 3.3.1 with additional edges between a subset of next nearest neighbors and two opposite nodes, as shown in fig. 3.4(a).*

- *Solid lines on fig. 3.4 represent the ring topology, which would result in a periodic decoupled state in absence of parameter heterogeneity. The state is admissible in case of adjacency or Laplacian coupling.*

- *Adding additional edges represented by dotted lines on fig. 3.4 would result in a quasiperiodic state. The state is admissible in case of adjacency or Laplacian coupling.*
- *Adding an edge represented by dashed line on fig. 3.4 makes that quasiperiodic state only admissible in case of Laplacian coupling.*

Following algorithm 3.4.0.1, we find the decoupled state that the network admits for the Laplacian coupling case. The steps of the algorithm, as well as their description, is shown on fig. 3.4. fig. 3.4 (d) shows the instantaneous state of the system. In general, even if all the oscillator natural frequencies are equal, the frequencies of splay clusters (corresponding to nodes colored red and blue on fig. 3.4 (c)) will differ because of the different intra-cluster connectivity structure (as evident on fig. 3.4 (c′)). This leads to multifrequency splay synchronization of identical oscillators without amplitude death.

This same algorithm can be applied to periodic lattices. The analysis of decoupled states in square and hexagonal 2D periodic lattices is presented in section 3.4.4. There, we show that diverse synchronization patterns can arise for the same regular network connectivity patterns.

Now, we consider adjacency coupling. If the external equitable partition is replaced by an equitable partition in the first step of algorithm 3.4.0.1, that algorithm can be used to obtain decoupled states for adjacency coupling. However, that does not cover the full range of possibilities for decoupled states arising in adjacency coupled networks. We provide a more general algorithm below.

ALGORITHM 3.4.0.2. *To find admissible decoupled states for* ***adjacency*** *coupling, it is sufficient to:*

(1) Divide the network nodes into non-overlapping sets of nodes $I_1, ..., I_k$. This partition is a candidate for assigning nodes into splay clusters C_p.

(2) For each $j = 1, ..., k$, consider a subset of the original network that only contains nodes in I_j and edges between these nodes. Check if there is an equitable partition of that subnetwork into cells of equal size ($I_j^1, ..., I_j^{m_j}$, where $|I_j^1| = ... = |I_j^{m_j}|$), s.t. the resulting quotient network is Z_{m_j}-symmetric. If so, I_j^l become candidates for fully synchronized clusters C_p^q.

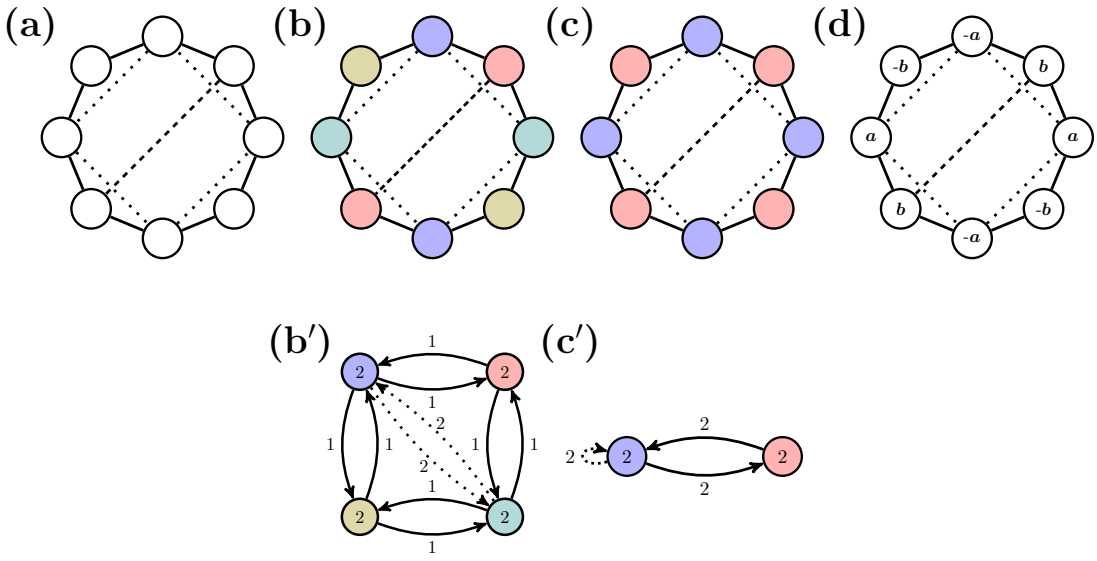

FIGURE 3.4. Obtaining the decoupled state using algorithm 3.4.0.1 for the network topology shown on (a). Subfigures (b)-(c) represent the steps to obtain the state. The top row shows network partitions, and the bottom rows demonstrate the quotient networks on various steps of algorithm 3.4.0.1. (b) shows the four fully synchronized clusters corresponding to the external equitable partition with the corresponding quotient network shown on (b′), once the self edges are removed. (c′) shows the quotient network with re-weighted edges that is now colored according to its orbital partition. (c) shows the original network colored according to the orbital quotient. The decoupled state consists of four fully synchronized clusters (shown in distinct colors on (b)) and two splay (rotating block) clusters (shown in distinct colors on (c)). (d) demonstrates the form of the state, where a and b are complex state variables.

(3) Check that the numbers of edges coming from nodes within each subset $(I_j^1, ..., I_j^{m_j})$ of I_j ***into*** *every node i that is not part of that cell, $i \notin I_j$, are equal.*

- *If the condition above is* ***not*** *satisfied, go back to step step 2 and try a new partition. In case that does not work, go to step 1 and try a new equitable partition.*
- *If the condition is satisfied, then a decoupled state is obtained. The partition $I_1, ..., I_k$ assigns the nodes into splay clusters C_p, and its refinement $I_j^1, ..., I_j^{m_j}$ provides the assignment into fully synchronized clusters C_p^q.*

Below, we provide an example of how the admissible networks for adjacency coupling may differ from those for Laplacian coupling, even for the same resulting decoupled state.

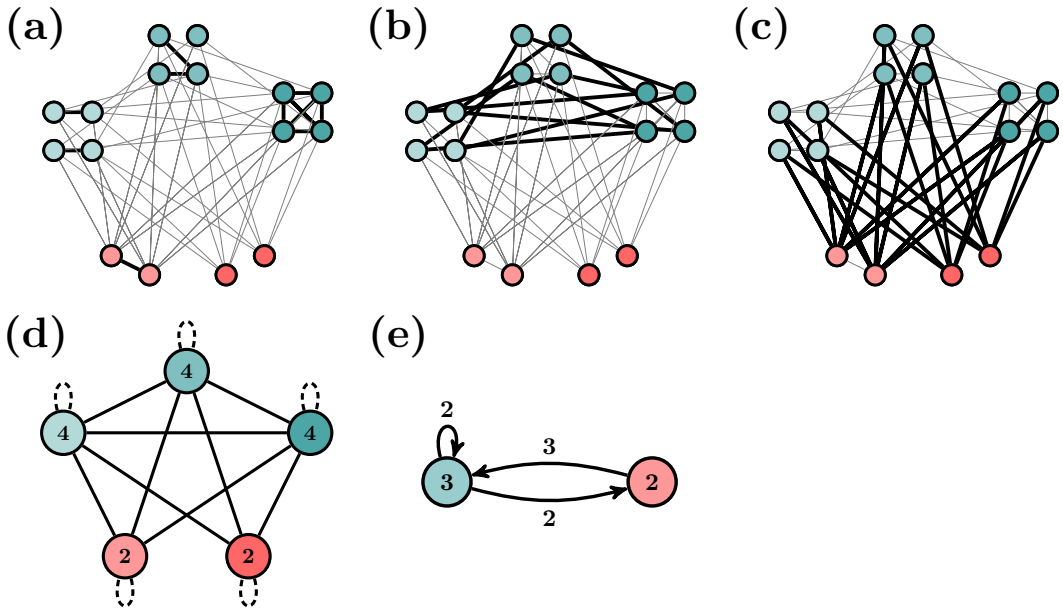

FIGURE 3.5. An example of a topology that allows decoupling in presence of Laplacian coupling, but not adjacency coupling. The subfigures (a-c) have different edges of the network highlighted in bold. (a): within fully synchronized clusters, any coupling is admissible for Laplacian coupling. (b): between fully synchronized sub-clusters that are in the same splay clusters. The quotient networks are $Z_3 \times Z_2$-symmetric. (c): between splay clusters. Each red node is connected to 2 nodes in each teal sub-cluster, each teal cluster connected to 2 nodes in each red sub-cluster. (d): external equitable partition. (e): orbital partition with respect to $Z_3 \times Z_2$. The dashed lines are edges that are not mandatory.

EXAMPLE 3.4.3. *We provide examples of two 16-node networks with different coupling topologies that admit a decoupled state. In both cases, the decoupled state consists of two splay clusters. The first cluster has 3 fully synchronized sub-clusters with 4 nodes each. The second consists of 2 fully synchronized sub-clusters with 2 nodes each.*

fig. 3.5 provides an example of a network topology that admits a decoupled state for Laplacian coupling, but not adjacency coupling. The network shown in fig. 3.6 is an example of a network topology that admits a decoupled state for adjacency coupling, but not Laplacian coupling.

*The configuration shown in fig. 3.5(a-c) is similar to remote synchronization [**111**]: one of the fully synchronized pairs of nodes, namely, two red nodes on the bottom right of fig. 3.5 have no edges directly connecting them to each other.*

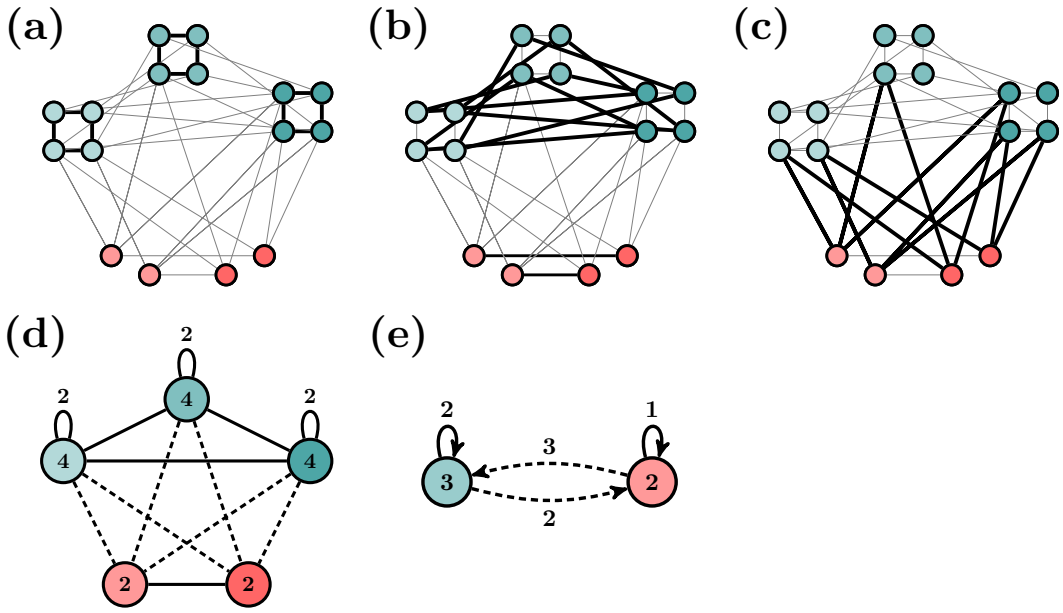

FIGURE 3.6. An example of a topology that allows decoupling in presence of adjacency coupling, but not Laplacian coupling. The subfigures have different edges of the network highlighted in bold. (a): within fully synchronized clusters. (b): between fully synchronized sub-clusters, within the same splay cluster. The quotient networks are $Z_3 \times Z_2$-symmetric. (c): between splay clusters. Each red node is connected to the same number of nodes in each teal sub-cluster, and vice versa. (d): external equitable partition. (e): orbital partition with respect to $Z_3 \times Z_2$. The dashed lines are edges that are not mandatory.

Although the algorithms in this section are most useful conceptually, the steps can be implemented using code published in recent literature. For instance, an efficient way to obtain equitable partitions from the network structure is described and implemented in Ref. [**69**], and orbital partitions can be determined using the supplementary code in Ref. [**114**].

3.4.3. Heterogeneous networks. So far, we considered decoupled states arising in the networks of oscillators with homogeneous individual oscillator parameters ψ and homogeneous coupling parameters κ and β. However, since the interaction dynamics between different decoupled clusters sum up to zero, and since the self-interactions do not affect the state for Laplacian coupling, decoupled states can also be observed if the homogeneity assumption is relaxed. Specifically, decoupling can be observed in modular networks with different modules corresponding to different node and edge parameters, and the decoupled state is robust to small discrepancies in parameters within

each modules [**97**]. Additionally, decoupling can be present in a multilayer network where each layer corresponds to a specific functional form of node dynamics and coupling parameters.

We denote the nodal parameters by ψ_i and the coupling parameters by ψ_{ij}. For both coupling schemes, the relaxed conditions require the following:

- Nodal parameters, denoted by ψ, satisfy $\psi_i = \psi_j$ if $i \in C_p$ and $j \in C_p$.
- Coupling parameters between different fully synchronized sub-clusters of each decoupled splay cluster satisfy $\psi_{ij} = \psi_{kl}$ (here, $i, k \in C_p^q$ and $j, l \in C_p^r$, $q \neq r$).

Additionally, for Laplacian coupling we require that the inter-cluster coupling parameters satisfy $\psi_{ij} = \psi_{kl}$ if $i, k \in C_p$ and $j, l \in C_q$ when $p \neq q$. If the nodes belong to the same synchronized cluster, no restrictions on the coupling strength are needed.

For adjacency coupling, we require each edge parameter ψ_{ij} from a fully synchronized cluster of C_p^q to a fully synchronized cluster C_r^s is matched by an edge $\psi_{ij} = \psi_{kl}$ of the same strength going into each of the clusters C_r^t where $s \neq t$. Additionally, we require all the intra-cluster coupling parameters within fully synchronized sub-clusters to have the same strength.

The conditions above can be understood both from the eigenvector approach in section 3.4.1 and the more structural approach in section 3.5.2. The restrictions presented here set constraints on the interactions within different blocks of the weighted coupling matrix so that the heterogeneity in parameters does not affect the relevant eigenvectors, therefore still allowing the decoupled state to be present, preserving the reasoning of section 3.4.1. Re-weighting the coupling matrix does introduce different types of edges and nodes to the networks in section 3.5.2, but these changes do not affect the structure of the relevant quotient networks, therefore keeping the decoupled states admissible if they were admissible in a homogeneous networks [**2**].

In addition to parameter heterogeneity, we can consider heterogeneity in nodal dynamics, resulting in a multilayer matrix with each type of dynamics corresponding to a distinct layer. An example of such a network could be a network of Stuart-Landau oscillators coupled to a network of nanoelectromechanical oscillators, with nodal dynamics defined in eq. (3.2) and eq. (3.3). Very similarly to the case of node parameter heterogeneity, this setup allows the decoupled state if $f_i(|z_j|, \psi)$ and $f_j(|z_j|, \psi)$ have the same functional form and parameters for $i \in C_p$ and $j \in C_p$.

3.4.4. Decoupled states on lattices. Generally, coupled periodic and chaotic oscillators placed on lattice topologies lead to a rich variety of spatio-temporal patterns, as shown in various analytic and numerical studies [**6**, **18**, **53**, **87**, **141**]. For instance, all possible balanced two-colorings for square lattices are presented in Ref. [**153**]. Since the lattice topology is highly symmetric, a variety of decoupled states is admissible on lattice networks.

The simplest example of a lattice system is an infinite 1D chain of oscillators. A state where even and odd nodes are decoupled and next nearest neighbors are in antiphase [**4**] is the only admissible decoupled state for such a system. This state is similar to the pattern observed in rings of $4N$ oscillators [**3**, **43**, **97**], which is a chain with periodic boundary conditions.

More complicated decoupling patterns can arise on 2D lattice coupling topologies. To illustrate them, we consider a periodic 8×8 square lattice, where each node has four immediate neighbors, and a periodic 8×8 hexagonal lattice, where each node has six neighbors. Though the analytic expressions for eigenvectors and eigenvalues of the Laplacian of periodic square and hexagonal lattices are available [**120**], their eigenvalue spectra are highly degenerate and enumerating the decoupled states based on the results of section 3.4.1 is therefore nontrivial. On the other hand, the approach from section 3.4.2 can be used, but it requires forming equitable partitions (also referred to as balanced k-colorings) of the lattice where $k \geq 4$.

Some of the resulting decoupling patterns, along with the quotient and orbital networks responsible for generating them, are demonstrated on figs. 3.7 and 3.8. To keep the examples minimal, we do not introduce node or edge heterogeneity. However, the states we present can also occur if the node and edge parameters satisfy the conditions of section 3.4.3.

First, we consider the square lattice case (fig. 3.7). We observe various patterns of decoupling, in many of which the pattern can be related to balanced 2-colorings [**153**]. Distinct colors represent distinct splay clusters, and different degrees of transparency represent different synchronized subclusters within each splay cluster. There are several partitions that lead to two decoupled clusters (fig. 3.7 (a-d)), one that leads to four decoupled clusters (fig. 3.7 (e)), and one that leads to eight (or, more generally, to n for $n \times n$ lattices), with the phase differences between nodes on different diagonals arbitrarily defined (fig. 3.7 (f)). In cases (d,e,f), the nodes are additionally effectively decoupled from their own cluster. In case of adjacency coupling, this means that the oscillator

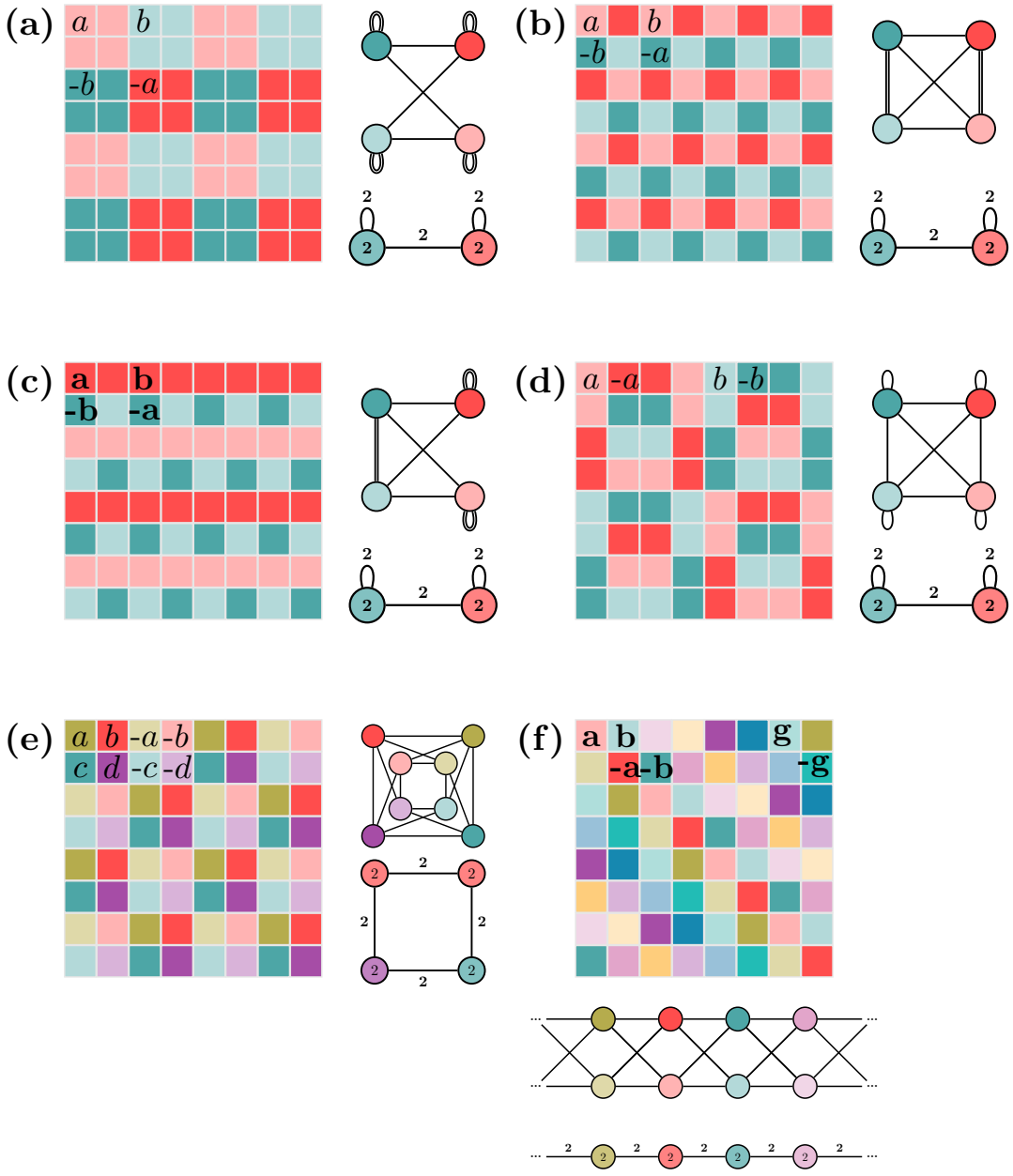

FIGURE 3.7. Decoupling in a periodic square lattice with nearest neighbor coupling (each node has 4 neighbors; in the visualization, the nodes are coupled if the edges of the squares touch). Subfigures (a-d) left: state of each node. Top right: external equitable partition defining the fully synchronized state (edges are unidirectional have weigh 1 for single line, 2 for double line). Bottom right: orbital partition defining splay clusters. Colors correspond to different splay clusters, and different brightness within each color corresponds to different fully synchronized sub-clusters. (a-d) has two splay clusters, (e) has four, (f) has n for a $n \times n$ periodic lattice.

frequencies and amplitudes in the decoupled state are the same as they would be in absence of any coupling.

Next, we consider the hexagonal lattice coupling structure (fig. 3.8). We observe two distinct partitions corresponding to two decoupled clusters (fig. 3.8 (a-b)), and one corresponding to three, four, six, and eight decoupled clusters (fig. 3.8 (c-f)). The nodes are effectively decoupled from their own cluster in partitions (a,c-g). The state in (e) is consists of four (or, more generally, n for $2n \times 2n$ lattices) separate clusters corresponding to every other row in the lattice and two decoupled clusters populating other rows. The state in (f) is similar to that in fig. 3.7 (e), where each pair of rows is separated by an arbitrary phase difference.

In networks of Stuart-Landau oscillators, amplitude death can coexist with the phenomena described above. For instance, if any of the nonzero amplitude splay clusters is replaced with a set of dead nodes, the state is still admissible. Additionally, we present an example illustrating a different possibility on fig. 3.8 (g). The state consists of three splay clusters and a cluster of dead nodes. Two of the splay clusters are the same as those shown on fig. 3.8 (c). The nodes in the third cluster of fig. 3.8 (c), shown in red, form a decoupled cluster and a cluster of dead nodes on fig. 3.8 (g). Two decoupled clusters are characterized by winding numbers $m_{1,2} = 3$, and the third cluster has $m_3 = 2$.

In some of the patterns, all the nodes are decoupled from their own splay cluster in addition to being decoupled from all the other splay clusters. That implies the state is not linearly stable if the nodal dynamics is described by phase-only oscillator dynamics such as those of nearest neighbor Kuramoto and Kuramoto-Sakaguchi model [**43**].

The analysis can be extended to higher dimensional lattices, in which even more complicated decoupling patterns could be observed. Stability of these patterns could be a subject of further investigation.

3.5. Stability calculations

3.5.1. General Jacobian structure. It is important to perform linear stability analysis of the decoupled state because it allows predicting which parameter regions will correspond to

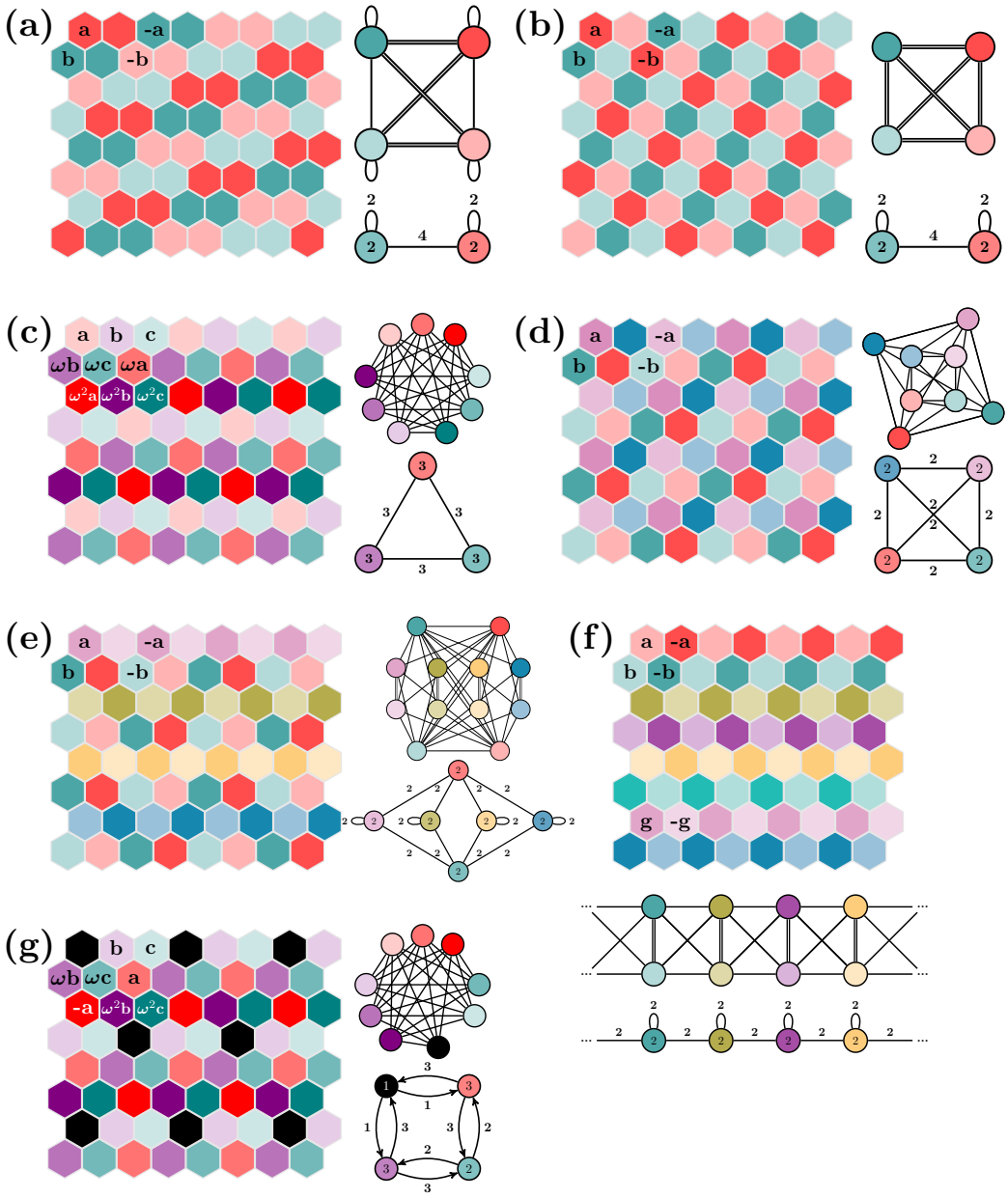

FIGURE 3.8. Decoupling in a periodic hexagonal lattice with nearest neighbor coupling (each node has 4 neighbors; in the visualization, the nodes are coupled if the edges of the hexagons touch). The meaning of parts of subfigures described under fig. 3.7. Subfigures (a-f) left: state of each node. Top right: external equitable partition defining the fully synchronized state (edges are unidirectional have weigh 1 for single line, 2 for double line). Bottom right: orbital partition defining splay clusters. (a-b) have two splay clusters, (c) has three, (d) four, (e) six, (f) has n for a $n \times n$ periodic lattice. Subfigure (g): decoupling pattern including amplitude death.

observing that state in simulations and experiments. Here, we present the general outline of linear stability calculation for decoupled states in equations of the form of eq. (3.1) for $N = \sum_{i=1}^{k} n_i m_i$.

The details of the stability calculation depend on the form of nodal dynamics, the decoupled state (periodic or quasiperiodic, equal or unequal winding numbers m_i), the type of coupling (Laplacian or adjacency matrix), and the coupling topology within splay clusters. In some cases, the stability calculations can be simplified using symmetry considerations, both by block diagonalizing using subgroups of the automorphism group leading to cluster synchronization [**114**] and by block diagonalizing by additionally using the symmetries of the splay states [**43**, **50**]. In other cases, symmetry methods may not be applicable.

Since the dynamics of each node correspond to two degrees of freedom, the Jacobian evaluated at the decoupled state is a $2N \times 2N$ matrix. For simplicity, we order the nodes according to the splay clusters to which they belong. The full Jacobian matrix can be written as:

$$J = \begin{pmatrix} J_{C_1,C_1} & \dots & J_{C_1,C_k} \\ \vdots & \ddots & \vdots \\ J_{C_k,C_1} & \dots & J_{C_k,C_k} \end{pmatrix}, \tag{3.17}$$

where each block J_{C_i,C_j} of size $2m_i n_i \times 2m_j n_j$ corresponds to the interactions between the splay clusters. Furthermore, each of these blocks is of the form:

$$J_{C_{p_1},C_{p_2}} = \begin{pmatrix} J_{C_{p_1}^{q_1},C_{p_2}^{q_1}} & \dots & J_{C_{p_1}^{q_1},C_{p_2}^{q_m}} \\ \vdots & \ddots & \vdots \\ J_{C_{p_1}^{q_m},C_{p_2}^{q_1}} & \dots & J_{C_{p_1}^{q_m},C_{p_2}^{q_m}} \end{pmatrix}, \tag{3.18}$$

where the finer blocks $J_{C_{p_j}^{q_i},C_{p_l}^{q_k}}$ correspond to the interactions between the fully synchronized sub-clusters. The fully synchronized sub-cluster blocks are of the form:

$$J_{C_{p_1}^{q_1},C_{p_2}^{q_2}} = \begin{pmatrix} J_{i_1,j_1} & \dots & J_{i_1,j_{n_2}} \\ \vdots & \ddots & \vdots \\ J_{i_{n_1},j_1} & \dots & J_{i_{n_1},j_{n_2}} \end{pmatrix}. \tag{3.19}$$

Here, $C_{p_1}^{q_1} = \{i_1, ..., i_{n_1}\}$, and $C_{p_2}^{q_2} = \{j_1, ..., j_{n_2}\}$. Finally, the Jacobian associated with each pair of oscillators is:

$$J_{ij} = \begin{pmatrix} J_{r_i,r_j} & J_{r_i,\theta_j} \\ J_{\theta_i,r_j} & J_{\theta_i,\theta_j} \end{pmatrix} = \begin{pmatrix} \frac{\delta \dot{r}_i}{\delta r_j} & \frac{\delta \dot{r}_i}{\delta \theta_j} \\ \frac{\delta \dot{\theta}_i}{\delta r_j} & \frac{\delta \dot{\theta}_i}{\delta \theta_j} \end{pmatrix}, \tag{3.20}$$

where δr_i and $\delta\theta_i$ are small perturbations of the amplitude and phase of the ith oscillator around the decoupled state.

For instance, if $m_1 = ... = m_k$, the full Jacobian J is a $2N \times 2N$ matrix, where $N = (n_1 + ... + n_k)m$. Then, for $i_1 = \sum_{j=1}^{p_1-1} mn_j + (p_1 - 1)q_1 + r_1$ and $i_2 = \sum_{j=1}^{p_2-1} mn_j + (p_2 - 1)q_2 + r_2$, J_{i_1,i_2} represents the interactions between the oscillators in $C_{p_1}^{q_1}$ and $C_{p_2}^{q_2}$ blocks.

Given a specified decoupled state, the Jacobian blocks J_{ij} (where $i \in C_{p_1}^{q_1}$ and $i \in C_{p_2}^{q_2}$) on that decoupled state can be evaluated explicitly:

$$J_{ij} = \begin{cases} \begin{pmatrix} \partial f_{r_i}/\partial r_i & \sum_{i \in C_p} \kappa A_{ij} r \sin\beta \\ \sum_{i \in C_p} \kappa A_{ij} \frac{1}{r} \sin\beta & \sum_{i \in C_p} -\kappa A_{ij} \cos\beta \end{pmatrix}, \\ \text{for } i = j; \\ A_{ij}\kappa \begin{pmatrix} \cos(\beta + \Delta_{p_1p_2}^{q_1q_2}) & -r\sin(\beta + \Delta_{p_1p_2}^{q_1q_2}) \\ \frac{1}{r}\sin(\beta + \Delta_{p_1p_2}^{q_1q_2}) & \cos(\beta + \Delta_{p_1p_2}^{q_1q_2}) \end{pmatrix}, \\ \text{for } i \in C_{p_1}^{q_1}, j \in C_{p_2}^{q_2}, \end{cases} \tag{3.21}$$

where we assume homogeneous coupling parameters. Here, for the general quasiperiodic case in case of uniform m, $\Delta_{p_1p_2}^{q_1q_2}(t) = \sigma_{p_1p_2}(t) + \sigma_{q_1q_2}$, where $\sigma_{q_1q_2} = \frac{2\pi}{m} \times ((q_1 - q_2) \mod m)$, and $\sigma_{p_1p_2}(t) = \sigma_{p_1p_2}(0) + \dot{\sigma}_{p_1p_2}t$ is a linearly evolving phase difference between the clusters.

If the Jacobian is time-independent, linear stability analysis can be performed by obtaining the largest real part of a Jacobian eigenvalue corresponding to transverse perturbations (as opposed to the neutrally stable perturbations of phases in the direction within the state correspond to k zero eigenvalues, where k is the number of splay clusters in the decoupled state). If the Jacobian is a periodic matrix (namely, only two clusters have an irrational frequency ratio), the stability analysis can be performed using Floquet theory. That is always possible when only two decoupled

clusters are present. If more than two clusters are present and no special restrictions are imposed on frequencies, the Jacobian is quasiperiodic and different methods are needed to perform stability analysis.

3.5.2. States arising directly from symmetries. Symmetries are extremely useful in analyzing various states of equivariant networked dynamical systems [**50**, **114**], determining the observability and controllability of such dynamical systems [**39**, **100**, **155**], as well as studying their global behaviors via transfer operators and their numerical approximations [**130**]. Likewise, if the decoupled state arises from symmetries alone, these symmetries can be used to assist in stability calculations using linear representation theory as shown below. Though the case of $m_i \neq m_j$ can appear as a result of symmetries, we first focus on the case of uniform m. The symmetries of the Jacobian in that case are a combination of the symmetries associated with the orbital partition of the network, and the symmetries leading to the splay state. The splay state symmetries show up as follows. If $i \in C_{p_1}^{q_1}$ and $j \in C_{p_2}^{q_2}$, $k \in C_{p_3}^{q_3}$ and $l \in C_{p_4}^{q_4}$, for $((q_1 - q_2) \mod m) = ((q_3 - q_4) \mod m)$ it is the case that $J_{ij} = J_{kl}$ if $A_{ij} = A_{kl}$ (in other words, the coupling within each block is defined by a circulant matrix). This simply follows from the general form of the dynamics we consider in eq. (3.1). Below we present the conditions under which these symmetries (e.g., discussed in [**4**]) can be used to simplify the linear stability calculations.

Let M be the coupling matrix, and let Γ be the automorphism group of the matrix. The group is formed by permutation matrices P_γ that act by relabeling the network nodes. Let $\Sigma_c \subseteq \Gamma$ be its subgroup such that its orbit partitions the nodes into decoupled splay clusters. Let $\Sigma_s \subset \Sigma_c$ be the subgroup such that its orbit partitions the nodes further into fully synchronized clusters. To obtain decoupled splay clusters of equal winding number m, we require Σ_c (and therefore Σ_s) to be subgroups of $(S_{n_1} \times ... \times S_{n_k}) \times Z_m$. Additionally, we require $Z_m \subseteq \Sigma_c$. Here, S_{n_i} refers to the symmetric group of degree n_i.

Since Σ_s leads to fully synchronized clusters, it can be used to block diagonalize the Jacobian according to its isotypic components (or, equivalently, irreducible representations) [**114**]. The symmetries of the splay states and their effect on the structure of the Jacobian, however, can also be taken into account, and the Jacobian can be block diagonalized according to the irreducible representations of Σ_c instead, leading to a finer structure [**43**, **50**]. This results in a new coordinate

system, defined by a linear transformation T, such that TJT^{-1} is block diagonal, and thus simplifies the calculation of its associated eigenvalues (static J case, periodic state) or Floquet exponents (for quasiperiodic state with linearly evolving inter-cluster phase differences). A more detailed outline of the process is presented in section 3.7.2.

We first consider how the considerations above can be applied to a previously discussed example of a ring of oscillators.

EXAMPLE 3.5.1. *We consider a ring of eight oscillators (similar to example 3.4.1). The automorphism group of the graph is the cyclic group* $\Gamma = Z_8$. *The subgroup of the full automorphism group,* $\Sigma_c = Z_4$, *corresponds to partitioning the nodes into four clusters according to its group orbit. The subgroup of* Σ_c, $\Sigma_s = Z_2$, *partitions each of the orbits into fully synchronized clusters. Using the results above, we can block diagonalize the Jacobian matrix using the irreducible representations of the symmetry group* Z_4, *going from a* 16×16 *matrix to one with* 4 *blocks, each of the size* 4×4. *A detailed analysis is presented in Ref. [**43**], where it is also shown that the symmetries of the time-dependent Jacobian are preserved for quasiperiodic states arising from the same symmetry group.*

Next, we present how to perform this simplification for a "cube" of eight oscillators. The ring and cube networks exhibit the same decoupled state, but the stability simplification process is different.

EXAMPLE 3.5.2. *We now consider a (3D) cube consisting of eight oscillators (a general discussion of decoupling in hypercubes can be found, e.g., in [**4**], but stability has not been addressed previously). The full symmetry group of such a network is* $\Gamma = S_4 \times Z_2$. *Its subgroup* $\Sigma_c = Z_2 \times Z_2$ *corresponds to fully synchronized clusters (shown on fig. 3.9). Its subgroup* $\Sigma_s = Z_2$ *corresponds to decoupling between even and odd nodes with antisynchronization between nodes in each cluster as shown on fig. 3.9, where only the nodes in inner and outer ring are fully synchronized among each other. A detailed stability calculation for an example of adjacency coupled Stuart Landau oscillators is presented in section 3.7.3. Again, the simplification results in going from a* 16×16 *matrix to* 4, 4×4 *blocks, but the linear transformation* T *is different from the one in example 3.5.1. We focus*

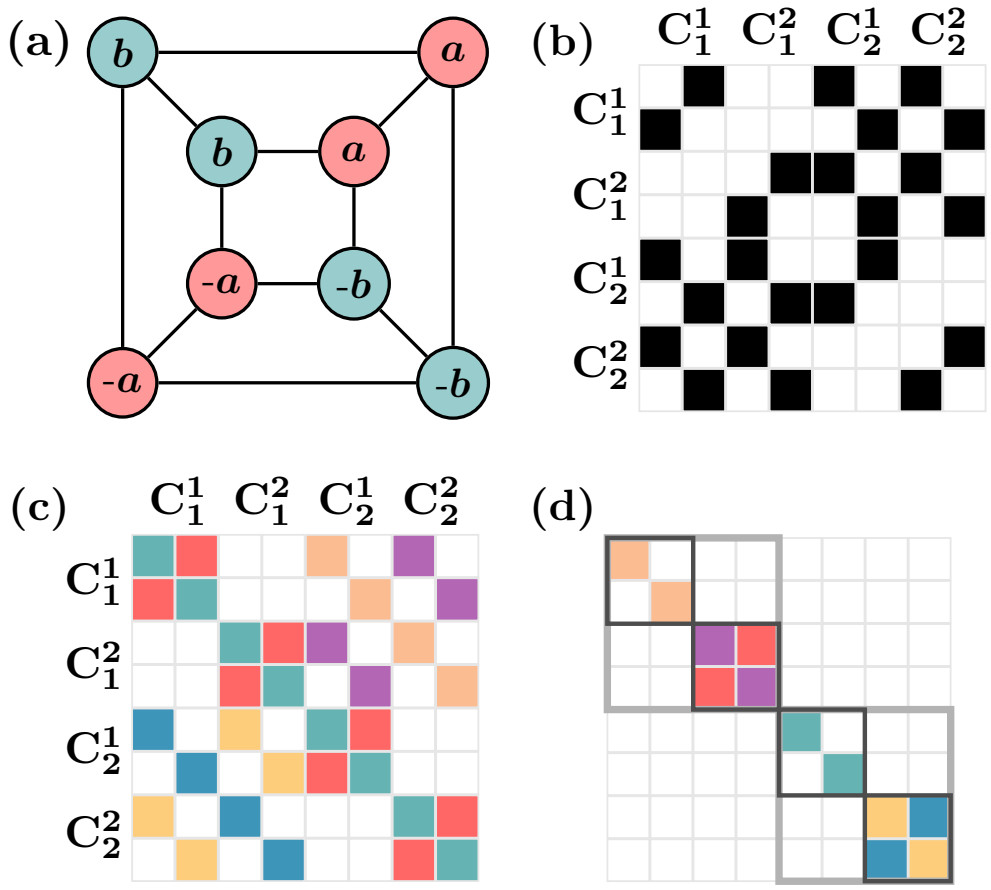

FIGURE 3.9. Example of a state on an eight-node coupled network and its Jacobian structure. (a) State of a network, where colors represent different decoupled clusters. (b) Adjacency matrix structure. (c-d) Jacobians in node and symmetry coordinates respectively. Colors represent different numerical values. Each colored block corresponds to a 2×2 matrix for amplitude and phase dynamics. (d) Dark gray lines correspond to Jacobian blocks according to fully synchronized cluster symmetries. Black corresponds to the finer structure obtained by decomposing according to Σ_c.

on the case of ***identical oscillators*** *for simplicity and consider adjacency and Laplacian coupling.*

3.5.3. Beyond symmetries. Isotypic component decomposition is not directly applicable if the state does not appear as a result of symmetries. However, the stability analysis can still be simplified [**134**, **139**, **163**]. Here, we present a low-dimensional example where the analysis can be performed even without the extra simplifications.

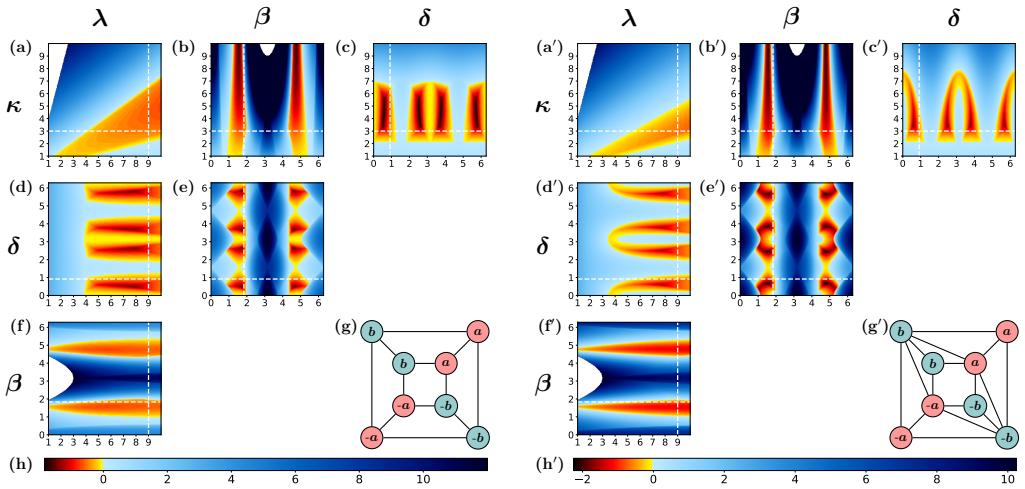

FIGURE 3.10. Linear stability of the decoupled state discussed in example 3.5.2 and section 3.7.3 for adjacency coupling. Left (a-h): coupling on a cube. Right: (a′-h′): coupling on a cube with additional edges. Subfigures (g) and (g') in the lower right corner of the stability plots show the coupling topologies linear stability was calculated for. Note that all the edges and all the nodes are assumed to have equal coupling and individual parameters. Largest transverse Jacobian eigenvalue is plotted for a set of parameters λ, σ, β, and δ (the angle between two splay clusters). Each subplot corresponds to the case where two of these parameters are fixed, and two are varied. Fixed parameters are selected from $\lambda = 9$, $\sigma = 3$, $\beta = 7\pi/12$, and $\delta = 7\pi/24$. Dashed white lines correspond to these fixed parameter values and can be used to guide comparing the subplots. Colors represent the magnitude of the real part of the maximum transverse eigenvalue of the Jacobian (blue for positive eigenvalue or linearly unstable solution, yellow and red for negative eigenvalue or linearly stable solution). The corresponding color bar is shown at the bottom of the figure. White spaces on the plots correspond to the parts of the space where there is no solution corresponding to real amplitude. The subfigures represent the following: (a) and (a′) λ vs κ; (b) and (b′) β vs κ; (c) and (c′) δ vs κ; (d) and (d′) λ vs δ; (e) and (e′) β vs δ; (f) and (f′) λ vs β; (e) and (e′) colormap.

We modify the network in example 3.5.2 to break the original network symmetries in a way that keeps the decoupled state admissible. The original topology is shown in fig. 3.10 (g). We demonstrate these topology modifications in fig. 3.10 (g′) and fig. 3.11 (g′). The coupling topology of fig. 3.10 (g′) corresponds to adding edges between different decoupled clusters such that the inter-cluster coupling terms still add up to zero. In this setting, the decoupled state can still appear in presence of adjacency coupling. We present its stability for various parameter regimes on fig. 3.10(a′-f′). The regions of parameter space where the state is stable are similar to those

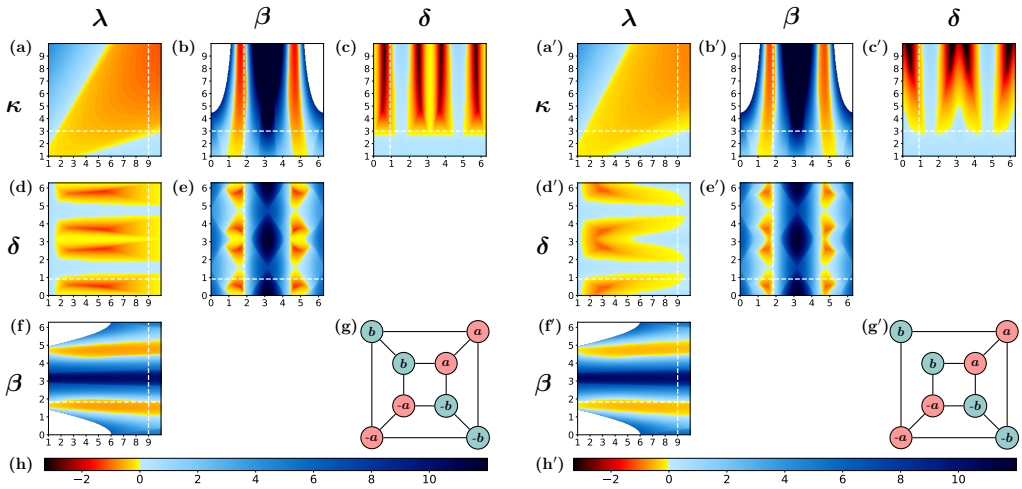

FIGURE 3.11. Linear stability of the decoupled state discussed in example 3.5.2 and section 3.7.3 for Laplacian coupling. Left (a-h): coupling on a cube. Right: (a′-h′): coupling on a cube with a removed edge. For fixed parameter values and subplot meanings see captions of fig. 3.10.

related to symmetric coupling, illustrated in fig. 3.10(a-g), though the details of the stability region boundaries differ. Similarly, we expect the modified topology to modify the shape of the state's basin of attraction once the parameters are fixed.

We also break the symmetry of the network in a way that makes the state admissible for Laplacian coupling by deleting an edge between two nodes in a fully synchronized cluster, as shown in fig. 3.11 (g'). The resulting stability diagrams are shown in fig. 3.11 (a′-f′). The stability diagrams show that symmetry breaking affects the shape of the stability regions, but preserves the possibility of observing these states in experiments, e.g., the experimental realization of networks of Stuart-Landau oscillators described in Ref. [**70**].

3.6. Conclusion and outlook

Synchronization phenomena, especially understanding the origins and stability of non-trivial synchronization patterns, are of great interest for both theoretical and practical reasons. Here we focus on states of synchronization that result from the canceling of terms in the dynamical equations of evolution that lead to decoupling of often physically coupled oscillators that rely both on the coupling structure and the phase shift invariance of the coupled dynamical equations. Such states show intriguing, emergent long-range order, such as next-nearest neighbor antiphase

synchronization with seeming independence between physically coupled nearest neighbors, as shown for the ring of 8 oscillators used as an example throughout this work (e.g., fig. 3.1 (e)). Here we consider the broad class of possible decoupled states that are accessible given the underlying network topology and the nature of the coupling between oscillators. Note that specific decoupled states have been studied in the literature previously based on symmetry considerations [**3**, **4**, **97**], but a unifying treatment of the class of states and their stability properties did not previously exist. Our work accomplishes this and also reveals that network symmetries alone are insufficient for identifying all possible decoupled states that a system can support, since the symmetries of the quotient network do not necessarily translate to the symmetries of the full network.

Specifically, we analyze the continua of decoupled states in networks of linearly coupled phase shift invariant limit cycle oscillators. We show that the eigendecomposition of the coupling matrix can reveal which decoupled states are admissible. We also formulate the admissibility criteria in the language of equitable and orbital partitions. This takes into account the balanced equivalence relations of the network as well as the symmetries of the associated quotient network and makes connections to symmetry groupoid and cluster synchronization literature. We demonstrate how various forms of decoupled states can arise in systems such as lattices of oscillators with periodic boundary conditions, and how partial amplitude death can a be part of these decoupled states.

Some of the most commonly considered cases of coupling for networked dynamical systems are the adjacency and Laplacian coupling schemes. Knowing the precise form of the coupling interactions lets us study the effect of the network structure on decoupling admissibility in great detail. We find that the Laplacian coupling scheme admits more flexibility in coupling between fully synchronized nodes, since the time evolution is not affected by the edges within fully synchronized clusters. Adjacency coupling, on the other hand, poses restrictions on the edges within fully synchronized clusters. However, it allows more flexibility in connections between different splay clusters, since the only condition that has to be imposed for the state to be admissible is that the contributions to each node from the splay clusters it does not belong to cancel out.

If the decoupled state is a direct result of network symmetries (as opposed to the symmetries of the quotient network), it is admissible for both adjacency and Laplacian coupling schemes. Additionally, in that case the stability analysis can be simplified by block diagonalizing the Jacobian

according to the irreducible representations of the symmetry group related to the state. We show how finer block sizes can be achieved by considering the symmetries beyond the automorphism group of the coupling matrix. We pick a simple eight node cube network, as well as those obtained from it by symmetry breaking edge addition and deletion, to illustrate the numerical linear stability analysis and determine what parameter regions can allow the observation of the decoupled state in simulations and experiment. We show that the stability regions are relatively robust to edge perturbations.

Our analysis of decoupled states is generalizable. For instance, it can be easily extended to networks with directed coupling, or even multilayer networks. In multilayer networks, decoupling could be present in one or more layers, or correspond to layers being decoupled from each other. In addition, the definition of the state itself can be extended to include dead nodes decoupled from all the other nodes, or, in case of Laplacian coupling, the nodes that are only attached to their cluster and therefore do not change the state of all the other nodes. In future work, it would be interesting to investigate the stability of decoupling combined with amplitude death, as that coexistence may be allowed for a larger set of network topologies. Moreover, decoupling is robust with respect to small parameter mismatch between individual oscillator parameters, as shown in experiments [**97**]. That robustness, as well as the fact that the state can be observed for diverse coupling topologies, e.g., modular coupling with all-to-all coupling between the modules, could mean decoupling can occur in natural systems such as biological networks and be related to behaviors such as remote mediated synchronization in the brain [**121**]. Since the stability analysis in presence of parameter heterogeneity exhibits sensitive dependence on the parameter values corresponding to islands of stability [**43**], such analysis is an important step towards understanding and predicting decoupling in experimental and natural systems.

3.7. Appendices

3.7.1. Decoupling in Stuart Landau oscillators. Here, we provide the form of the decoupled solution for Stuart-Landau oscillator networks and show how it leads to phenomena that have not been explicitly discussed in Stuart-Landau literature. The dynamics in presence of adjacency

coupling can be expressed as:

$$\dot{z}_j = (\lambda_j + i\omega_j - |z_j|^2)z_j + \sum_k M_{jk}\kappa_{jk}e^{i\beta_{jk}}z_k. \tag{3.22}$$

Here, M can be an adjacency matrix or a Laplacian matrix. Equivalently, in phase-amplitude coordinates:

$$\begin{aligned} \dot{r}_j &= (\lambda_j - r_j^2)r_j + \sum_k M_{jk}\kappa_{jk}r_k\cos(\beta_{jk} + \theta_k - \theta_j), \\ \dot{\theta}_j &= \omega_j + \sum_k M_{jk}\kappa_{jk}\frac{r_k}{r_j}\sin(\beta_{jk} + \theta_k - \theta_j). \end{aligned} \tag{3.23}$$

If $j \in C_p$, the only nodes that have effect on j also belong to C_p. Let

$$\tilde{\lambda} = \sum_{k\in C_p} A_{jk}\kappa_p\cos(\beta_p + \theta_k - \theta_j) \quad \text{and} \quad \tilde{\omega} = \sum_{k\in C_p} A_{jk}\kappa_p\sin(\beta_p + \theta_k - \theta_j). \tag{3.24}$$

The adjacency coupling dynamics on the decoupled state can be expressed as:

$$r_j = \sqrt{\lambda_j + \tilde{\lambda}_p}, \quad \theta_j = \theta_j(0) + (\omega_j + \tilde{\omega})t. \tag{3.25}$$

Here, the parameters β_p and κ_p are the in-cluster coupling parameters, $\theta_j(0)$ satisfy the decoupled state conditions.

For instance, if the oscillators are not directly coupled to the any other ones in their group C_p (e.g., ring topology in example 3.3.1), and the decoupled state is admissible, the solution takes form:

$$r_j = \sqrt{\lambda_j}, \quad \dot{\theta}_j = \omega_j. \tag{3.26}$$

The oscillators move at their natural frequencies in the same manner they would in absence of coupling. Their amplitudes and frequencies are uniform within splay clusters, but may differ between the clusters if parameter heterogeneity is present.

For Laplacian coupling with $M = A - D$, the dynamics is:

$$r_{j\in C_p} = \sqrt{\lambda_p + \tilde{\lambda}_p - \sum_{C_p} A_{jk}\kappa_p \cos\beta}, \tag{3.27}$$

$$\theta_{j\in C_p} = \theta_j(0) + \left(\omega_p + \tilde{\omega} - \sum_{C_p} A_{jk}\kappa_p \sin\beta\right) t. \tag{3.28}$$

Here, each coupling edge introduces a shift in oscillator amplitudes and phases.

3.7.2. Adding state symmetries to cluster synchronization. As shown in the section 3.5.2, the Jacobian of the dynamics on decoupled states commutes with the permutations generated by the actions of the group Σ_c, the orbits of which form *splay* clusters (not just the subgroup Σ_s and associated fully synchronized sub-clusters).

To block diagonalize the Jacobian matrix, we take the following steps. First, we find the projection operators $T^{(l)}$ from the following expression:

$$T^{(l)} = \frac{d^{(l)}}{h} \sum_{\kappa} \chi_{\kappa}^{(l)} \sum_{g\in\kappa} R_g \tag{3.29}$$

Here, $d^{(l)}$ is the dimension of the lth irreducible representation of Σ_c, h is the size of the symmetry group Σ_c, κ is a conjugacy class, χ_κ are the characters corresponding to a conjugacy class κ and an irreducible representation l, and R_g are the linear representations of group elements $g \in \Sigma_c$ in a form of permutation matrices.

Stacking the eigenvectors ot $T^{(l)}$ provides a projection matrix T, which can be used to transform the Jacobian into a block diagonal form: $J_{BD} = TJT^{-1}$. A more detailed description of the process as applied to clusters of identically synchronized oscillators can be found in recent cluster synchronization literature [**114**], and the process of obtaining the projection can be simplified using computational group theory tools developed to address this problem [**57**].

3.7.3. Detailed example of stability calculations. Here, we provide explicit stability matrix block diagonalization for example 3.5.1 and a periodic solution. We consider the Stuart Landau

oscillator dynamics:

$$\dot{z}_j = (\lambda + i\omega - |z_j|^2)z_j + \sum_k M_{jk}\kappa e^{i\beta} z_k. \tag{3.30}$$

The adjacency matrix A and the form of the decoupled state of interest z_{dc} are:

$$A = \left(\begin{array}{cc|cc|cc|cc} 0&1&0&0&1&0&1&0\\ 1&0&0&0&0&1&0&1\\ \hline 0&0&0&1&1&0&1&0\\ 0&0&1&0&0&1&0&1\\ \hline 1&0&1&0&0&1&0&0\\ 0&1&0&1&1&0&0&0\\ \hline 1&0&1&0&0&0&0&1\\ 0&1&0&1&0&0&1&0 \end{array}\right),\ z_{\mathrm{dc}} = \begin{pmatrix} a\\ a\\ -a\\ -a\\ b\\ b\\ -b\\ -b \end{pmatrix}. \tag{3.31}$$

where $|a| = |b|$. In case of adjacency coupling, $M = A$, and $M = A - D$ for Laplacian coupling. The time evolution in case of adjacency coupling is defined by:

$$r_j(t) = \sqrt{\lambda + \kappa\cos\beta},\ \dot{\theta}_j(t) = \omega + \kappa\sin\beta. \tag{3.32}$$

If the coupling is Laplacian,

$$\begin{aligned} r_j(t) &= \sqrt{\lambda - 2\kappa\cos\beta},\\ \dot{\theta}_j(t) &= \omega - 2\kappa\sin\beta. \end{aligned} \tag{3.33}$$

Let $\Sigma_c = Z_2 \times Z_2$ be the group defining the splay clusters, as discussed in section 3.5. The group has two commuting generators (we denote them by α and β, and the identity element by e), and the corresponding representations acting on the coupling matrix are:

$$R_\alpha = I_{4\times 4} \otimes \begin{pmatrix} 0&1\\ 1&0 \end{pmatrix}, \tag{3.34}$$

$$R_\beta = I_{2\times 2} \otimes \begin{pmatrix} 0&1\\ 1&0 \end{pmatrix} \otimes I_{2\times 2}. \tag{3.35}$$

All elements of this group commute with the adjacency matrix A (as well as L). The group has four irreducible representations, with characters presented in the table below.

	e	α	β	$\alpha\beta$
χ_{11}	1	1	1	1
χ_{12}	1	-1	1	-1
χ_{21}	1	1	-1	-1
χ_{22}	1	-1	-1	1

The projections onto the isotypic component basis are then defined by their nontrivial eigenvectors:

$$T_{11} = \begin{pmatrix} 1 & 1 & 1 & 1 & 0 & 0 & 0 & 0 \\ 0 & 0 & 0 & 0 & 1 & 1 & 1 & 1 \end{pmatrix}, \tag{3.36}$$

$$T_{12} = \begin{pmatrix} 1 & 1 & -1 & -1 & 0 & 0 & 0 & 0 \\ 0 & 0 & 0 & 0 & 1 & 1 & -1 & -1 \end{pmatrix}, \tag{3.37}$$

$$T_{21} = \begin{pmatrix} 1 & -1 & 1 & -1 & 0 & 0 & 0 & 0 \\ 0 & 0 & 0 & 0 & -1 & 1 & -1 & 1 \end{pmatrix}, \tag{3.38}$$

$$T_{22} = \begin{pmatrix} 1 & -1 & -1 & 1 & 0 & 0 & 0 & 0 \\ 0 & 0 & 0 & 0 & -1 & 1 & 1 & -1 \end{pmatrix}. \tag{3.39}$$

The transformation matrix can be obtained by vertically stacking these projection matrices.

To illustrate the stability calculation, we first provide the form of the Jacobian evaluated at the decoupled state:

$$J = \left(\begin{array}{cc|cc|cc|cc} J_D & J_{11}^{11} & 0 & 0 & J_{12}^{11} & 0 & J_{12}^{12} & 0 \\ J_{11}^{11} & J_D & 0 & 0 & 0 & J_{12}^{11} & 0 & J_{12}^{12} \\ \hline 0 & 0 & J_D & J_{11}^{11} & J_{12}^{12} & 0 & J_{12}^{11} & 0 \\ 0 & 0 & J_{11}^{11} & J_D & 0 & J_{12}^{12} & 0 & J_{12}^{11} \\ \hline J_{21}^{11} & 0 & J_{21}^{21} & 0 & J_D & J_{11}^{11} & 0 & 0 \\ 0 & J_{21}^{11} & 0 & J_{21}^{21} & J_{11}^{11} & J_D & 0 & 0 \\ \hline J_{21}^{21} & 0 & J_{21}^{11} & 0 & 0 & 0 & J_D & J_{11}^{11} \\ 0 & J_{21}^{21} & 0 & J_{21}^{11} & 0 & 0 & J_{11}^{11} & J_D \end{array}\right). \tag{3.40}$$

Here, each element is a 2×2 block. Except for the self-interaction blocks, J_D (denoted by J_D^A and J_D^L respectively), the blocks are the same for adjacency and Laplacian coupling. The blocks

are defined by:

$$J_D^A = \begin{pmatrix} \lambda - 3r^2 & \kappa r \sin\beta \\ -\kappa/r \sin\beta & -\kappa\cos\beta \end{pmatrix}, \quad J_D^L = \begin{pmatrix} \lambda - 3r^2 - 3\kappa\cos\beta & \kappa r\sin\beta \\ -\kappa/r\sin\beta & -\kappa\cos\beta \end{pmatrix},$$

$$J_{11}^{11} = \kappa \begin{pmatrix} \cos\beta & -r\sin\beta \\ r\sin\beta & \cos\beta \end{pmatrix}, \quad J_{12}^{11} = \kappa \begin{pmatrix} \sin\delta & r\cos\delta \\ r\cos\delta & -\sin\delta \end{pmatrix}, \; J_{12}^{12} = -J_{12}^{11}, \tag{3.41}$$

$$J_{21}^{11} = \kappa \begin{pmatrix} -\sin\delta & r\cos\delta \\ r\cos\delta & \sin\delta \end{pmatrix}, \; J_{21}^{21} = -J_{21}^{11},$$

where $\delta = \delta_{12} + \beta$, and J_D^A and J_D^L refer to J_D in case of adjacency and Laplacian coupling respectively, and the values of r can be obtained from eq. (3.32) and eq. (3.33) for the adjacency and Laplacian cases respectively. Then $J_{BD} = J_1 \oplus J_2 \oplus J_3 \oplus J_4$, where:

$$J_1 = \begin{pmatrix} J_D + J_{11} & 0 \\ 0 & J_D + J_{11} \end{pmatrix}, \quad J_2 = \begin{pmatrix} J_D + J_{11} & J_{12}^{11} - J_{12}^{12} \\ J_{21}^{11} - J_{21}^{21} & J_D + J_{11} \end{pmatrix}$$

$$J_3 = \begin{pmatrix} J_D - J_{11} & 0 \\ 0 & J_D - J_{11} \end{pmatrix}, \quad J_4 = \begin{pmatrix} J_D - J_{11} & -J_{12}^{11} + J_{12}^{12} \\ -J_{21}^{11} + J_{21}^{21} & J_D - J_{11} \end{pmatrix}. \tag{3.42}$$

Additional zero structure within J_1 and J_3 arises from the form of eq. (3.41). The eigenvalues of J_1 and J_3 can be computed analytically. This reduced the size of the Jacobian blocks and speeds up the stability computations.

We present a linear stability diagram for such a system as a function of parameter values λ, κ, β, and $\delta_{1,2}$ in fig. 3.10 and fig. 3.11 for adjacency and Laplacian cases respectively. Colors show the value of the maximum transverse Lyapunov exponent $\eta_{\max}$. We note that the symmetries of equations lead to $\mathrm{Re}(\eta(\delta))_{\max} = \mathrm{Re}(\eta(\pi/2 - \delta))_{\max}$, $\mathrm{Re}(\eta(\delta))_{\max} = \mathrm{Re}(\eta(-\delta))_{\max}$, and $\mathrm{Re}(\eta(\beta))_{\max} = \mathrm{Re}(\eta(-\beta))_{\max}$, where ηs stand for the Jacobian eigenvalues, and all the parameters not stated in parentheses (e.g., $\lambda, \omega, \kappa, \delta_{12}$ for $\eta(\beta)$) are kept constant.

CHAPTER 4

Analyzing states beyond full synchronization on hypergraphs requires methods beyond projected networks

Preprint available as Salova, A., & D'Souza, R. M. (2021). Analyzing states beyond full synchronization on hypergraphs requires methods beyond projected networks. arXiv preprint arXiv:2107.13712.

A common approach for analyzing hypergraphs is to consider the projected adjacency or Laplacian matrices for each order of interactions (e.g., dyadic, triadic, etc.). However, this method can lose information about the hypergraph structure and is not universally applicable for studying dynamical processes on hypergraphs, which we demonstrate through the framework of cluster synchronization. Specifically, we show that the projected network does not always correspond to a unique hypergraph structure. This means the projection does not always properly predict the true dynamics unfolding on the hypergraph. Additionally, we show that the symmetry group consisting of permutations that preserve the hypergraph structure can be distinct from the symmetry group of its projected matrix. Thus, considering the full hypergraph is required for analyzing the most general types of dynamics on hypergraphs. We show that a formulation based on node clusters and the corresponding edge clusters induced by the node partitioning, enables the analysis of admissible patterns of cluster synchronization and their effective dynamics. Additionally, we show that the coupling matrix projections corresponding to each edge cluster synchronization pattern, and not just to each order of interactions, are necessary for understanding the structure of the Jacobian matrix and performing the linear stability calculations efficiently.

4.1. Introduction

The framework of dynamical systems on dyadic networks provides a useful tool for modeling the behavior of many systems, including those from biological, social, and engineered realms [**16**, **34**,**35**,**119**,**123**]. However, some systems have higher order non-additive interactions which require going beyond dyadic interactions [**17**,**24**]. Hypergraphs are a natural extension of dyadic networks that allow the study of a wider range of systems by capturing higher-order interactions. Naturally, adding higher order interactions requires modifying tools from systems with dyadic interactions to be applicable to dynamics on hypergraphs and also developing new tools to analyze the system's behavior.

There are several ways higher order dynamics can be defined. Namely, dynamics can be defined on the nodes interacting via hyperedges of different orders [**45**, **85**, **93**, **136**, **137**, **138**, **159**, **162**]. Alternatively, especially if the dynamics is defined on a simplicial complex, the dynamical signals can be defined on simplices of different dimensions [**41**,**47**,**101**]. Here, we take the former approach. Specifically, we consider dynamics on undirected hypergraphs, where the evolution of each node depends on the state of its neighbors via dyadic and higher order interactions. Additionally, we assume that some sets of nodes within the system have similar internal dynamics, and some sets of edges have similar coupling forms. We specifically study cluster synchronization where groups of oscillators in the system have fully synchronized trajectories, but distinct groups follow distinct trajectories. The framework of cluster synchronization is useful for analyzing intricate patterns of synchronization in dynamical systems on hypergraphs and it illustrates the difference between analysis based on full hypergraph considerations and those based on dyadic projections.

To study synchronization in higher order systems, the generalization of the dyadic graph adjacency and Laplacian matrices are useful tools. Several ways to generalize these matrices from the perspective of node interactions have been recently proposed [**30**,**37**,**45**,**93**]. These generalizations are based on projecting the higher order edges onto dyadic cliques and finding the adjacency or Laplacian of a resulting network for each order of interactions. Specifically, the projections of this form are sufficient to formulate stability conditions for full synchronization on undirected hypergraphs [**37**, **45**, **93**] and chemical hypergraphs [**105**] or even some cases of cluster synchronization, such as non-intertwined cluster synchronization [**162**]. A downside of hypergraph projection is the

non-applicability of such analysis to more intricate types of synchronization dynamics in higher order systems. In this manuscript, we demonstrate that the hypergraph projection description is not sufficient for analyzing cluster synchronization in the most general case.

First we show that the projection is not always in one-to-one correspondence with the original higher order system. In other words, several non-isomorphic hypergraphs can have the same projection onto a dyadic network. Specifically we demonstrate that distinct hypergraphs can have the same projection, yet the effective interactions on the hypergraphs can be distinct even for the same pattern of cluster synchronization (i.e., which nodes follow the same trajectory, and which do not). It is these effective interactions between the clusters that determine the dynamical behavior. Projections are sensitive enough for capturing full synchronization dynamics and its stability properties, but do not necessarily capture more intricate patterns of synchronization.

We next compare the symmetries of the full hypergraph with the symmetries of its dyadic projections to show that the hypergraph does not always admit the same cluster synchronization patterns as one would deduce from its dyadic projections. Symmetry considerations, namely the orbits of the symmetry group of the system (as well as its subgroups), can be used to determine some of the admissible cluster synchronization states [**50**, **114**]. While the symmetries of the projected hypergraph are often in direct correspondence with the symmetries of the original hypergraph [**45**], we demonstrate that for some topologies, some of the symmetries of the projected network do not preserve the hypergraph structure (also discussed in Ref. [**107**]).

Our final contribution is showing how projected networks can be used for stability calculations. In systems with purely dyadic interactions, cluster synchronization states do not necessarily arise from symmetries alone [**142**]. They can also arise from more general balanced equivalence relations. This is also the case for systems with higher order interactions, both for Laplacian-like coupling [**126**, **129**] and more general couplings discussed in this manuscript. To analyze general cluster synchronization patterns whether they arise from symmetries or more generally from equitable partitions, we define the concept of *edge clusters* with each edge cluster corresponding to a specific *edge synchronization pattern*. We demonstrate that one needs to define a separate projected adjacency matrix for each edge synchronization pattern and hyperedge order to fully

capture the structure of the Jacobian matrix used for linear stability analysis (discussed in detail in section 4.8.1).

Linear stability calculations can be simplified using simultaneous block diagonalization [**163**]. We demonstrate that the set of matrices that need to be simultaneously block diagonalized to analyze cluster synchronization on hypergraphs includes the projected adjacency matrices for each edge pattern of synchronization for interactions beyond dyadic. In contrast, stability analysis for dyadic interactions does not require tracking the individual edge synchronization patterns.

The rest of the manuscript is organized as follows. section 4.2 provides the basic formulation for dynamical systems on undirected hypergraphs and the general conditions for cluster synchronization in such systems based on node and edge partitions. section 4.3 demonstrates that the hypergraph projection does not always allow us to unambiguously reconstruct the original hypergraph up to an isomorphism, which can produce misleading predictions for the effective dynamics of cluster synchronization states. In section 4.4 we consider symmetries and show that some of the orbital partitions of the projected hypergraph do not describe the admissible cluster synchronization states of the original hypergraph, thus projected adjacency matrices are not always sufficient to determine the admissible patterns of synchronization on hypergraphs. section 4.6 demonstrates that the projected hypergraph adjacency matrices combined with the cluster synchronization indicator matrices are not sufficient to fully represent the structure of the Jacobian and simplify its analysis in the case of the most general hypergraph structure and pattern of synchronization. Instead, we show how to use projections corresponding to different cluster synchronization patterns to perform the linear stability analysis. Finally, we discuss our results and future directions in section 4.7.

4.2. Background: cluster synchronization oh hypergraphs

4.2.1. Hypergraph structure and dynamics. First, we define the general form of the dynamics on hypergraphs that is being considered. A hypergraph is defined by a set of N nodes and a set of hyperedges $e_j \in \mathcal{E}$. In this work, we focus on undirected hyperedges. Let $\mathcal{E}_i \subset \mathcal{E}$ be the set of hyperedges that contain node i. Each hyperedge $e_j \in \mathcal{E}_i$ contains a set of nodes $e_j = \{i, j_1, ..., j_{m-1}\}$. The order of the hyperedge e_j is m, which is the number of nodes including i that are part of it. Thus, $m = 2$ corresponds to dyadic edges, $m = 3$ to triadic edges, etc.

Using notation similar to Ref. [**37**], we can express the evolution of the state of each node in the system, $x_i \in R^n$, as:

$$\dot{x}_i = F_i(x_i) + \sum_{e \in \mathcal{E}_i} G_e(x_i, x_{e\setminus i}). \tag{4.1}$$

Here, the function $F_i(x_i)$ describes the evolution of uncoupled nodes, and the function $G_e(x_i, x_{e\setminus i})$ is a coupling function corresponding to the influence of the hyperedge e on node i, where x_i is the state of the node i itself, and $x_{e\setminus i}$ is the state of the rest of the edge. This setup is general, including the case when the interaction hypergraph is a simplicial complex which has the additional requirement that each subset of nodes in the hyperedge forms a hyperedge of lower order.

Often, some degree of homogeneity is present within the nodal dynamics, $F_i(x_i)$, of different nodes i as well as in the coupling dynamics, $G_e(x_i, x_{e\setminus i})$. In that case, one can use the hypergraph structure to find nontrivial partitions into sets of nodes that can fully synchronize. In the simplest case, all the self-dynamics are characterized by the same function F and the coupling dynamics of a given order m are characterized by the same function $G^{(m)}$. In that case, it is sufficient to consider adjacency structures (e.g., adjacency tensors) with binary entries.

The exact higher order adjacency structure can be defined in terms of the collection of m incidence matrices $I^{(m)}$, one for each order m. Let $\mathcal{E}_i^{(m)}$ be the set of hyperedges of order m containing the node i. Then, the nonzero elements of the incidence matrix are $[I^{(m)}]_{i,e} = 1$ if $e \in \mathcal{E}_i^{(m)}$. Additionally, we assume undirected coupling, so $[I^{(m)}]_{i,e} = 1$ for all $i \in e$.

With these simplifications, the dynamics of eq. (4.1) can be expressed as:

$$\dot{x}_i = F(x_i) + \sum_{m=2}^{d} \sigma^{(m)} \sum_{e \in \mathcal{E}^{(m)}} [I^{(m)}]_{i,e} G^{(m)}(x_i, x_{e\setminus i}), \tag{4.2}$$

where due to undirected coupling we assume that the function $G^{(m)}(x_i, x_{e\setminus i})$ is invariant under any reordering of nodes in $x_{e\setminus i}$.

In Ref. [**129**], we cover the stability analysis in the case of Laplacian and Laplacian-like coupling. Here, we assume more general undirected coupling. In the case of undirected coupling, the presence of the hyperedge $\{i_1, ..., i_k, ..., i_m\}$ providing input to node i_1 via the coupling function $G^{(m)}$, s.t. $\dot{x}_{i_1} = ... + G^{(m)}(x_{i_1}, ..., x_{i_k}, ..., x_{i_m})$, implies that hyperedge affects x_{i_k} via the

same coupling function, s.t. $\dot{x}_{i_k} = ... + G^{(m)}(x_{i_k}, ..., x_{i_1}, ..., x_{i_m})$. Additionally, the coupling function responsible for providing input into node x_{i_1} has to be invariant with respect to permutations of the elements corresponding to the nodes providing this input within a hyperedge, namely, $G^{(m)}(x_{i_1}, ..., x_{i_k}, ..., x_{i_{k'}}, ...) = G^{(m)}(x_{i_1}, ..., x_{i_{k'}}, ..., x_{i_k}, ...)$. For a concrete example of triadic coupling, consider the extension of the Kuramoto model to triadic interactions presented in Ref. [**160**], with $G^{(3)}(x_i, x_j, x_k) = K \sin(\theta_j + \theta_k - 2\theta_i)$, where we set the coupling strengths $\sigma^{(3)}$ to be identical for all triadic edges. First, we note that $G^{(3)}(x_i, x_j, x_k) = G^{(3)}(x_i, x_k, x_j)$. In addition, for the coupling to be undirected, we require that $I_{i,e} = I_{j,e} = I_{k,e}$, where the edge e consists of nodes i, j, and k.

4.2.2. Bipartite representation of a hypergraph. While incidence matrices are a useful and compact representation of the hypergraph structure, sometimes it is helpful to deal with square matrices instead. Thus, hypergraphs represented via a bipartite graph will be useful for much of the analysis herein. The adjacency matrix $\mathcal{M}$ of the bipartite representation of a hypergraph is of the form:

$$\mathcal{M} = \begin{pmatrix} 0_{N\times N} & I_{N\times M} \\ I^T_{N\times N} & 0_{M\times M} \end{pmatrix}, \tag{4.3}$$

where N is the number of nodes in the hypergraph, M is the number of edges, and I is its incidence matrix. While this matrix is less compact than the incidence matrix, this bipartite graph representation allows the use of standard dyadic interaction tools in analyzing systems with higher order interactions, as $\mathcal{M}$ is a square matrix.

An important caveat here is that one needs to additionally take into account that the elements of $\mathcal{M}$ represent the relations between nodes and edges, and not simply the interactions between the nodes. This is discussed in more detail in section 4.3 in the context of hypergraph isomorphism and section 4.4 in relation to admissible patterns of cluster synchronization.

4.2.3. Dyadic projections of hypergraphs. A common way to analyze hypergraph structure and full synchronization dynamics is by using the projection of the hypergraph structure onto a dyadic coupling matrix for each order of interaction. Depending on the type of the coupling

function, either an adjacency or Laplacian projection can be used. In several recent publications [**30**, **37**, **45**, **93**], the projected matrices for each order of interactions are defined as:

$$\mathcal{A}^{(m)} = I^{(m)}[I^{(m)}]^T - \mathcal{D}^{(m)}, \tag{4.4}$$

where $[\mathcal{D}^{(m)}]_{ii} = \sum_j I_{ij}^{(m)}$ and has zero off-diagonal elements.

This projection is useful in analyzing, for instance, the stability of full synchronization in systems with higher order interactions, by either forming an aggregate projection matrix with different edge orders being assigned different weights [**30**, **37**, **93**], or considering projected Laplacians in case of noninvasive coupling [**45**]. However, in some cases, this projection loses information about the original hypergraph even for a given order of interactions (e.g., triadic), as discussed in section 4.3 and section 4.4. Additionally, these projections are insufficient for cluster synchronization analysis, which is why we need to define such a projection for every *edge pattern of synchronization*, as discussed in section 4.6.

4.2.4. Admissible patterns of cluster synchronization on hypergraphs. While projection matrices are useful in analyzing full synchronization, collective behavior of coupled dynamical systems is more complicated when the nodes are not fully synchronized. Often, it is useful to analyze these behaviors using the framework of cluster synchronization, where the nodes in the same clusters C_i are fully synchronized due to receiving the same dynamical input, but their behavior is distinct from all the other clusters C_j. Cluster synchronization can arise as a form of symmetry breaking in systems with identical nodes and edges (or hyperedges of the same order) that allow full synchronization. However, it can also be present in systems with multiple node and edge types, such as multilayer networks, in which full synchronization solutions are not admissible.

Patterns of cluster synchronization have been extensively analyzed for systems with dyadic interactions [**18**, **31**, **114**, **127**], with a few recent advances to higher order systems. Cluster synchronization of coupled map lattices on chemical hypergraphs was recently analyzed in Ref. [**21**], but the setup is distinct from the general structure and dynamics considered in this manuscript. Stability of cluster synchronization in systems like the one in eq. (4.2) is analyzed in Ref. [**162**]. However, the question of admissibility of different patterns is not discussed there, and the analysis is limited to non-intertwined clusters. Finally, cluster synchronization on hypergraphs is briefly

discussed in Ref. [**45**]. However, the reference only discusses the patterns of synchronization arising from symmetries and does not discuss the ones arising from more general partitions (e.g., discussed in Ref. [**129**] and later herein). Additionally, the conditions for symmetry-based clusters in Ref. [**45**] may not be sufficient for general hypergraphs, and additional checks must be performed as discussed in detail in section 4.4.

In this section, we demonstrate how to find the admissible cluster synchronization patterns by partitioning the nodes into node clusters, and the edges into edge clusters based on the node clusters those edges span. The framework is similar to that in Ref. [**129**], but we do not restrict the coupling functions to *Laplacian-like* coupling. As an example of cluster synchronization, consider fig. 4.1(a). The hypergraph structure shown on the left admits a cluster synchronization pattern with two node clusters, shown in purple and teal. Each purple node p obtains input from two hyperedges, one of the form $C^{(3)}_{ppp}$ (containing three nodes in the purple cluster) and one $C^{(3)}_{ptt}$. Each teal node t gets input from two edges of the form $C^{(3)}_{ptt}$. We will index the node clusters as C_j (where j can refer to a cluster number or a cluster "color"). Here, the node clusters are $C_1 = C_p = \{1, 2, 3\}$ and $C_2 = C_t = \{4, 5, 6\}$. The edge clusters induced by node partition (i.e., hyperedges which span equivalent node clusters, and, therefore, have equivalent node trajectories) are denoted by $C^{(m)}_j$. In this example, $C^{(3)}_1 = C^{(3)}_{ppp} = \{[1, 2, 3]\}$ and $C^{(3)}_2 = C^{(3)}_{ptt} = \{[1, 4, 5], [2, 4, 6], [3, 5, 6]\}$. The bipartite graph in fig. 4.1(a) (right) demonstrates the relations between nodes (circles) and edges (triangles). The bipartite graph makes it clear that there are two triadic edge clusters ($C^{(3)}_1$ shown in olive and $C^{(3)}_2$ shown in yellow) induced by the node clusters.

The cluster synchronization pattern in fig. 4.1(a) is not the only admissible pattern. fig. 4.1 (a-d) shows four distinct example partitions, using direct hypergraph representation (left column) and its bipartite representation (right column).

Mathematically, the condition for an admissible cluster synchronization state based on the incidence matrix is

$$\sum_{e_j \in C^{(m)}_k} I^{(m)}_{ij} = \sum_{e_j \in C^{(m)}_k} I^{(m)}_{i'j} \tag{4.5}$$

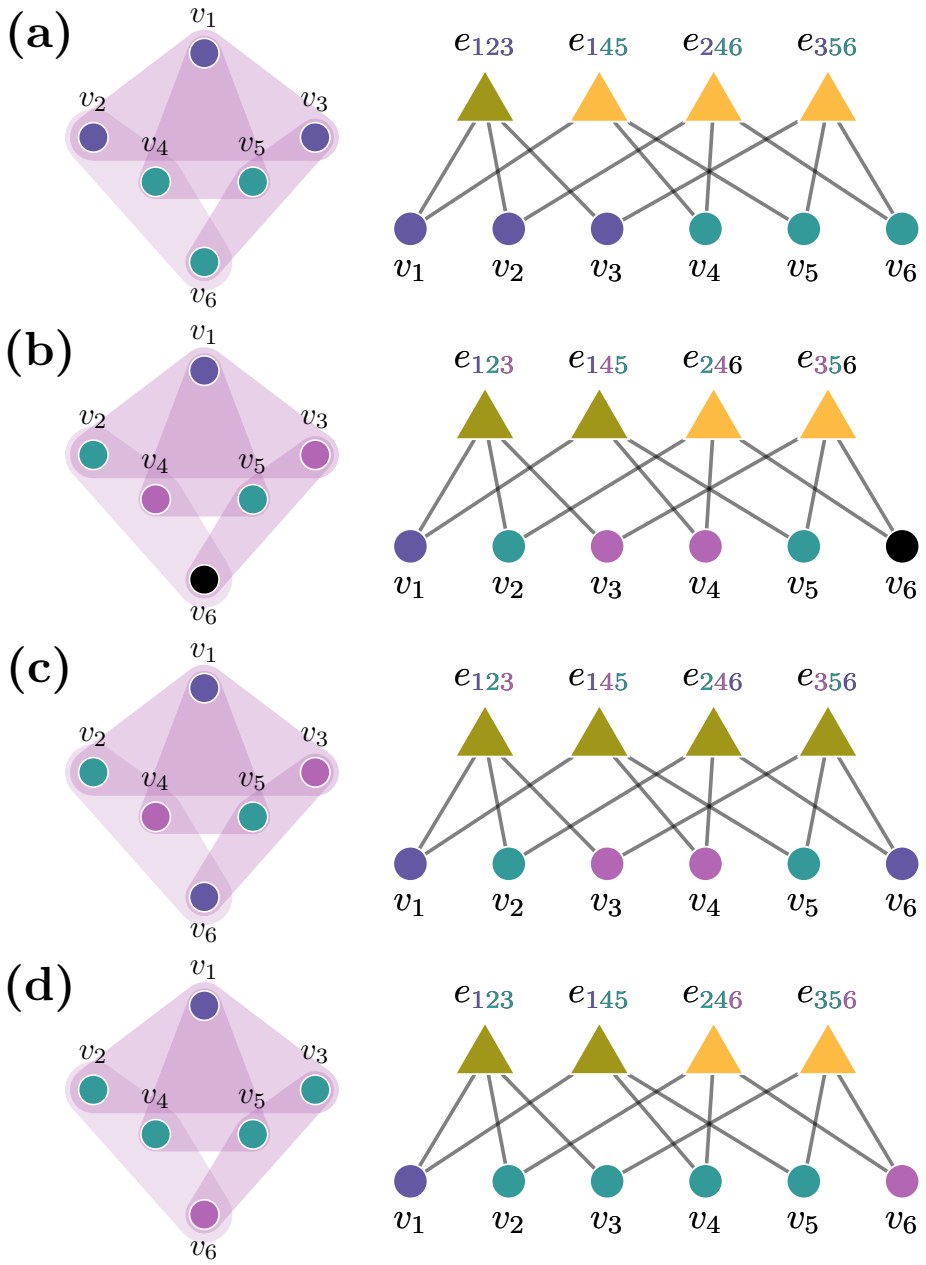

FIGURE 4.1. Synchronization patterns in hypergraphs. Left column: hypergraph, right column: equivalent bipartite representation. [(a-d)] Distinct cluster synchronization patterns.

where $i, i' \in C_l$, and the summation is performed over all the columns of $I^{(m)}$ corresponding to the edges in the kth edge cluster of order m, denoted by $C_k^{(m)}$. eq. (5.2) has to hold for all the orders of interaction and edge clusters, unless the specific form of the coupling function makes some edge

clusters irrelevant to cluster synchronization admissibility (e.g., fully synchronized hyperedges in Ref. [**129**]).

The effective interactions between different clusters are contained in the *quotient hypergraph*, where

$$I_{\text{eff}}^{(m)} = \mathcal{P}_n I^{(m)} (\mathcal{P}_e^{(m)})^T, \tag{4.6}$$

where $\mathcal{P}_n$ $(K \times N)$ and $\mathcal{P}_e^{(m)}$ $(K_m \times N)$ are the indicator matrices corresponding to node and edge partitions, and $I^{(m)}$ is the mth order incidence matrix. The nonzero elements of the indicator matrices $\mathcal{P}_n$ and $\mathcal{P}_e^{(m)}$ are defined by $[\mathcal{P}_n]_{i,j} = 1$ if node i belongs to node cluster C_j, and $[\mathcal{P}_e^{(m)}]_{i,j} = 1$ if the mth order edge i belongs to the mth order edge cluster $C_j^{(m)}$.

Note that eq. (5.2) can be easily modified to handle the case where there are different types of nodes and hyperedges in the system. If distinct node types are present, only the ones within the same type are expected to fully synchronize. To put it in the form of eq. (5.2), we can form a trivial incidence matrix $I^{(1)}$, where $I_i^{(1)} = I_j^{(1)}$ if and only if the nodes i and j are of the same type, and add those incidence matrices to the set that needs to be tested in eq. (5.2). If distinct hyperedge types are present, eq. (5.2) has to hold for each edge interaction order m and for each edge type.

Equivalently, the bipartite graph adjacency matrix (eq. (4.3)) can be used to partition nodes and edges into clusters using the methods applicable to systems with dyadic interactions (even for systems with different types of nodes and hyperedges). Importantly, since we distinguish between nodes and edges, they need to be partitioned into clusters separately (corresponding to the case of two distinct types of nodes in systems with dyadic interactions). It is also important to note that for each *node* partition obtained from the bipartite representation, only the coarsest *edge* partition is properly identified. For instance, fig. 4.2 demonstrates two partitions admissible on the bipartite graph, whose structure corresponds to the hypergraph with six nodes (shown as circles in the bipartite graph) and four triadic edges (shown as shaded triangles). However, only one of the resulting partitions (fig. 4.2 top right) is an admissible partition of the nodes and hyperedges of the hypergraph itself. fig. 4.2 bottom right shows that partitioning the bipartite representation can misidentify the edge partitions induced by the node partitions. In this case, all hyperedges contain

the same nodes (purple, teal, violet), and thus have to belong to the same edge cluster, although the bipartite representation divides them into two edge clusters.

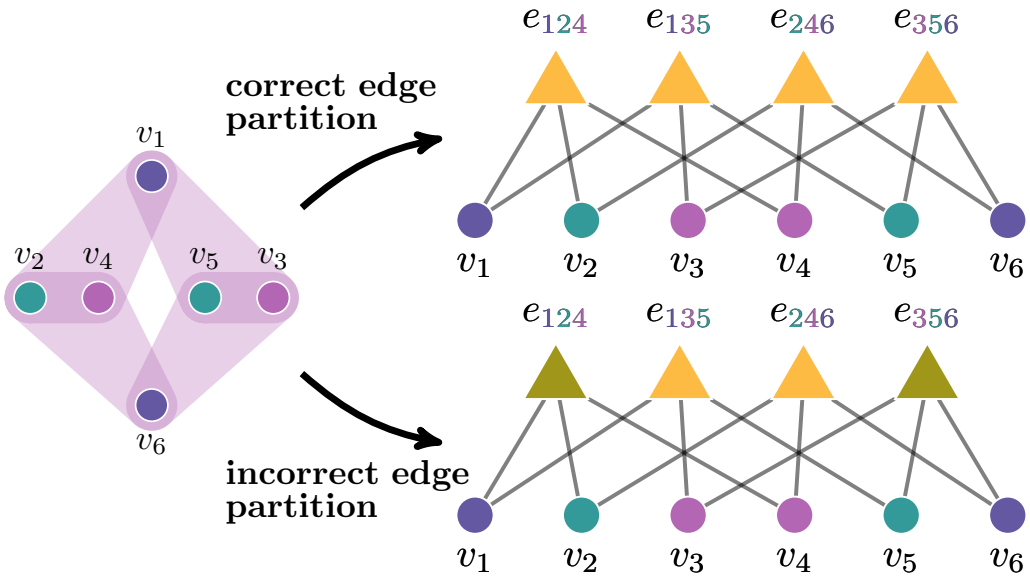

FIGURE 4.2. Left: cluster synchronization pattern on a hypergraph. Right: equitable partitions of the corresponding bipartite network. Only the top partition represents the correct node and edge partition of the hypergraph. In the bottom partition, the hyperedges e_{124} and e_{356} are incorrectly assigned into a cluster distinct from that containing e_{135} and e_{246}, even though all the hyperedges consist of one violet, one purple, and one teal node.

4.3. Hypergraph dyadic projection: loss of information on structure and effective dynamics

Hypergraph projections can be used to analyze fully synchronized states and their stability [**37**, **45**]. However, this tool is not always useful in analyzing general dynamics on hypergraphs, including cluster synchronization. Initial results obtained in Ref. [**37**] led its authors to conjecture that it is possible to create a hypergraph projection (with the adjacency matrix calculated as a weighted sum of terms defined in eq. (4.4)) that fully preserves the information about the hypergraph structure. However, we show the projection as defined in eq. (4.4) does not necessarily correspond to a unique hypergraph. In fact, these distinct hypergraphs that get mapped onto the same single projection do not even have to be isomorphic, as we show next in section 4.3.1. As a result, sometimes the

hypergraphs with the same node clusters and projected adjacency matrix have distinct quotient hypergraphs, and thus different cluster synchronization dynamics.

4.3.1. Example: non-isomorphic hypergraphs with distinct effective dynamics but identical dyadic projection. Identical hypergraphs, as well as isomorphic hypergraphs, produce identical dynamical behavior, including cluster synchronization. However, the hypergraphs that map onto the same projected network are not necessarily identical or isomorphic, and therefore can produce distinct dynamical behavior despite having the same projection. This can be investigated computationally, especially since the problem can be considered on a single order of higher order interactions at the time, because distinct orders can be distinguished in the projection.

To obtain hypergraphs that are not isomorphic, but which have the same projected dyadic adjacency matrix, it is sufficient to find two distinct incidence matrices, $I_1^{(m)}$ and $I_2^{(m)}$, that satisfy

$$I_1^{(m)}[I_1^{(m)}]^T - D^{(m)} = I_2^{(m)}[I_2^{(m)}]^T - D^{(m)} = \mathcal{A}^{(m)}, \tag{4.7}$$

with no nontrivial permutational matrix P satisfying

$$P(\mathcal{M}_1 + \mathcal{R}) = (\mathcal{M}_2 + \mathcal{R})P, \tag{4.8}$$

where $\mathcal{M}_1$ and $\mathcal{M}_2$ are the respective adjacency matrices corresponding to the bipartite graph representation of the original hypergraphs. Here, $\mathcal{R}$ is a diagonal matrix whose purpose is to avoid permuting nodes with edges. It has diagonal entries $\mathcal{R}_{ii} = \alpha$ if $i \leq N$ and $\mathcal{R}_{ii} = \beta$ if $i > N$. In numerical calculations, α and β can be set to be distinct random numbers.

As an example, consider two distinct hypergraphs with triadic interactions, each with six nodes and seven hyperedges. The first is shown in the box shaded in purple in fig. 5.1(a), and the second in the box shaded in olive in fig. 5.1(d). Both fig. 5.1(a) and fig. 5.1(d) are the union of the two simpler hypergraphs shown in the respective boxes. The hypergraphs in the left column of fig. 5.1(a) and (d) are isomorphic but distinct, whereas the right column hypergraphs are identical. Note, the full hypergraphs in fig. 5.1(a) and (d) are not isomorphic. The graph isomorphism problem is notoriously complicated. However, we used the *networkx.is_isomorphic* Python package [**56**] to verify that indeed $\mathcal{M}_1 + \mathcal{R}$ corresponding to fig. 5.1(a) is not isomorphic to $\mathcal{M}_2 + \mathcal{R}$ corresponding

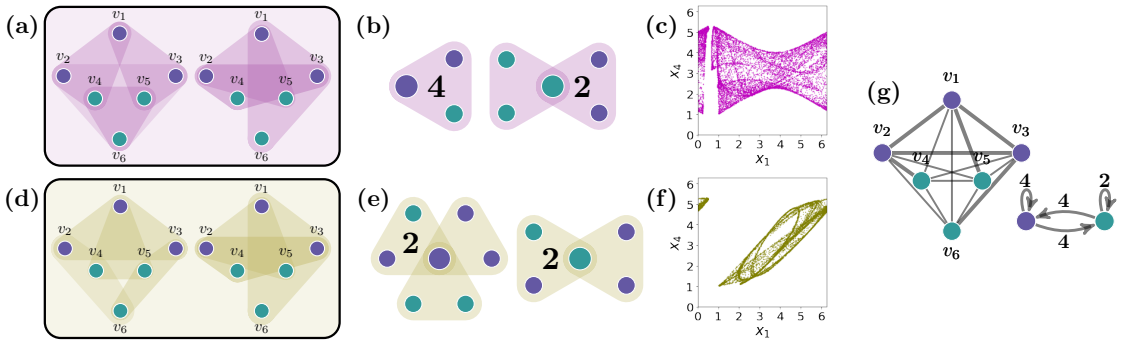

FIGURE 4.3. Synchronization patterns in hypergraphs. Teal and violet node colors correspond to distinct node synchronization clusters. [(a) and (d)] Hypergraph structure of two distinct hypergraphs (violet box (a) and olive box (d)) containing the union of hypergraphs shown on the left and on the right. The left hypergraphs in (a) and (d) are distinct, but isomorphic to each other. The right hypergraphs in these boxes are fully identical. [(b) and (e)] Distinct quotient hypergraphs for cases (a) and (d) respectively. [(c) and (f)] State of node 4 (x_4) vs state of node 1 (x_1) using eq. (4.12) dynamics evolved for 10^4 time steps for the two-cluster state on hypergraphs (a) and (d) respectively. Node 1 belongs to the violet cluster, node 4 belongs to the teal cluster. (g) The same projected network (left) and its quotient network (right) results for both cases (a) and (d). Thick lines correspond to edges of weight two, and thin lines correspond to those of weight one.

to fig. 5.1(d). We denote their incidence matrices by I_1 and I_2. The corresponding projected dyadic graph for both of the above hypergraphs, containing edges of weight 1 and 2 (shown in thin and thick lines respectively), is demonstrated in fig. 5.1(g). Its adjacency matrix is

$$\mathcal{A}^{(3)} = I_1^{(3)}(I_1^{(3)})^T - \mathcal{D}^{(3)} = I_2^{(3)}(I_2^{(3)})^T - \mathcal{D}^{(3)} = \begin{pmatrix} 0 & 1 & 1 & 2 & 2 & 2 \\ 1 & 0 & 1 & 2 & 1 & 1 \\ 1 & 1 & 0 & 1 & 2 & 1 \\ 2 & 2 & 1 & 0 & 2 & 1 \\ 2 & 1 & 2 & 2 & 0 & 1 \\ 2 & 1 & 1 & 1 & 1 & 0 \end{pmatrix}.$$

Thus, the conditions from eq. (4.7) hold: two non-isomorphic hypergraphs, fig. 5.1(a) and (d), s.t. no nontrivial permutation satisfies eq. (4.8) for their bipartite adjacency matrices $\mathcal{M}_1$ and $\mathcal{M}_2$, have the same projected adjacency matrix.

The fact that non-isomorphic hypergraphs may have the same projected graph has consequences on the cluster synchronization dynamics. Specifically, the inability to reconstruct the original hypergraph may lead to an ambiguity in effective dynamics in a hypergraph, even if the node assignment into clusters is the same between the two hypergraphs. As an example, consider the

coloring of nodes on fig. 5.1. In all its subfigures, teal and violet nodes represent distinct clusters. This cluster assignment is admissible in both hypergraphs in fig. 5.1(a) and (d). The corresponding quotient hypergraphs are shown respectively in fig. 5.1(b) and (e). These hypergraphs represent the effective dynamics of each type of node (teal and violet). As very clearly visible in fig. 5.1, these quotient hypergraphs are qualitatively different. The dynamics on each type of nodes in case of fig. 5.1(b) is:

$$\begin{aligned} \dot{x}_p &= F(x_p) + 4G^{(3)}(x_p, x_p, x_t), \\ \dot{x}_t &= F(x_t) + G^{(3)}(x_t, x_t, x_t) + 2G^{(3)}(x_t, x_p, x_p), \end{aligned} \tag{4.9}$$

whereas in case of fig. 5.1(e) it is:

$$\begin{aligned} \dot{x}_p =& F(x_p) + 2G^{(3)}(x_p, x_p, x_t) + G^{(3)}(x_p, x_p, x_p) + G(x_p, x_t, x_t), \\ \dot{x}_t =& F(x_t) + 2G^{(3)}(x_t, x_p, x_t) + G^{(3)}(x_t, x_p, x_p), \end{aligned} \tag{4.10}$$

leading to distinct behaviors.

To provide a concrete example of distinct trajectories arising from eq. (4.9) and eq. (4.10), we consider the discrete time dynamics:

$$x_i^{t+1} = F(x_i^t) + \sigma^{(3)} \sum_{e \in \mathcal{E}^{(m)}} [I^{(3)}]_{i,e} G^{(3)}(x^t_{e\setminus i}), \tag{4.11}$$

where x_i^t is the state of the node i at time t, and the self evolution and coupling functions are defined as:

$$F(x_i^t) = \alpha \frac{1 - \cos(x_i^t)}{2} + \frac{\pi}{6}, \quad G^{(3)}(x_j^t, x_k^t) = \frac{1 - \cos(x_j^t + x_k^t)}{2}. \tag{4.12}$$

This oscillator dynamics is the optoelectronic dynamics defined in Ref. [**31**] with added triadic interactions. We also use this dynamics in section 4.6.2. Here, we chose the parameters $\alpha = 0.5$ and $\sigma^{(3)} = 1.5$. fig. 5.1(c) demonstrates the dynamics of two clusters (teal and violet) on the hypergraph shown in fig. 5.1(a), and fig. 5.1(f) demonstrates the dynamics of these clusters on the hypergraph shown in fig. 5.1(d). The dynamics of the two-cluster state are clearly distinct for these different hypergraph topologies with the same projected network.

Here, we covered one of the mechanisms that leads to non-isomorphic hypergraphs having the same projected adjacency matrix. Namely, it requires picking two isomorphic hypergraphs, and breaking the isomorphism by adding the same set of additional hyperedges. Clearly, if additional identical interactions of any order are present in both hypergraphs, eq. (4.7) still holds and the hypergraphs will have the same projection.

Note that in case of complete synchronization, distinct hypergraphs with the same dyadic projection produce the same effective behavior, so this phenomenon only arises for more complicated dynamical states.

4.3.2. Does loss of information from the projection occur frequently in randomly selected hypergraphs? To estimate if the information loss from projecting the hypergraph is frequent for a given number of nodes (n_{nodes}) and hyperedges (n_{edges}), we investigate how often the condition in eq. (4.7) holds for pairs of hypergraphs with hyperedges added at random.

It is known that bipartite network projections may exhibit data loss. In fact, it was shown that in some cases, non-isomorphic bipartite networks with incidence matrices I_1 and I_2 can have identical projections corresponding to node and edge interactions, i.e., $I_1 I_1^T = I_2 I_2^T$ and $I_1^T I_1 = I_2^T I_2$, but those cases are rare [**71**]. Here, we consider a similar problem in the context of hypergraphs, but only require the node interaction projections to be identical. In fact, for the example discussed in fig. 5.1, $I_1^T I_1 \neq I_2^T I_2$. This leaves us a wider range of options to explore. On the other hand, since we consider hypergraph projections where different edge orders can be distinguished, we only focus on matrices I with constant column sums, where these sums equal to the edge order. This restriction narrows down the types of incidence matrices we consider.

Here, we focus on the case of triadic interactions on hypergraphs. First, we create $10,000$ random hypergraphs by randomly selecting with replacement three distinct nodes that will be connected by a hyperedge n_{edges} times for each of the hypergraphs consisting of n_{nodes} nodes. We note that the resulting hypergraphs may have duplicate edges, isolated nodes, or several connected components. We accept this since in real hypergraphs, more than one edge order can be present, so the nodes that are isolated for a specific interaction order may not be isolated when all orders of interactions are considered. But we also compare the results to those considering only fully connected hypergraphs. Then, we remove the "duplicate" isomorphic hypergraphs. Finally, we

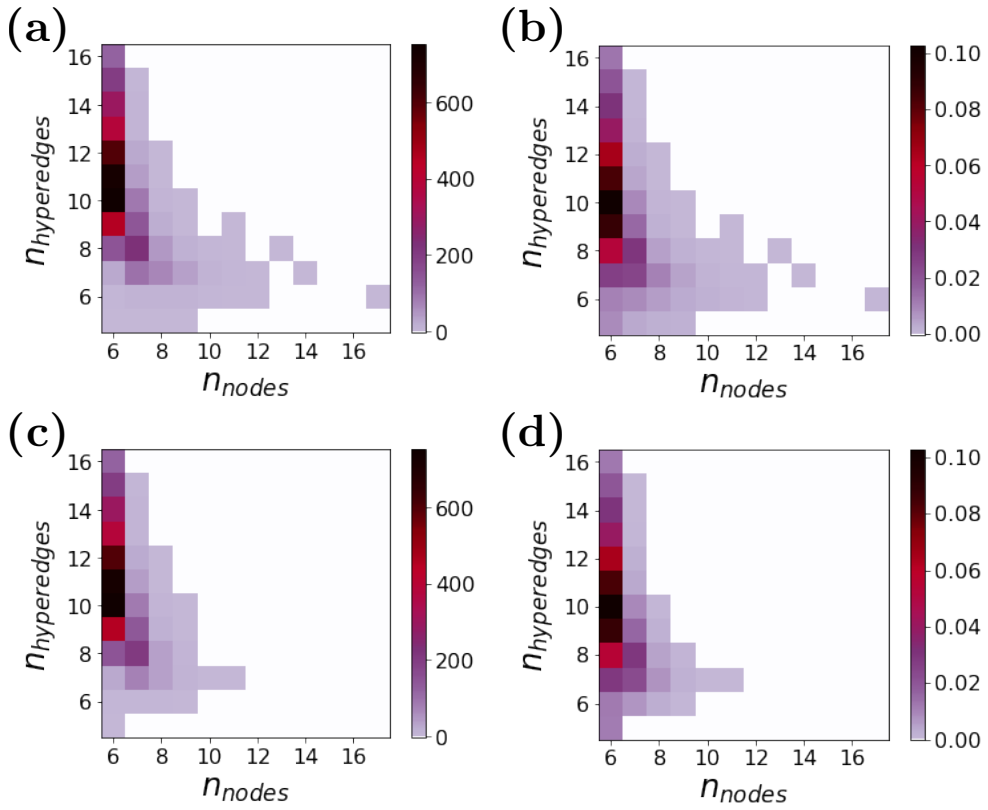

FIGURE 4.4. (a) Number and (b) fraction of pairs of non-isomorphic hypergraphs sharing the same projection for a given number of nodes and triadic hyperedges. (c) Number and (d) fraction of pairs of non-isomorphic fully connected hypergraphs sharing the same projection.

find the non-isomorphic hypergraphs satisfying eq. (4.7) and calculate the number and fractions of such pairs for each number of nodes and hyperedges. The results calculated for small numbers of nodes and hyperedges are presented in fig. 4.4. We note that while these hypergraphs are not common, they could still occur as motifs in larger hypergraphs. For example, consider two identical hypergraphs. Adding different extra hyperedges to the same subset of their nodes, s.t. those hyperedges satisfy eq. (4.7) makes the whole hypergraph satisfy eq. (4.7), producing two hypergraphs that are not isomorphic but have the same projection.

4.4. Symmetry differences between hypergraphs and their dyadic projections

Structural symmetries of hypergraphs and dyadic networks determine some of the types of synchronization patterns admissible in the system and assist in determining their stability. We

demonstrate that in some cases, there are symmetries of the projected adjacency matrix that are not the symmetries of the original hypergraph.

Specifically, consider the permutations of each order of interactions defined in Ref. [**45**]

$$P\mathcal{L}^{(m)} = \mathcal{L}^{(m)}P, \tag{4.13}$$

or, equivalently,

$$P\mathcal{A}^{(m)} = \mathcal{A}^{(m)}P, \tag{4.14}$$

where the permutation matrices P satisfying eq. (4.14) for each order of interactions form the symmetry group. For the examples studied in Ref. [**45**], the resulting symmetry group is associated with cluster synchronization states on simplicial complexes. We demonstrate that is not always the case, both in case of dynamics on simplicial complexes, or, more generally, hypergraphs. While this issue does not arise very often in randomly selected large hypergraphs, it is still important to know that using the conditions in Ref. [**45**] to obtain the patterns of cluster synchronization requires an extra step of checking that each specific pattern is admissible on the full hypergraph and not just the projections of every order. Thus, next in section 4.4.1, we develop the conditions for cluster synchronization to arise from symmetries that hold for any hypergraph structure.

4.4.1. Hypergraph symmetries. Equitable partitions (groupings of nodes into clusters, in which nodes in the same cluster receive the same input from that cluster as well as all the other clusters) give rise to the admissible cluster synchronization states for a given hypergraph structure. Equitable partitions that result from structural symmetries of the hypergraph are called orbital partitions and are a special case of more general equitable partitions [**50**, **54**]. For instance, all the partitions shown in fig. 4.1 are orbital partitions, while the ones shown later in fig. 4.7 are not. Even more flexibility is allowed for Laplacian-like coupling which requires only external equitable partitions (groupings of nodes into clusters, in which nodes in the same cluster receive the same input from all the *other* clusters, meaning that the hyperedges only containing one type of node cluster, e.g., the edge e_{123} in fig. 4.1(a), can be ignored for admissibility purposes), and patterns

arising from symmetries are less common in that case [**129**]. In summary, orbital partitions are a subset of equitable partitions, which are the subset of external equitable partitions.

Our focus in this section is structural symmetries. First, we state the algorithm for finding symmetry induced cluster synchronization patterns in systems with dyadic interactions. The automorphism group of the dyadic adjacency matrix A is formed by a set of permutation matrices P, s.t. $PA = AP$. Any subgroup of that group can be linked to an admissible cluster synchronization pattern via orbital partitions. Namely, all the subsets of the network nodes that get mapped to themselves (and thus belong to the same cell of the orbital partition) can be completely synchronized [**114**]. The approach can be generalized to systems with different types of nodes and interactions, e.g., multilayer networks of coupled oscillators where cluster synchronization requires compatibility between intra- and interlayer symmetries [**38**].

Symmetries of dyadic projected networks can not be immediately translated to those of a system with higher order interactions similarly to more general equitable partition methods. Instead, one has to consider the full hypergraph and the node and edge permutations simultaneously to assess the hypergraph synchronization patterns from the symmetry perspective. Symmetries, such as the ones analyzed in Ref. [**107**] for directed hypergraphs, arise from the hypergraph automorphism group with elements P represented as permutation matrices. We formulate the cluster synchronization condition in terms of the symmetries of the undirected hyperedges of each order m as:

$$PI = IP_{\text{edge}}. \tag{4.15}$$

Here, $P_{N\times N}$ is a permutation matrix that reorders the nodes, and $[P_{\text{edge}}]_{M\times M}$ corresponds to the permutations of the edge labels if node labels are permuted. These hyperedge permutation matrices are defined as follows:

$$[P_{\text{edge}}]_{e_i,e_j} = [P]_{i_1 j_1}...[P]_{i_m j_m}, \tag{4.16}$$

where $e_i = \{i_1, ..., i_m\}$ and $e_j = \{j_1, ..., j_m\}$ are the hyperedges. The orbits of the subgroups of the automorphism group with elements P determine the admissible cluster synchronization patterns.

Note that I here is an aggregate matrix combining all the interaction orders. Alternatively, we could consider the incidence matrices for different orders of interactions, $I^{(m)}$, separately. Then,

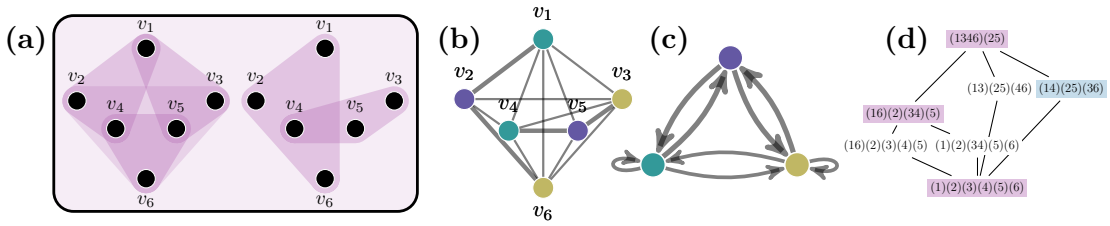

FIGURE 4.5. Symmetries of the dyadic projection (b) identify some patterns that are not admissible on the original hypergraph (a). (a) Hypergraph structure. (b) Hypergraph projection with a pattern of synchronization not admissible for the original hypergraph. (c) Quotient hypergraph of the projected network. (d) Lattice of partitions representing the admissible synchronization patterns obtained from the projection in (b). Only patterns highlighted in violet are admissible for the original hypergraph. Blue: pattern on [(b-c)].

the largest common subgroup of the symmetry groups of all the interaction orders determines the automorphism group of the hypergraph.

As an example, consider the incidence matrix corresponding to the hypergraph structure in fig. 4.1

$$I^{(3)} = \begin{array}{c} \\ 1 \\ 2 \\ 3 \\ 4 \\ 5 \\ 6 \end{array} \begin{array}{c} \begin{array}{cccc} [123] & [145] & [246] & [356] \end{array} \\ \begin{pmatrix} 1 & 1 & & \\ 1 & & 1 & \\ 1 & & & 1 \\ & 1 & 1 & \\ & 1 & & 1 \\ & & 1 & 1 \end{pmatrix} \end{array}. \tag{4.17}$$

One of the pairs containing a node permutation and its induced edge permutation satisfying eq. (4.15) is

$$P = (1)(6)(2,3)(4,5), \quad P_{\text{edge}} = ([1,2,3],[1,4,5])([2,4,6],[3,5,6]). \tag{4.18}$$

Permuting the nodes and edges simultaneously leaves the structure of the hypergraph in fig. 4.1 invariant.

4.4.2. Symmetries and square projection matrices. Projected adjacency (or, if appropriate, Laplacian) matrices are useful to study cluster synchronization from the symmetry perspective [**45**]. However, in some cases, synchronization patterns obtained from the projected matrix are not admissible as synchronization patterns of the original hypergraph.

In section 4.4.1, we demonstrated how the symmetries of a hypergraph can be obtained from the incidence matrix. Equivalently, such symmetries can be deduced from the adjacency matrix $\mathcal{M}$ of the hypergraph's bipartite representation with the additional requirement that the permutations are of the form where nodes are permuted with nodes, and edges are permuted with edges. Similarly to section 4.3.1, we add a diagonal matrix $\mathcal{R}$ to ensure that. The conditions are then

$$P_{\mathcal{M}}(\mathcal{M}+\mathcal{R}) = (\mathcal{M}+\mathcal{R})P_{\mathcal{M}}, \tag{4.19}$$

where $P_{\mathcal{M}}$ is an $(N+M)\times(N+M)$-dimensional permutation matrix. Just like in the case of other balanced equivalence relations, only the coarsest edge partitions for each node partition would be the ones that actually correspond to the hyperedge permutations. However, all the partitions of the nodes themselves are valid.

If instead of the full hypergraph we consider the projection matrix, its symmetries (elements of the automorphism group) satisfy the condition

$$P_{\mathcal{A}}^{(m)}\mathcal{A}^{(m)} = \mathcal{A}^{(m)}P_{\mathcal{A}}^{(m)}, \tag{4.20}$$

for each order m. Here, the permutation matrix $P_{\mathcal{A}}$ is an $N\times N$-dimensional permutation matrix.

First, we note that the node partitions for the original hypergraph obtained using eq. (4.19) are always a subset of those for the projection shown in eq. (4.20). This means that the admissible patterns on the hypergraph can be a proper subset of those that are admissible on the dyadic projection. In many specific hypergraph cases, the conditions in eq. (4.19) and eq. (4.20) result in equivalent group orbits, thus corresponding to identical sets of admissible cluster synchronization patterns. However, in fig. 4.5, we present an example when this equivalence does not hold. Specifically, fig. 4.5(a) shows a hypergraph with six nodes and six hyperedges. This hypergraph admits three patterns of synchronization corresponding to the orbital partitions that are shaded in violet in fig. 4.5(d). fig. 4.5(b) demonstrates the structure of the dyadic projection of the hypergraph. This

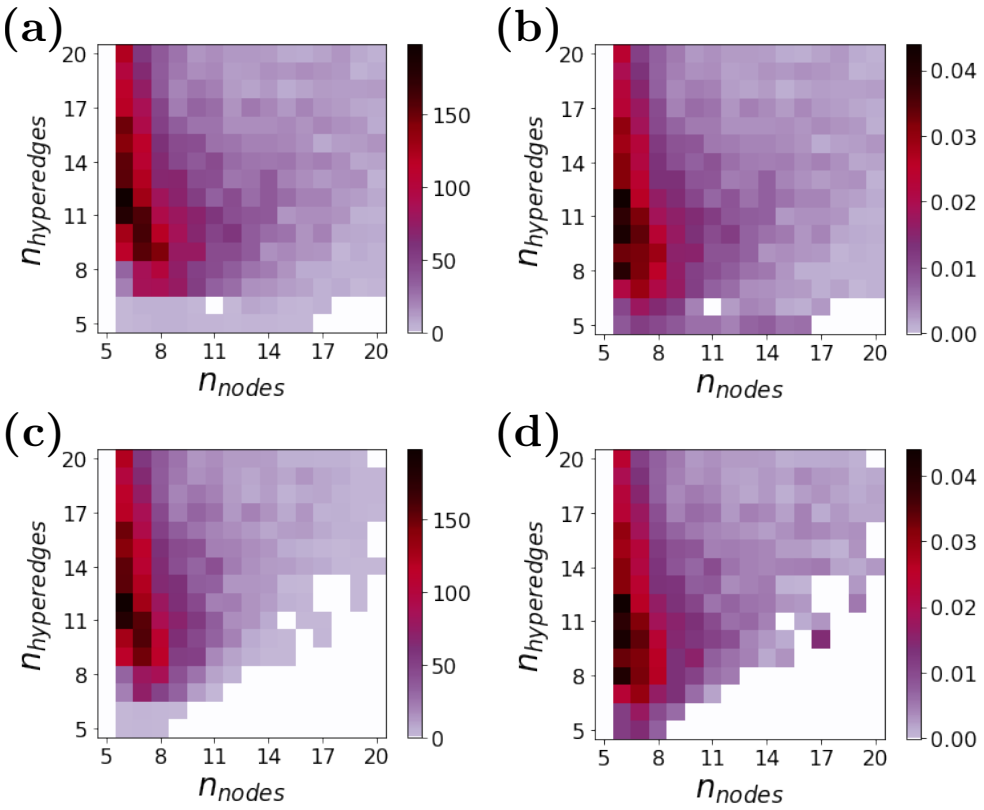

FIGURE 4.6. (a) Number and (b) fraction of hypergraphs with an automorphism group containing less elements than that of its projected network. (c) Number and (d) fraction of non-isomorphic fully connected hypergraphs with an automorphism group containing less elements than that of its projected network.

projection admits the full seven orbital partitions shown in fig. 4.5(d). One particular partition shaded in blue in fig. 4.5(d) is specifically illustrated in fig. 4.5(b), where node colors correspond to a cluster assignment arising from eq. (4.20). fig. 4.5(c) demonstrates the quotient network corresponding to the blue partition. Note that the blue partition does not correspond to a valid pattern of synchronization on the hypergraph in fig. 4.5(a) since it does not satisfy eq. (4.19).

4.4.3. How often are the symmetries of the hypergraph distinct from those of the projected network? We aim to get an idea of how often the automorphism group of the hypergraph does not have the same number of elements as that of its dyadic projection, which would result in different admissible cluster synchronization patterns. To do so, we generate a set of random non-isomorphic hypergraphs, similarly to section 4.3.2. We then find the number of node partitions induced by the symmetry group of the bipartite network representing the hypergraph

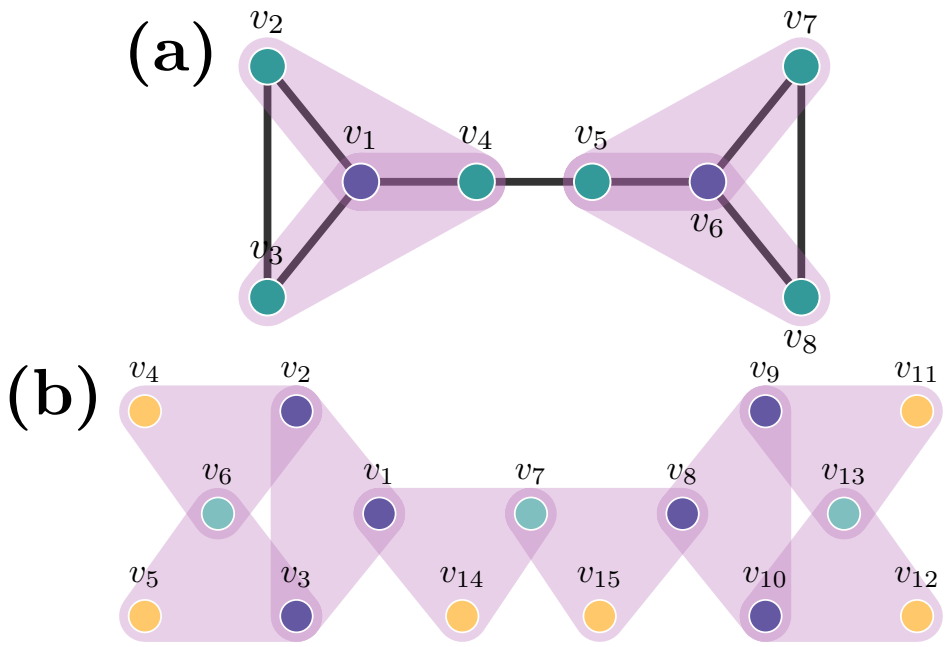

FIGURE 4.7. Examples of cluster synchronization patterns arising from equitable partitions that are not orbital partitions (in other words, patterns did not arise from symmetries). (a) Hypergraph with dyadic and triadic interactions. (b) Hypergraph with only triadic interactions.

and compare that to the number of partitions induced by the symmetry group of the projected adjacency matrix, counting the number of cases in which these numbers are not the same.

Our results are presented in fig. 4.6, where subfigures (a)-(b) consider all the hypergraphs we generate, and (c)-(d) only take into account hypergraphs with one connected component. While the number of occurrences when the hypergraph and the projection differ becomes relatively rare as the size of the hypergraph increases, the fact that they can differ means that if using, for instance, the method from Ref. [**45**], an extra step of checking which of the orbital partitions of the projected hypergraph are the orbital partitions of the original hypergraph is required.

4.5. Mismatch between equitable partitions of the hypergraph and the dyadic projection

Beyond symmetries, more generally, admissible cluster synchronization patterns arise from equitable partitions (e.g., consider the cluster synchronization patterns in fig. 4.7(a,b)). One of the

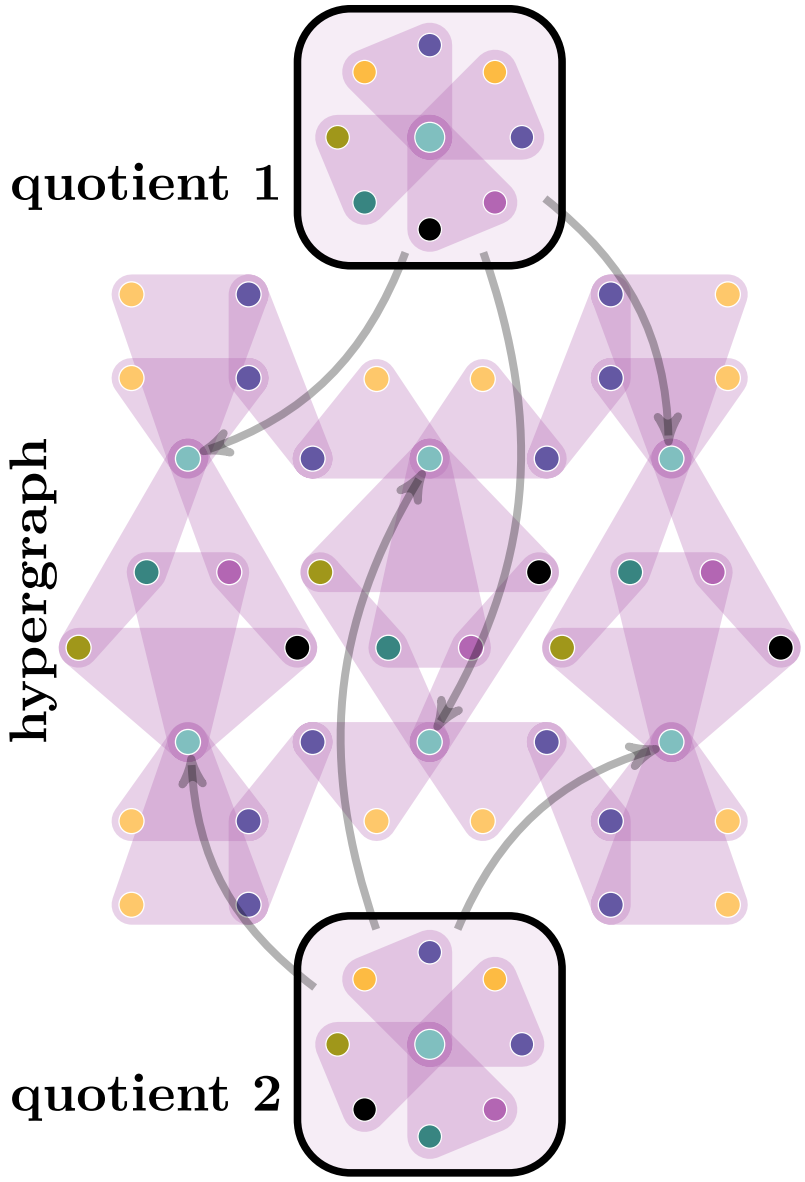

FIGURE 4.8. Example of a pattern that is not symmetry-induced, but follows from a more general equitable partition, which is not admissible on a hypergraph but is admissible on its projection. Top and bottom sub-figures (boxed, labeled as *quotient 1* and *quotient 2*) demonstrate the effective interactions of the nodes the arrows are pointing to. Since the effective interactions are distinct, the pattern is not admissible.

natural mechanisms for the latter is Laplacian and Laplacian-like coupling, where the fully synchronized edges do not add any dynamical contributions to the states of their nodes, and only

affect the system's stability [**129**]. However, even for systems with non-diffusive (adjacency) coupling, clusters do not necessarily arise from the symmetries alone. Two such examples are shown in fig. 4.7. Here, fig. 4.7(a) is an example where the dyadic synchronization pattern does not arise from symmetries, with extra hyperedges added to form a system with higher order interactions. This can hold for systems with no dyadic interactions as well, as shown by the synchronization pattern in fig. 4.7(b).

If a pattern of synchronization arises from an equitable partition that is not an orbital partition, similar mismatch between the states of the full hypergraph and its projection can be observed. For instance, fig. 4.8 demonstrates a pattern which is not symmetry induced but arises from an equitable partition. This pattern of cluster synchronization is not admissible for the full hypergraph, but is admissible on its projection.

Additionally, for some types of coupling functions partitions more general than equitable partitions are sufficient, and it is also possible in that case that that the hypergraphs have the same projection but different admissible states. For instance, consider triadic coupling of the form

$$G(x_i, x_j, x_k) = g(x_j - x_i)g(x_k - x_i), \tag{4.21}$$

where $g(x_i, x_i) = 0$, on a hypergraph with purely triadic interactions. The admissibility conditions for a cluster synchronization state given this coupling function are similar to eq. (5.2), with the caveat that a hyperedge influencing the node $i \in C_k$ can be ignored if any other node j on a hyperedge is a part of the same cluster as i, i.e., $j \in C_k$, since then $G(x_i, x_j, x_k) = 0$ when evaluated on that cluster synchronization state. Consider the isomorphic hypergraphs in fig. 4.9(a) (violet) and fig. 4.9(b) (olive). For the coupling form defined by eq. (4.21), the same cluster assignment is admissible on fig. 4.9(a) (each node in a given cluster receives the same dynamical input), but not admissible on fig. 4.9(b) (nodes 1, 2, and 3 are assigned to the same cluster, but node 3 receives the dynamical input that is different from that received by nodes 1 and 2). Since the violet and olive hypergraphs have the same dyadic projection, dyadic projection alone would not be sufficient to determine which states are admissible for a given hypergraph structure. Therefore, having full information about the hypergraph structure is essential if the coupling functions allow us to relax some of the partition admissibility conditions.

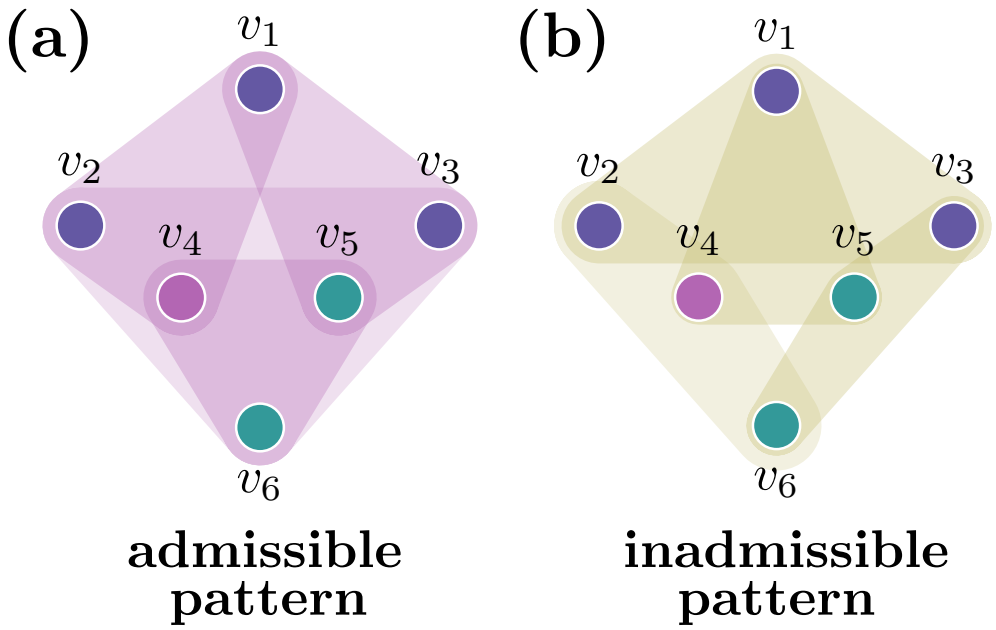

FIGURE 4.9. Three cluster pattern of synchronization (nodes in different clusters shown in different colors) on hypergraphs with the same dyadic projection. Assuming the coupling type defined in eq. (4.21), this pattern of synchronization is admissible on the violet hypergraph (a), but not the olive hypergraph (b).

4.6. Stability calculations: Jacobian block diagonalization

4.6.1. Background and dyadic interactions. Here we consider the general case where equitable partitions and external equitable partitions determine admissible cluster synchronization patterns.

Simultaneous block diagonalization, which can be based on symmetry considerations or balanced equivalence relations, is a useful tool that allows dimensionality reduction in cluster synchronization stability calculations. Tools for performing such reduction in the case of systems with dyadic interactions have been developed for systems such as networks with different types of edges, temporal networks, multilayer networks, and beyond.

Symmetry methods do not always provide the most refined block diagonal Jacobian structure [**162**]. As shown in section 4.4, while in most cases the symmetries of the hypergraph coincide with those of the projected matrix, this is not always the case. Regardless, once the symmetry group and group orbits are obtained, the irreducible representations of the symmetry group produce the block diagonalization of the Jacobian. The details of this process are discussed in section 4.8.2.

When cluster synchronization partitions come from more general balanced equivalence relations, such as equitable or external equitable partitions, different methods must be used. In systems with purely dyadic interactions, simultaneous block diagonalization of the coupling matrix and the diagonal indicator matrices corresponding to different clusters,

$$\{A, E_1, ..., E_K\}, \tag{4.22}$$

block diagonalizes the Jacobian in a simple case of identical time-independent coupling. This dimensionality reduction can be performed using the algorithm from Refs. [**162**, **163**]. Next, in section 4.6.2, we demonstrate how these results can be generalized to analyze cluster synchronization on hypergraphs.

4.6.2. Stability of cluster synchronization on hypergraphs. Here, we demonstrate how to perform and simplify symmetry-independent stability analysis for general undirected coupling (as opposed to Laplacian and Laplacian-like coupling discussed in Ref. [**129**]). The form of the dynamical equations and undirected coupling are discussed in eq. (4.2). In this section, we develop cluster synchronization analysis for general patterns. The more specialized case of stability analysis of cluster synchronization patterns arising from symmetries is discussed in section 4.8.2.

As discussed in section 4.2.3, a projected adjacency matrix for an interaction order m can be defined as:

$$\mathcal{A}^{(m)} = I^{(m)}[I^{(m)}]^T - \mathcal{D}^{(m)}, \tag{4.23}$$

where $[\mathcal{D}^{(m)}]_{ii} = \sum_j I_{ij}^{(m)}$ and has zero off-diagonal elements. To analyze cluster synchronization on hypergraphs, instead of simply using $\mathcal{A}^{(m)}$, we need to define a projected adjacency matrix $\mathcal{A}_k^{(m)}$ for each interaction order m and *edge cluster* (distinct pattern of synchronization on a hyperedge of order m induced by node clusters) indexed by k. Here,

$$\mathcal{A}_k^{(m)} = I_k^{(m)}[I_k^{(m)}]^T - \mathcal{D}_k^{(m)}, \tag{4.24}$$

where $I_k^{(m)}$ is an $N \times |C_k^{(m)}|$ matrix (here, $|C_k^{(m)}|$ denotes the number of unique elements in the edge cluster $C_k^{(m)}$) consisting of the columns of $I^{(m)}$ corresponding to the hyperedges in the kth

cluster of order m. Additionally, $\mathcal{D}_k^{(m)}$ is a diagonal matrix of node degrees corresponding to the number of edges with that synchronization pattern ($[\mathcal{D}_k^{(m)}]_{ii} = \sum_{j=1}^{N} [I_k^{(m)}]_{ij}$).

Then, the variational equation determining the linear stability of cluster synchronization states can be expressed as:

$$\begin{aligned}\delta\dot{x} = \Bigg(& \sum_{k=1}^{K} E_k \otimes JF(s_k) - \sum_{m=2}^{d} \sigma^{(m)} \cdot \\ & \Big[\sum_{k=1}^{K_m} \sum_{l \in \{C_k^{(m)}\}} \sum_{p \in \{C_k^{(m)} \setminus l\}} E_l \mathcal{A}_k^{(m)} E_p \otimes JG^{(m)}(s_l, s_p, s_{C_k^{(m)} \setminus l,p}) \\ & + \sum_{k=1}^{K_m} \sum_{l \in \{C_k^{(m)}\}} E_l \mathcal{D}_k^{(m)} \otimes JG^{(m)}(s_l, s_{C_k^{(m)} \setminus l}) \Big] \Bigg) \delta x.\end{aligned} \tag{4.25}$$

Here, $\{C_k^{(m)}\}$ is the set of *unique* node clusters included in the kth edge cluster. Additionally, $s_{C_k^{(m)} \setminus l}$ defines the set of all trajectories of nodes included in edge cluster $C_k^{(m)}$, excluding the one in the cluster C_l. Note that all node clusters and all edge clusters of all orders contribute to eq. (4.25).

The terms contributing to the off-diagonal Jacobian elements are defined as

$$[JG^{(m)}(s_l, s_p, s_{C_k^{(m)} \setminus l,p})]_{q,r} = \left. \frac{\partial G_q^{(m)}\left(x_i, x_j, x_{k_1} ..., x_{k_{m-2}}\right)}{\partial [x_j]_r} \right|_{\substack{x_i = s_l, x_j = s_p, \\ x_{k_v} = [s_{C_k^{(m)} \setminus l,p}]_v}}. \tag{4.26}$$

Similarly, the diagonal elements consist of

$$\begin{aligned}[JF(s_k)]_{q,r} &= \left. \frac{\partial F_q(x_i)}{\partial [x_i]_r} \right|_{x_i = s_k}, \\ [JG^{(m)}(s_l, s_{C_k^{(m)} \setminus l})]_{q,r} &= \left. \frac{\partial G_q^{(m)}\left(x_i, x_{k_1} ..., x_{k_{m-1}}\right)}{\partial [x_i]_r} \right|_{\substack{x_i = s_l, \\ x_{k_v} = [s_{C_k^{(m)} \setminus l}]_v}}.\end{aligned} \tag{4.27}$$

In addition, we note that if $i \in C_k$ and $j \in C_k$, $[\mathcal{D}_k^{(m)}]_{ii} = [\mathcal{D}_k^{(m)}]_{jj}$ from the cluster synchronization admissibility conditions.

While eq. (4.25) requires a lot of notation, the implication is simple: block diagonalization of the Jacobian requires the simultaneous block diagonalization of the set of cluster indicator matrices,

the dyadic adjacency projection, and the projections for each higher order edge cluster:

$$\{E_1, ..., E_K, \mathcal{A}^{(2)}, \mathcal{A}_1^{(3)}, ..., \mathcal{A}_{K_3}^{(3)}, ..., \mathcal{A}_1^{(d)}, ..., \mathcal{A}_{K_d}^{(d)}\}. \tag{4.28}$$

The reason why only considering $\mathcal{A}^{(2)}$ for dyadic interactions is sufficient is discussed in section 4.8.1.

For some topologies and synchronization patterns in systems with higher order interactions, it is only necessary to simultaneously block diagonalize the cluster indicator matrices and the projections of higher order coupling matrices, i.e.

$$\{E_1, ..., E_K, \mathcal{A}^{(2)}, ..., \mathcal{A}^{(d)}\}. \tag{4.29}$$

One of such cases, in addition to complete synchronization, is the case of noninvasive clusters [**162**], where each node in cluster C_i receives the input from the same set of nodes in cluster C_j. Others include the case when there is only one edge pattern in the hypergraph for coupling of each order, i.e. there is only one matrix $\mathcal{A}_1^{(m)} = \mathcal{A}^{(m)}$ (e.g., fig. 4.1(c)), discussed in more detail in section 4.8.1.

For more general cases, such as the cluster synchronization patterns shown in fig. 4.1(a,b,d) and in figs. 4.7 and 5.1, the conditions in eq. (4.29) are not sufficient. Thus, the direct analogy with dyadic coupling does not work, and the entire set of matrices in eq. (4.28) is required for simultaneous block diagonalization.

To provide a concrete example, we consider the dynamics of a form:

$$x_i^{t+1} = F(x_i^t) + \sum_{m=2}^{d} \sum_{e \in \mathcal{E}^{(m)}} [I^{(m)}]_{i,e} G^{(m)}(x_{e\setminus i}^t), \tag{4.30}$$

which is a discrete time analogue of eq. (4.2). Additionally, we impose the optoelectronic oscillator dynamics as discussed in Ref. [**31**] but add higher order terms. Namely, we use

$$F(x_i^t) = \alpha \frac{1 - \cos(x_i^t)}{2} + \frac{\pi}{6}, \quad G^{(2)}(x_j^t) = \sigma^{(2)} \frac{1 - \cos(x_j^t)}{2}, \tag{4.31}$$

where $\alpha = 2\pi/3 - 4\sigma^{(2)}$, with additional higher order terms

$$G^{(3)}(x_j^t, x_k^t) = \sigma^{(3)} \frac{1 - \cos(x_j^t + x_k^t)}{2} \tag{4.32}$$

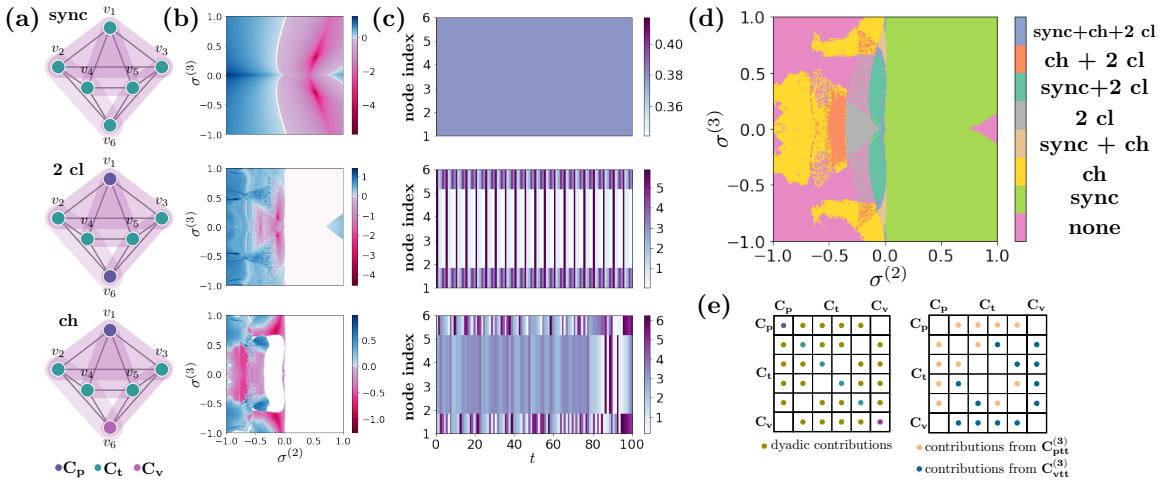

FIGURE 4.10. Stability of complete and cluster synchronization for a hypergraph of optoelectronic oscillators. (a) Synchronization patterns: full synchronization (top row), two clusters (middle row), and three-cluster chimera state (bottom row). (b) Linear stability (maximum transverse Lyapunov exponent) as a function of coupling strengths $\sigma^{(2)}$ and $\sigma^{(3)}$ for the states in part (a) based on 2.5×10^4 time steps. White regions are due to not seeing a specific state in simulations on the quotient hypergraph for 20 initial conditions. (c) Representative trajectories for each state. Full synchronization state is a fixed point, 2-cluster state is periodic with period 5, 3-cluster state can be considered a chimera state and is chaotic. (d) Regions of stability of these states plotted together. It is evident there are regions where the system is multistable. (e) Matrices that need to be simultaneously block diagonalized for stability calculation. Distinct matrices shown in distinct colors. Diagonal elements correspond to the cluster indicator matrices E_i.

introduced to add triadic hyperedge interactions. Finally, we combine this dynamics with the hypergraph structure displayed in fig. 5.3(a) to define our example system.

The hypergraph in fig. 5.3(a) consists of six coupled oscillators and supports a variety of cluster synchronization states: twenty two distinct cluster synchronization patterns are admissible, including the two extreme states where all the node trajectories are distinct and the fully synchronized state. To narrow down our analysis, we focus on three states: the fully synchronized, two-cluster, and three-cluster state as shown respectively in the rows of fig. 5.3(a). The stability properties are shown in fig. 5.3(b), and example trajectories in fig. 5.3(c). The three-cluster state can be considered a chimera state in some regions of the phase space, since each cluster exhibits chaotic behavior that is not frequency synchronized with the other clusters (an example trajectory is shown in fig. 5.3(c) bottom row). The set of matrices that need to be block diagonalized to analyze this

state is demonstrated in fig. 5.3(e). It is evident that higher order interactions have a large effect on stability, as stability regions change significantly when the triadic coupling $\sigma^{(3)}$ becomes nonzero. The numerically calculated stability regions of all three states are shown together in fig. 5.3(d) as a function of $\sigma^{(2)}$ and $\sigma^{(3)}$.

4.7. Conclusion

In this manuscript, we consider the applicability of dyadic methods for analyzing systems with higher order interactions in the context of cluster synchronization. Specifically, we consider the questions of admissibility and stability of the cluster synchronization states on hypergraphs. We show that the dyadic projection cannot be used in the most general instance and instead develop an analysis based on node and edge clusters which is sufficient.

First, we demonstrate that it is not always possible to reconstruct the hypergraph from its projected network. Since it is possible to construct the projections that distinguish between different orders of interactions, we focused our attention on distinct orders of interaction. While the cases when the information about the hypergraph is lost in the projections appear to be rare, they have strong implications on the analysis of cluster dynamics when distinct hypergraphs with identical projections both admit a specific cluster synchronization state, but have distinct quotient network structure dictating distinct dynamical evolution, as shown in fig. 5.1.

Additionally, we investigate how the patterns of synchronization admissible on the hypergraph are related to those admissible on its dyadic projected network and demonstrate that these patterns do not have to be the same. We explicitly provide examples where some of the symmetries of the projected hypergraph do not preserve the structure of the hypergraph itself, making these patterns of synchronization inadmissible.

Dyadic methods still can be used to find the admissible patterns on a hypergraph by using the adjacency matrix of the corresponding bipartite graph with additional diagonal elements. However, for large hypergraphs, it may be more efficient to find the admissible patterns on the projected network and then manually check their admissibility on the original hypergraph.

Finally, while projected networks are sufficient to define the structure of the Jacobian for the stability calculation of the *fully* synchronized state, it does not capture the full structure of the

Jacobian for cluster synchronization. For networks with purely dyadic interactions, additional diagonal matrices describing the distinct patterns of synchronization are needed to capture the Jacobian structure. However, in case of higher order interactions, even that is not sufficient. We show that for higher order interactions we generally need multiple projection matrices, each corresponding to a specific order of interactions and specific *edge* pattern of synchronization. These matrices are also useful in simplifying the stability calculations as shown in eq. (4.28).

The results on the admissibility of cluster synchronization obtained in this manuscript are easily generalizable to directed hypergraphs, just like the results for admissible clusters on dyadic networks generalize to networks with directed edges. The admissibility analysis we develop is valid for any cluster synchronization pattern on directed hypergraphs, provided that the edge clusters assignments take the hyperedge directedness into account. Linear stability analysis for patterns arising from symmetries, as discussed in section 4.8.2, is also valid for directed hypergraphs. The simplification of linear stability analysis and its interpretation for patterns arising beyond symmetry considerations can use the results from Refs. [**25**, **92**], which will again need to be generalized to higher order interactions.

In summary, hypergraph structures support a rich variety of dynamical phenomena, and hyperedges of all orders contribute to the dynamical evolution and stability calculations (see for instance eq. (4.25)). A formalism in terms of node clusters and edge clusters provides a principled way to organize the calculations for states beyond full synchronization. Such an approach may enable detailed analysis of the interplay between dyadic and higher order interactions and its impact on dynamical phenomena that can not be observed in systems with strictly dyadic interactions.

4.8. Appendices

4.8.1. When projected matrices are enough for stability calculations. Here, we consider the cases in which the non-diagonal elements of each block of the Jacobian (i.e., each part corresponding to the interactions of specific clusters C_i and C_j) coming from the same interaction order, denoted as $J^{(m)}_{C_i,C_j}$ contains only zeros and identical nonzero elements.

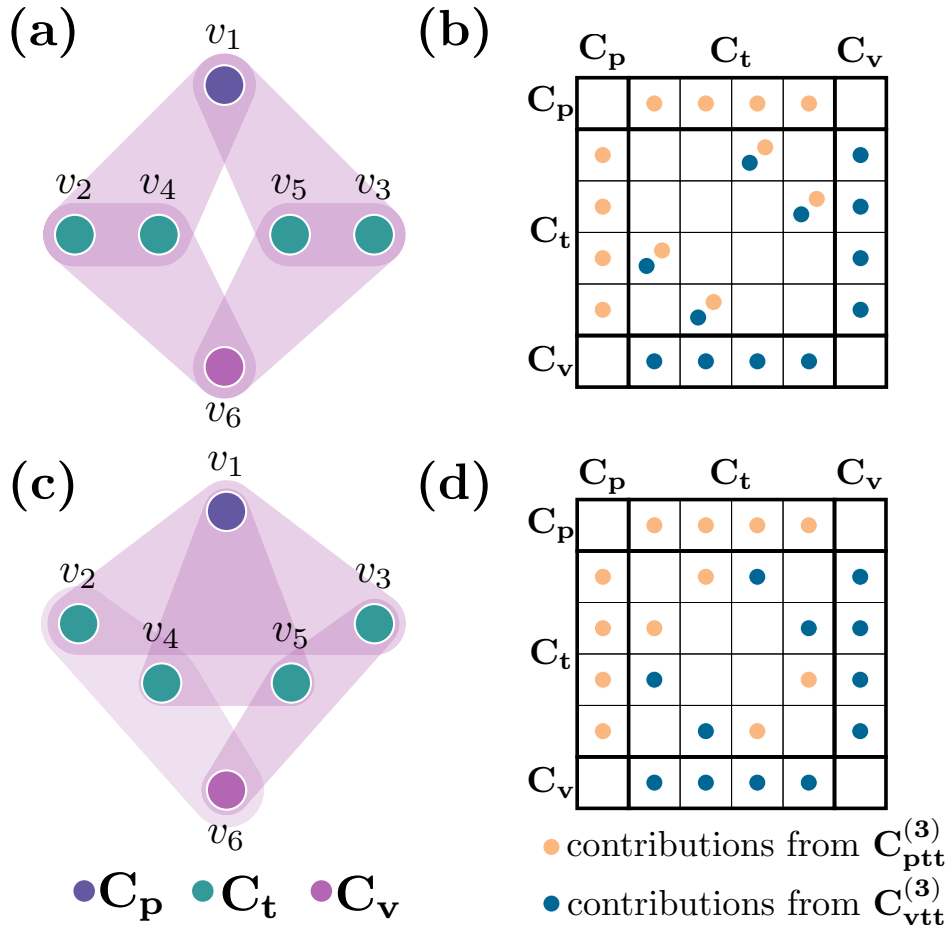

FIGURE 4.11. Example of a hypergraph and node clusters that it allows using eq. (4.29) for simultaneous block diagonalization. (a) Hypergraph and its node clusters, shown in distinct colors. (b) Jacobian structure. Distinct colors correspond to distinct edge contributions (e.g., orange corresponds to the derivatives of $G^{(3)}(s_1, s_2, s_3)$)

.

The condition above clearly holds for systems with purely dyadic interactions, since each *edge cluster* (e.g., connecting nodes in C_i to nodes in C_j) only contributes to the Jacobian blocks $J^{(2)}_{C_i,C_j}$ and $J^{(2)}_{C_j,C_i}$.

The first way for the condition to hold for higher order edges is when for each pair of node clusters on a hyperedge, the edge cluster they are contained in is unique. In this case, the elements contributing to $J^{(m)}_{C_i,C_j}$ are either zero, or equal and unambiguously determined from eq. (4.27). For instance, consider the cluster synchronization pattern in fig. 4.7(a): the condition holds for its

hyperedge clusters, $C^{(3)}_{ptt}$ and $C^{(3)}_{ppp}$. Similarly, it works for fig. 4.7(c): there is only one edge cluster, $C^{(3)}_{tvp}$. That condition, however, does not hold for fig. 4.7(b) and (d).

Now, assume there are several distinct edge clusters that contain the nodes from clusters C_i and C_j, i.e., including a pair of edge clusters satisfying $\{i,j\} \subset C^{(m)}_k$ and $\{i,j\} \subset C^{(m)}_l$. Then, for every hyperedge in edge cluster $C^{(m)}_l$ containing the nodes $a \in C_i$ and $b \in C_j$, there has to exist a corresponding hyperedge in edge cluster $C^{(m)}_k$ that contains the nodes a and b. This has to hold for every pair of such hyperedge clusters. The condition formulated here ensures that the nonzero off-diagonal Jacobian elements corresponding to the mth order interactions within each block are equal, and that they can be expressed as:

$$J^{(m)}_{a,b} = \sum_k JG^{(m)}(s_i, s_j, s_{C^{(m)}_k \setminus i,j}), \tag{4.33}$$

where $a \in C_i$, $b \in C_j$, and $\{i,j\} \subset C^{(m)}_k$.

As an example illustrating the discussion above, consider fig. 4.11(a) with three node clusters, C_p, C_t, and C_v, and two edge clusters, $C^{(3)}_{ttp}$ and $C^{(3)}_{ttv}$. There are two types of edges that contain two teal nodes, but both pairs (2 and 4; 3 and 5) are contained exactly once in each type of hyperedges present in the hypergraph ($C^{(3)}_{ttp}$ and $C^{(3)}_{ttv}$), thus satisfying the requirements in the paragraph above. As illustrated in fig. 4.11(b), each block J_{C_a,C_b} contains the same contributions within its nonzero elements, thus, the full adjacency matrix projections (eq. (4.29)) can be used for simultaneous block diagonalization. In contrast, consider fig. 4.11(c) with a hypergraph that supports the exact same pattern of synchronization but requires more intricate stability calculations. Block diagonalizing the Jacobian for fig. 4.11(c), the structure of which is schematically illustrated in fig. 4.11(d), requires a set of matrices from eq. (4.28), and exhibits different stability properties.

In summary, while under some circumstances block diagonalizing the matrices in eq. (4.29) is sufficient, eq. (4.28) is required in the most general case.

4.8.2. Stability calculations for patterns arising from orbital partitions. In the manuscript we discussed how some of the cluster synchronization patterns can be determined from symmetries (orbital partitions). Due to a general result from equivariant dynamical systems theory, the Jacobian evaluated on a cluster synchronization state commutes with the elements of the

symmetry group whose orbital partition determines the structure of that cluster synchronization state [**50**] (we denote the actions of these elements by P). Therefore, the following holds:

$$\mathcal{J}_{\text{cs}} P = P \mathcal{J}_{\text{cs}}. \tag{4.34}$$

where $\mathcal{J}_{\text{cs}}$ is the full Jacobian of the system ($\delta \dot{x} = \mathcal{J}_{\text{cs}} \delta x$) evaluated at a particular cluster synchronization state. As a result, the Jacobian can be block diagonalized using the matrices that block diagonalize the symmetry group elements P.

The individual terms of the variational equation for linear stability, eq. (4.25), can also be used to demonstrate why the full Jacobian commutes with the symmetry group action. First, we note that the diagonal cluster indicator matrices E_k commute with the permutations P ($PE_k = E_k P$), since the permutations P only permute the nodes within a specific cluster. Additionally, for the same reason, the matrices P commute with the diagonal matrices $\mathcal{D}_k^{(m)}$. We can also define the matrices $E_k^{(m)}$ to be diagonal matrices, s.t. $[E_k^{(m)}]_{ii} = 1$ if the ith hyperedge of order m belongs to $C_k^{(m)}$, and $[E_k^{(m)}]_{ii} = 0$ otherwise. Similarly, the permutations P_{edge} (as defined in eq. (4.16)) commute with the matrices $E_k^{(m)}$, as they only permute the edges within a specific edge cluster.

Finally, we use eq. (4.15) to show that the matrices $\mathcal{A}_k^{(m)} = I_k^{(m)} [I_k^{(m)}]^T - \mathcal{D}_k^{(m)}$ commute with the action of the symmetry group:

$$\begin{aligned} P I_k^{(m)} [I_k^{(m)}]^T &= P I^{(m)} E_k^{(m)} [I^{(m)} E_k^{(m)}]^T = I^{(m)} P_{\text{edge}} E_k^{(m)} [I^{(m)}]^T \\ &= I^{(m)} E_k^{(m)} P_{\text{edge}} [I^{(m)}]^T = I^{(m)} E_k^{(m)} [I^{(m)} P_{edge}^T]^T = I^{(m)} E_k^{(m)} [I^{(m)}]^T P, \end{aligned} \tag{4.35}$$

using that $P^T = P^{-1}$ is an element of the symmetry group that preserves the structure of the hypergraph and generates the orbital partition leading to the cluster synchronization pattern we consider. Therefore, all the terms of eq. (4.25) commute with the symmetry group elements P, and as a result, eq. (4.34) holds.

Group representation theory can be used to block diagonalize the Jacobian to simplify the stability calculations in a similar way they are used for systems with dyadic interactions [**114**,**140**]. Alternatively, other simultaneous block diagonalization methods are applicable and can result in a finer block diagonal structure [**163**].

The steps in symmetry-based block diagonalization may appear simpler than those discussed in section 4.6. Additionally, they apply to both directed and undirected hypergraphs. However, the calculation of irreducible representations that are then used to find the transformation of $\mathcal{J}_{\text{cs}}$ into the block diagonal form is more computationally expensive [**162**]. Moreover, the method is only applicable to systems where the state arises from symmetries, and not the larger class of systems with patterns of cluster synchronization arising from balanced equivalence relations.

CHAPTER 5

Cluster synchronization on hypergraphs

Preprint available as Salova, A., & D'Souza, R. M. (2021). Cluster synchronization on hypergraphs. arXiv preprint arXiv:2101.05464.

We develop the formalism to analyze cluster synchronization for dynamical elements coupled via hypergraphs beyond pairwise interactions. We introduce the notion of edge partitions and show how node and edge partitions allow us to identify admissible cluster synchronization states and simplify their linear stability calculations. The analysis in terms of node and edge partitions provides a principled way to track dynamics on hypergraphs, and the projected Laplacian matrices based on each edge cluster are essential to block diagonalizing the Jacobian in order to reduce the dimensionality of the stability analysis. Our work enables detailed analysis of patterns of synchronization beyond full synchronization and beyond dyadic interactions.

5.1. Introduction

Patterns of synchronization in complex interdependent dynamical systems can be essential to their function. Often, such systems are modeled by networks of agents with dyadic interactions between them [**110**]. However, studying dyadic interactions is not always sufficient. Higher order edges may be required to describe many systems, including chemical [**67**], biological [**72**], and coauthorship interactions [**59**, **94**], and processes such as consensus dynamics [**108**], making it necessary to go beyond the pairwise interaction analysis [**17**]. A hypergraph can be used to encode the structure of these higher order interactions.

Cluster synchronization is a type of synchronization where different groups of oscillators in the system follow distinct synchronized trajectories. Studies of cluster synchronization have focused on phenomena on networks with dyadic interactions, including a broad class of important behaviors such as remote synchronization and chimera states [**31**, **46**] with wide areas of applicability from

neuroscience and ecological networks to opinion dynamics [**38**, **63**, **91**, **109**, **154**]. Ideas from graph and equivariant dynamical systems theory can be applied to deduce admissible patterns of cluster synchronization on dyadic networks and simplify their stability analysis [**18**, **114**].

Recently, many contributions to analyzing synchronization on hypergraphs and simplicial complexes have been made. For instance, several recent works study full synchronization in phase oscillator models, where higher order interactions extend the range of available models and lead to new behaviors [**9**, **22**, **23**, **101**, **136**, **138**]. Performing stability analysis is crucial to determine which synchronization patterns can be observed in experiments or natural systems. Some recent works extend the master stability function formalism, originally formulated for dyadic interactions, to higher order structures to analyze full synchronization and its stability [**30**, **37**, **45**, **80**, **106**], as well as non-intertwined cluster synchronization [**162**] and cluster synchronization on chemical hypergraphs [**21**]. However, the admissibility and stability of cluster synchronization states in arbitrary systems of dynamical elements coupled via hypergraphs has not yet been considered.

In this manuscript, we formulate the conditions for cluster synchronization on hypergraph structures using external equitable partitions. Our analysis is formulated in terms of partitioning the nodes into node clusters and, additionally, "edge clusters" induced by the node partition for each order of the interactions (e.g., dyadic edge clusters, triadic edge clusters, etc.). This allows us to simplify the stability calculation by grouping the contributions to node dynamics via each of the distinct edge clusters. We then generalize the results from Refs. [**64**, **114**, **163**] (which are formulated on networks with dyadic interactions) to a hypergraph setting and show how to block diagonalize the Jacobian to simplify the stability analysis beyond dyadic interactions and non-intertwined clusters. We release accompanying code that can be used for admissibility and stability calculations [**126**].

5.2. Background

First, we define the general form of the dynamics on hypergraphs that is being considered. A hypergraph consists of a set of N nodes and a set of hyperedges $e_j \in \mathcal{E}$. In this work, we focus on undirected hyperedges. Let $\mathcal{E}_i \subset \mathcal{E}$ be the set of hyperedges that contain node i. Each hyperedge $e_j \in \mathcal{E}_i$ contains a set of nodes $e_j = \{i, j_1, ..., j_{m-1}\}$. The order of the hyperedge e_j is m, which

is the number of nodes including i that are part of it. Thus, $m = 2$ corresponds to dyadic edges, $m = 3$ to triadic edges, etc.

For each edge order m, the adjacency structure can be defined in terms of the collection of m incidence matrices $I^{(m)}$ (as illustrated in Fig.3 of Ref. [**17**]). Let $\mathcal{E}_i^{(m)}$ be the set of hyperedges of order m containing the node i. Then, for the simplest case of homogeneous edge coupling dynamics for each edge order m, the nonzero elements of the incidence matrix are $[I^{(m)}]_{i,e} = 1$ if $e \in \mathcal{E}_i^{(m)}$.

We can express the evolution of the state of each node in the system, $x_i \in R^n$, as:

$$\dot{x}_i = F(x_i) + \sum_{m=2}^{d} \sigma^{(m)} \sum_{e \in \mathcal{E}^{(m)}} [I^{(m)}]_{i,e} G^{(m)}(x_i, x_{e\setminus i}), \tag{5.1}$$

where d is the maximum edge order present in the hypergraph. Here, $\sigma^{(m)}$ denotes the strength of the mth order coupling.

The function $F(x_i)$ describes the internal dynamics of the node i, and the function $G(x_i, x_{e\setminus i})$ is a coupling function corresponding to the influence of the hyperedge e on node i, where x_i is the state of the node i itself, and $x_{e\setminus i}$ is the state of the rest of the edge. This setup is general, including the case when the interaction hypergraph is a simplicial complex and the additional requirement that each subset of nodes in a hyperedge forms a hyperedge of lower order must be satisfied.

In this manuscript, we focus on noninvasive coupling functions. Specifically, we assume that the coupling function is Laplacian or Laplacian-like for dyadic interactions and Laplacian-like for higher-order interactions. Laplacian coupling for dyadic interactions is of the form $G(x_i, x_j) = H(x_j) - H(x_i)$. Laplacian-like coupling for edges of order m is of the form $G^{(m)}\left(\sum_{l=1}^{m-1} x_{j_l} - (m-1)x_i\right)$. Coupling functions of this form are natural, for instance, for higher order networks of phase oscillators [**138**], and are not limited to systems with one-dimensional node states.

5.3. Cluster synchronization

Cluster synchronization is manifested by groups of nodes following the same trajectory over time, $x_{i_1}(t) = ... = x_{i_L}(t)$, where the groups are not fully synchronized with one another. We call each group of synchronized nodes a "node cluster" and denote them by $C_1, C_2 \ldots, C_K$ assuming K distinct groups exist. The set of dynamic trajectories followed by the nodes in each cluster, the

"node cluster trajectories", can be expressed as $s_1(t), ..., s_K(t)$. The trajectories are time-dependent, but we assume the time-dependence is implicit and use the notation $s_1, ..., s_K$ for compactness.

Likewise, we consider "edge clusters" and "edge cluster trajectories". A hyperedge of order m can be characterized by the node clusters to which the m nodes it connects together belong. All the hyperedges of order m with the same set of node clusters is called an edge cluster and denoted by $C_1^{(m)}, C_2^{(m)}, \ldots, C_{K_m}^{(m)}$, assuming K_m distinct edge clusters exist for each order m. The edge cluster trajectories are denoted by $s_{C_1^{(m)}}, s_{C_2^{(m)}}, \ldots, s_{C_{K_m}^{(m)}}$, where $s_{C_j^{(m)}}$ is the set of dynamic trajectories followed by the nodes involved in the jth edge cluster. A concrete example of node and edge clusters will be given in Fig. 5.1. The node and edge clusters with their corresponding trajectories will be used to facilitate stability calculations.

For dynamical systems on networks with purely dyadic interactions, equitable partitions can be used to determine the synchronized clusters [**69**, **131**] as well as other patterns of synchronization [**127**]. Equitable partitions divide the network into cells, where each node in a cell C_i receives the same input from any cell C_j including the nodes within its own cell, $i = j$. Each cell of the network defines a cluster of nodes that could be synchronized. In case of noninvasive coupling, as is the focus of this manuscript, the conditions above only have to hold for $i \neq j$ (in which case the partition is called an external equitable partition), since the terms representing the effect of nodes within the same cluster upon one another becomes zero if evaluated on that state.

The same idea holds for higher order interaction networks, where the equitable partitions now need to be defined in terms of the interactions of all orders. The conditions can be relaxed to external equitable partitions if the coupling functions are noninvasive, such as the Laplacian-like coupling considered herein. Namely, we can ignore the input into every node i belonging to the cluster C_k from all the hyperedges that only connect the nodes in C_k. General undirected coupling is considered in Ref. [**128**].

More explicitly, the partitioning can be achieved by considering the incidence matrix. The nodes can be separated into non-overlapping cells of "node clusters". This node partition induces a partition of edges into "edge clusters", according to what combination of node clusters those edges contain (we only need to consider the unordered set of included node clusters in the case of Laplacian-like coupling as the edges are undirected). The partition is equitable if each node in a

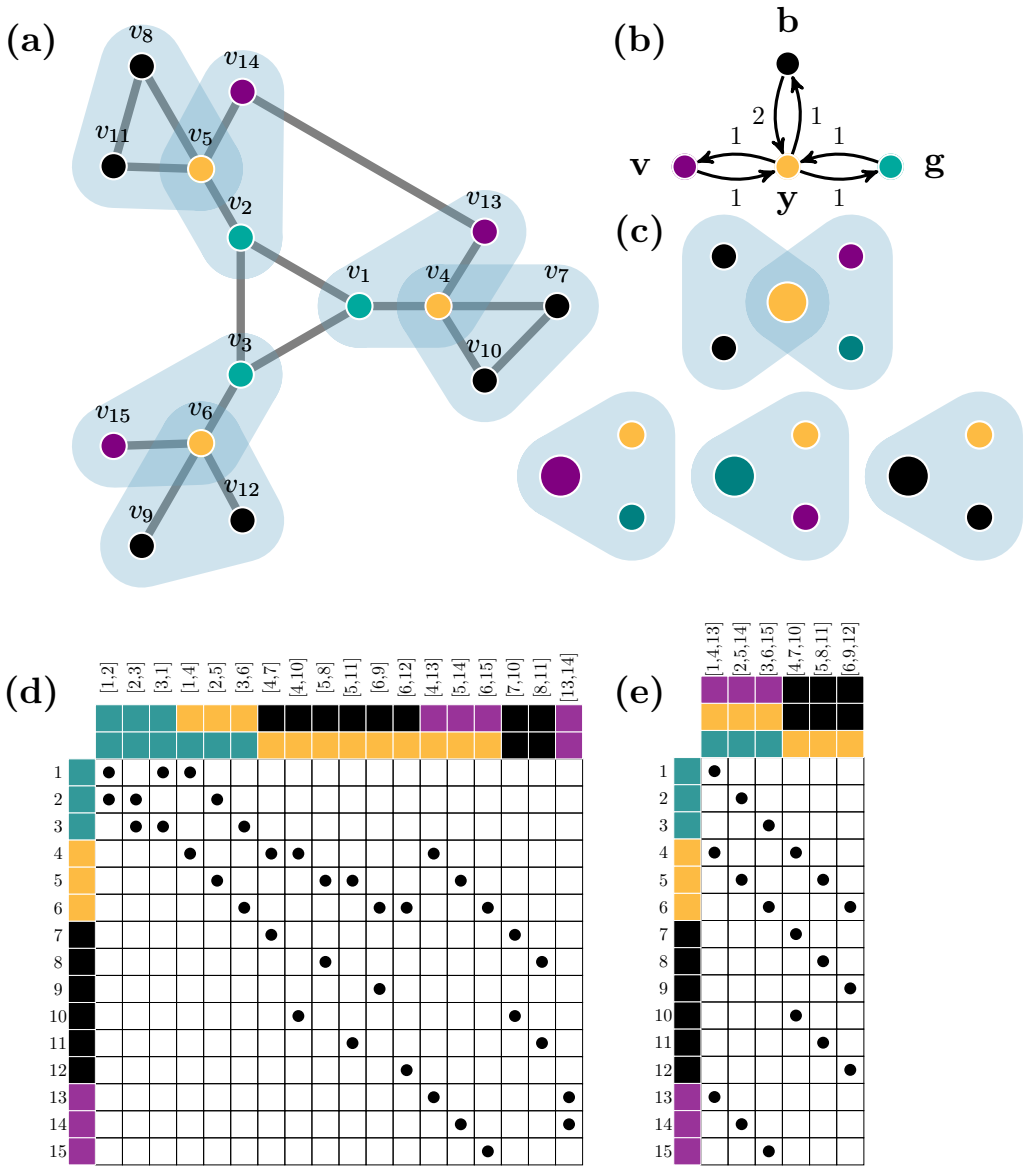

FIGURE 5.1. An admissible pattern of synchronization into four clusters of nodes based on an external equitable partition. (a) The hypergraph. (b) The dyadic quotient network. (c) The triadic quotient network, with nodes undergoing that effective dynamics shown in larger size. [(d)-(e)] Incidence matrices for dyadic and triadic interactions respectively. Dots represent ones. Row label colors represent the node clusters, column label colors represent the edge clusters induced by the node clusters. (d) shows there are 6 types of dyadic edge clusters and (e) shows there are two types of triadic edge clusters.

given node cluster gets the same input from each edge cluster. We demonstrate this on a concrete example by considering the hypergraph structure shown in fig. 5.1.

The structure of the hypergraph in fig. 5.1 is an extension of the network shown in Fig.1 in Ref. [**163**], with extra hyperedges added to represent the higher order interactions, and extra edges added to highlight that strict symmetry conditions are not necessary for our framework. We need to specify certain aspects of the dynamics for the system as well and for this we impose conditions on the coupling functions. Namely, we assume that $G^{(2)}$ is Laplacian and $G^{(3)}$ is Laplacian-like.

Many distinct partitions, each one corresponding to a different pattern of cluster synchronization, can be admissible for a given hypergraph. To illustrate a specific example, we focus on the four cluster synchronization pattern shown in figure fig. 5.1(a). We can divide the nodes into four non-overlapping cells (i.e., synchronized clusters) which we label by their number for convenience in mathematical formulas, C_1, C_2, C_3, C_4, or equivalently by their color for convenience when referring to the figure, C_g, C_y, C_b, C_v, corresponding to green, yellow, black, and violet. $C_1 = C_g = \{1, 2, 3\}$, $C_2 = C_y = \{4, 5, 6\}$, $C_3 = C_b = \{7, 8, 9, 10, 11, 12\}$, and $C_4 = C_v = \{13, 14, 15\}$. There are 6 distinct dyadic order edge clusters as shown by the identical color combinations in the column labels of fig. 5.1(d). There are two distinct triadic order edge clusters corresponding to the identical color combinations in the column labels of fig. 5.1(e), where $C_1^{(3)} = C_{gyv}^{(3)} = \{[1, 4, 13], [2, 5, 14], [3, 6, 15]\}$ and $C_2^{(3)} = C_{ybb}^{(3)} = \{[4, 7, 10], [5, 8, 11], [6, 9, 12]\}$. These node and edge clusters together form an external equitable partition. Therefore, this particular partition corresponds to an admissible pattern of synchronization. Additionally, we use the notation $C_j \in C_k^{(m)}$ to denote the node clusters that are included in the kth edge cluster, for instance $C_1^{(3)} = \{C_g, C_y, C_v\} = \{C_1, C_2, C_4\}$, written respectively in terms of colors and then index number.

The condition for cluster synchronization in hypergraphs with Laplacian-like coupling can be written as:

$$\sum_{e_j \in C_k^{(m)}} I_{ij}^{(m)} = \sum_{e_j \in C_k^{(m)}} I_{i'j}^{(m)}, \tag{5.2}$$

for $i, i' \in C_l$, where we are summing over the m-th order hyperedges e_j that are in edge cluster $C_k^{(m)}$, where the terms coming from edge clusters $C_k^{(m)}$ that contain only nodes in C_l can be ignored due to noninvasive coupling.

The effective dynamics of cluster synchronized states can be expressed via the *quotient hypergraphs* which represent the interactions between nodes of different clusters. The structure of that effective quotient hypergraph for the state shown in fig. 5.1(a) is contained in the effective incidence matrices, $I_{\text{eff}}^{(m)}$, defined as:

$$I_{\text{eff}}^{(2)} = \begin{array}{c} \\ b \\ y \\ v \\ g \end{array} \begin{array}{c} \begin{array}{ccc} [by] & [yv] & [yg] \end{array} \\ \begin{pmatrix} 1 & & \\ 2 & 1 & 1 \\ & 1 & \\ & & 1 \end{pmatrix} \end{array}, \quad I_{\text{eff}}^{(3)} = \begin{array}{c} \\ b \\ y \\ v \\ g \end{array} \begin{array}{c} \begin{array}{cc} [bby] & [gyv] \end{array} \\ \begin{pmatrix} 1 & \\ 1 & 1 \\ & 1 \\ & 1 \end{pmatrix} \end{array}. \tag{5.3}$$

(See Ref. [**128**] for more details on calculating $I_{\text{eff}}^{(m)}$.) The quotient hypergraph (illustrated in fig. 5.1 (b-c)) can be used to read out the time evolution of each node. For instance, every node in the yellow cluster evolves according to:

$$\begin{aligned} \dot{x}_y = & F(x_y) + G^{(2)}(x_g - x_y) \\ & + G^{(2)}(x_v - x_y) + 2G^{(2)}(x_b - x_y) \\ & + G^{(3)}(x_b + x_b - 2x_y) + G^{(3)}(x_v + x_g - 2x_y), \end{aligned} \tag{5.4}$$

with analogous equations describing the time evolution of completely synchronized nodes belonging to other clusters. Here, $G^{(m)}$ is expressed taking into account the Laplacian-like coupling assumption.

5.4. Stability

Stability analysis of cluster synchronization patterns on dyadic networks is well understood [**31**, **114**]. However, in the presence of higher order coupling, the Jacobian acquires additional terms. Here, we show how all the terms in the Jacobian can be block diagonalized by using the incidence matrices for a given cluster synchronization pattern, thus enabling stability calculations for general dynamics on hypergraphs.

First, we define a Laplacian corresponding to the kth edge cluster (i.e., synchronization pattern) of order m as follows:

$$\mathcal{L}_k^{(m)} = m\mathcal{D}_k^{(m)} - I_k^{(m)}[I_k^{(m)}]^T, \tag{5.5}$$

where $I_k^{(m)}$ is an $N \times |C_k^{(m)}|$ matrix (here, $|C_k^{(m)}|$ denotes the number of unique elements in the edge cluster $C_k^{(m)}$) consisting of the columns of $I^{(m)}$ that correspond to the hyperedges in the kth cluster of order m. For instance, for the *bby* 3rd order hyperedge cluster of the hypergraph in fig. 5.1, $I_k^{(m)}$ is obtained by keeping the last 3 columns of $I^{(m)}$. Additionally, $\mathcal{D}_k^{(m)}$ is a diagonal matrix with elements $[\mathcal{D}_k^{(m)}]_{ii}$ corresponding to the number of mth order edges in the kth edge cluster node i is part of ($[\mathcal{D}_k^{(m)}]_{ii} = \sum_{j=1}^{N} [I_k^{(m)}]_{ij}$).

The variational equation for linear stability depends on all node clusters and all edge clusters of all orders. For a specific pattern of cluster synchronization, it is:

$$\begin{aligned}\delta\dot{x} = \Bigg(&\sum_{k=1}^{K} E_k \otimes JF(s_k) - \sum_{m=2}^{d} \sigma^{(m)} \cdot \\ &\Big(\sum_{k=1}^{K_m} \sum_{l \in \{C_k^{(m)}\}} E_l \mathcal{L}_k^{(m)} \otimes JG^{(m)}(s_l, s_{C_k^{(m)} \setminus l}) \Big) \Bigg) \delta x,\end{aligned} \tag{5.6}$$

where E_k denotes the diagonal cluster indicator matrix encoding which nodes are in cluster C_k ($[E_k]_{ii} = 1$ if $i \in C_k$ and $[E_k]_{ii} = 0$ otherwise). Additionally, $\{C_k^{(m)}\}$ is a set of *unique* node clusters included in the kth edge cluster, (e.g., in Fig. 5.1, $\{C_{ybb}^{(3)}\} = \{y, b\}$). Finally, $s_{C_k^{(m)} \setminus l}$ is the set of all the trajectories of nodes included in edge cluster $C_k^{(m)}$, excluding those nodes in node cluster l. The partial derivatives are computed as:

$$\begin{aligned}JG^{(m)}(s_l, s_{C_k^{(m)} \setminus l})_{p,q} &\frac{\partial G_p^{(m)} \left(\sum_{j=1}^{m-1} x_j - (m-1)x_0 \right)}{\partial [x_2]_q} \Bigg|_{\substack{x_0 = s_l, \\ x_j = [s_{C_k^{(m)} \setminus l}]_j}} \\ &= \frac{\partial G_p^{(m)}(z)}{\partial z_q} \Bigg|_{z = \sum_{j=1}^{m-1} [s_{C_k^{(m)} \setminus l}]_j - (m-1)s_l},\end{aligned} \tag{5.7}$$

where $[s_{C_k^{(m)} \setminus l}]_j$ is the jth trajectory in the set $s_{C_k^{(m)} \setminus l}$.

The key implication of eqs. (5.6) and (5.7) is that to block diagonalize the Jacobian for the entire system of Laplacian-like coupled oscillators, it is sufficient to simultaneously block diagonalize the following matrices:

$$\{E_1, ..., E_K, \mathcal{L}^{(2)}, \mathcal{L}_1^{(3)}, ..., \mathcal{L}_{K_3}^{(3)}, ..., \mathcal{L}_1^{(d)}, ..., \mathcal{L}_{K_d}^{(d)}\}. \tag{5.8}$$

The form of the projected Laplacians describing a specific pattern of cluster synchronization (the $\mathcal{L}_k^{(m)}$ matrices) is similar to that of the generalized Laplacian [**93**].

An example of simultaneous block diagonalization is shown in fig. 5.2. There, we impose Laplacian coupling on dyadic edges, and Laplacian-like coupling on triadic edges. We observe that in the first case (two clusters, shown in fig. 5.2(a,c-e)), it is sufficient to simultaneously block diagonalize the cluster indicator matrices (E_y and E_b), the dyadic Laplacian, and the projected triadic Laplacian, since each node participates in a unique triadic edge pattern. However, in the second case (four clusters, shown in fig. 5.2(b,f-h)), for the triadic interactions it is necessary to simultaneously block diagonalize two matrices corresponding to the two distinct triadic order edge clusters (shown in fig. 5.2(g)).

The results relevant for binary hyperedges are easily generalizable to systems with different types of nodes and edges, and thus are applicable to multilayered networks [**38**]. Generally, only the nodes of the same type get fully synchronized. Additionally, synchronization requires that the input to each node in the cluster from all types of edges is the same. Thus, we need to cluster the edges not only based on the node clusters, but also on the edge types. Given the appropriate cluster assignment, the Jacobian block diagonalization is still obtained by simultaneously block diagonalizing the set of matrices in eq. (5.8).

We consider an example of a system with different types of hyperedges shown in fig. 5.3(a), where distinct colors (blue and violet) illustrate distinct hyperedge types and we consider a state with two distinct node clusters (denoted with black and yellow colored nodes). The different hyperedge types are also highlighted in fig. 5.3(b-c) with different colors corresponding to different edge types in the labeled incidence matrices. eq. (5.2) establishing the condition for cluster synchronization holds for all types of edges and all coupling orders.

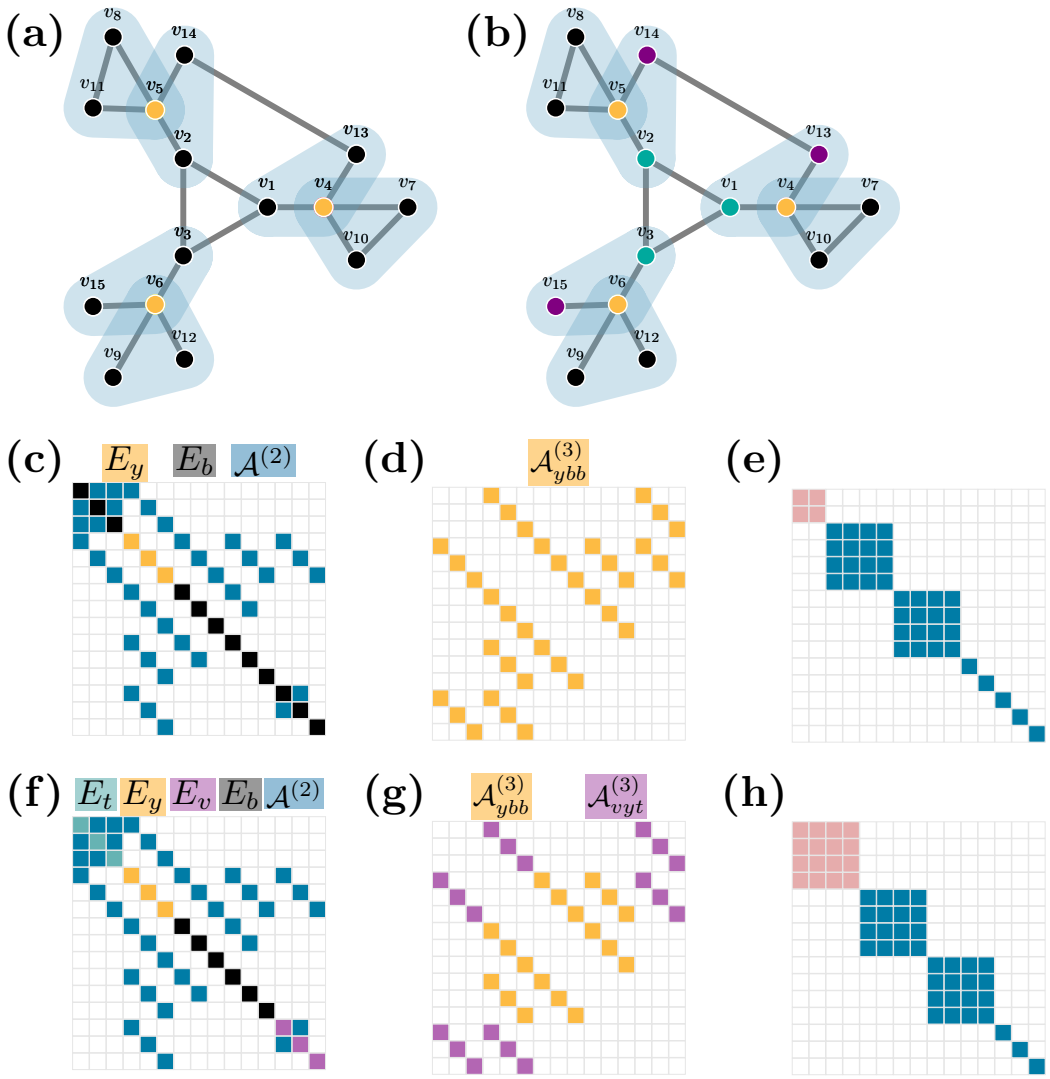

FIGURE 5.2. Block diagonalizing the Jacobian evaluated on cluster synchronization states. [(a,b)] Admissible states with two (left column) and four (right column) clusters. [(c,d)] and [(f,g)] The set of matrices that need to be simultaneously block diagonalized. [(e,h)] Blocks of the resulting Jacobian. Pink and blue correspond to parallel and transverse perturbation blocks respectively.

In order to obtain concrete linear stability results, we need to impose specific dynamical equations to describe the evolution of the system. We use the optoelectric oscillator dynamics used in experiments in Ref. [**61**] and considered in [**162**, **163**], with one-dimensional discrete time node

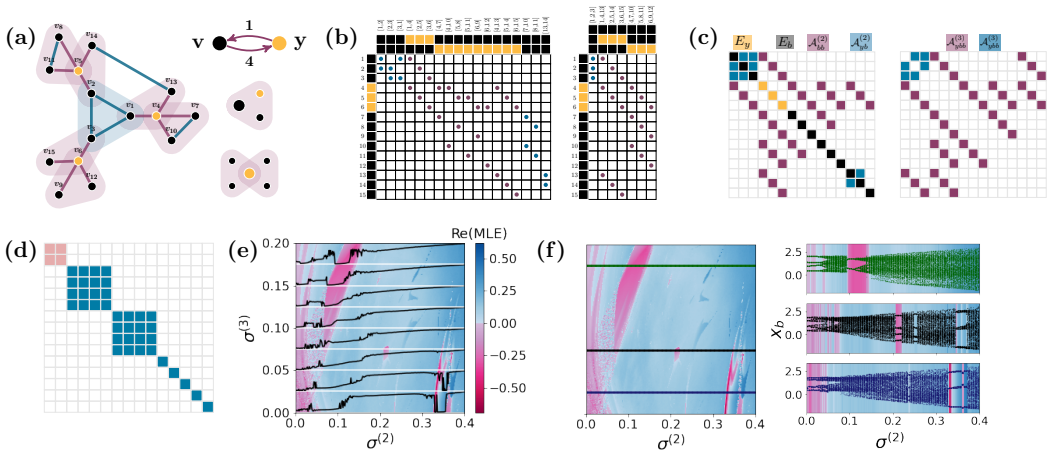

FIGURE 5.3. Example linear stability calculation for the system discussed in eqs. (5.9) and (5.10). The calculations were performed using the accompanying code, Ref. [**126**]. (a) Left: a hypergraph with attractive (blue) and repulsive (violet) coupling (eq. (5.10)) and with nodes that obey the same dynamical equations (eq. (5.9)). Right: the quotient networks representing dyadic and triadic interactions. (b) Structure of $I^{(2)}$ (left) and $I^{(3)}$ (right). Black and yellow represent the distinct clusters, blue and violet represent the distinct coupling types. (c) Matrices used in simultaneous block diagonalization to perform the stability analysis. (d) Jacobian structure after block diagonalization. Pink and blue represent parallel and transverse perturbation blocks respectively. (e) Linear stability diagram for a fixed parameter $\beta = 1.8$ and various values of dyadic and triadic coupling strengths, $\sigma^{(2)}$ and $\sigma^{(3)}$. Pink areas are linearly stable, blue areas are not linearly stable. Black lines correspond to direct simulation of standard deviations from the average cluster trajectory for each of the $\sigma^{(3)}$ values in white. (f) Left: stability diagram with three distinct parameters $\sigma^{(3)}$ shown with different colored solid lines. Right: bifurcation diagram for the three distinct values of $\sigma^{(3)}$ shown in the corresponding color. Horizontal axis represents the dyadic coupling strength, vertical axis corresponds to the states of black nodes x_{black} at the past 100 time steps. Background colors represent the calculated linear stability for each value of $\sigma^{(2)}$.

dynamics

$$F(x_i) = \beta \sin^2(x_i + \pi/4) \tag{5.9}$$

and coupling functions

$$\begin{aligned} G^{(2)}(x_i, x_j) =& \delta_{ij}\sigma^{(2)}[F(x_j) - F(x_i)], \\ G^{(3)}(x_i, x_j, x_k) =& \delta_{ijk}\sigma^{(3)} \sin(x_i + x_j - 2x_k). \end{aligned} \tag{5.10}$$

Here, the values of δ_{ij} and δ_{ijk} are selected from values $\{-1, 1\}$ and correspond to repulsive and attractive hyperedges respectively. To avoid complications from multistability, we pick a two cluster state for our analysis and we make edges connecting only the nodes that are in the same cluster attractive and all the other edges repulsive. Keeping the parameter β constant, we vary $\sigma^{(2)}$ and $\sigma^{(3)}$ to determine the linear stability regions for different parameter regimes. We present our findings for this example system in fig. 5.3. Figure 5.3(a-b) shows the analogous plots to Fig. 5.1(a-e) with the state, the quotient networks, and incidence matrices respectively. Figure 5.3(c) shows the set of matrices that need to be simultaneously block diagonalized. Figure 5.3(e) is the linear stability plot demonstrating sensitive dependence on both parameters $\sigma^{(2)}$ and $\sigma^{(3)}$, with the changes in the stability properties of the system showing correspondence to different regions of the bifurcation diagram shown in Figure 5.3(f).

5.5. Conclusion

Systems of dynamical elements coupled on hypergraphs can show intricate synchronization patterns beyond full synchronization, such as cluster synchronization. We show how to use the structure of the incidence matrices to determine the admissibility of cluster synchronization patterns and analyze their stability properties. To do so, we need to consider not only the partition into node clusters, but also the partition into hyperedge clusters that is induced by the synchronization pattern of the entire set of nodes coupled on each hyperedge. Our formulation in terms of node and edge clusters provides a general way to organize the analysis of dynamical processes on hypergraphs.

A crucial aspect of analyzing synchronization patterns is their stability analysis. We demonstrate how to organize and reduce the dimension of stability calculations. Unlike previous work, our analysis is not restricted to dyadic interactions, full synchronization [**45**], or non-intertwined clusters [**162**]. Our results open up an opportunity for detailed analysis of systems of theoretical and practical significance, as well as investigating the role of higher order interactions in stabilizing or destabilizing different states.

Bibliography

[1] D. M. Abrams and S. H. Strogatz, *Chimera states for coupled oscillators*, Physical Review Letters, 93 (2004).

[2] M. A. Aguiar and A. P. S. Dias, *Synchronization and equitable partitions in weighted networks*, Chaos: An Interdisciplinary Journal of Nonlinear Science, 28 (2018), p. 073105.

[3] J. Alexander and G. Auchmuty, *Global bifurcations of phase-locked oscillators*, Archive for Rational Mechanics and Analysis, 93 (1986), pp. 253–270.

[4] J. C. Alexander and B. Fiedler, *Global decoupling of coupled symmetric oscillators.*, in Differential Equations, New York, 1989, Marcel Dekker Inc., pp. 7–16.

[5] R. G. Andrzejak, C. Rummel, F. Mormann, and K. Schindler, *All together now: Analogies between chimera state collapses and epileptic seizures*, Scientific reports, 6 (2016), pp. 1–10.

[6] F. Antoneli and I. Stewart, *Symmetry and synchrony in coupled cell networks 2: Group networks*, International Journal of Bifurcation and Chaos, 17 (2007), pp. 935–951.

[7] P. Ashwin and O. Burylko, *Weak chimeras in minimal networks of coupled phase oscillators*, Chaos: An Interdisciplinary Journal of Nonlinear Science, 25 (2015), p. 013106.

[8] P. Ashwin, S. Coombes, and R. Nicks, *Mathematical frameworks for oscillatory network dynamics in neuroscience*, The Journal of Mathematical Neuroscience, 6 (2016), p. 2.

[9] P. Ashwin and A. Rodrigues, *Hopf normal form with sn symmetry and reduction to systems of nonlinearly coupled phase oscillators*, Physica D: Nonlinear Phenomena, 325 (2016), pp. 14–24.

[10] P. Ashwin and J. W. Swift, *The dynamics of n weakly coupled identical oscillators*, Journal of Nonlinear Science, 2 (1992), pp. 69–108.

[11] F. M. Atay, *Total and partial amplitude death in networks of diffusively coupled oscillators*, Physica D: Nonlinear Phenomena, 183 (2003), pp. 1–18.

[12] N. Aubry, W.-Y. Lian, and E. S. Titi, *Preserving symmetries in the proper orthogonal decomposition*, SIAM Journal on Scientific Computing, 14 (1993), pp. 483–505.

[13] S. Bagheri, *Koopman-mode decomposition of the cylinder wake*, Journal of Fluid Mechanics, 726 (2013), pp. 596–623.

[14] ——, *Effects of weak noise on oscillating flows: Linking quality factor, Floquet modes, and Koopman spectrum*, Physics of Fluids, 26 (2014), p. 094104.

[15] E. Barany, M. Dellnitz, and M. Golubitsky, *Detecting the symmetry of attractors*, Physica D: Nonlinear Phenomena, 67 (1993), pp. 66–87.

[16] A. Barrat, M. Barthelemy, and A. Vespignani, *Dynamical processes on complex networks*, Cambridge university press, 2008.

[17] F. Battiston, G. Cencetti, I. Iacopini, V. Latora, M. Lucas, A. Patania, J.-G. Young, and G. Petri, *Networks beyond pairwise interactions: structure and dynamics*, Physics Reports, (2020).

[18] V. N. Belykh, G. V. Osipov, V. S. Petrov, J. A. Suykens, and J. Vandewalle, *Cluster synchronization in oscillatory networks*, Chaos: An Interdisciplinary Journal of Nonlinear Science, 18 (2008), p. 037106.

[19] A. Ben-Israel and T. N. Greville, *Generalized inverses: theory and applications*, vol. 15, Springer Science & Business Media, 2003.

[20] R. Berner, E. Scholl, and S. Yanchuk, *Multiclusters in networks of adaptively coupled phase oscillators*, SIAM Journal on Applied Dynamical Systems, 18 (2019), pp. 2227–2266.

[21] T. Böhle, C. Kuehn, R. Mulas, and J. Jost, *Coupled hypergraph maps and chaotic cluster synchronization*, arXiv preprint arXiv:2102.02272, (2021).

[22] C. Bick, P. Ashwin, and A. Rodrigues, *Chaos in generically coupled phase oscillator networks with nonpairwise interactions*, Chaos: An Interdisciplinary Journal of Nonlinear Science, 26 (2016), p. 094814.

[23] C. Bick, T. Böhle, and C. Kuehn, *Multi-population phase oscillator networks with higher-order interactions*, arXiv preprint arXiv:2012.04943, (2020).

[24] C. Bick, E. Gross, H. A. Harrington, and M. T. Schaub, *What are higher-order networks?*, arXiv preprint arXiv:2104.11329, (2021).

[25] F. M. Brady, Y. Zhang, and A. E. Motter, *Forget partitions: Cluster synchronization in directed networks generate hierarchies*, arXiv preprint arXiv:2106.13220, (2021).

[26] E. Brown, P. Holmes, and J. Moehlis, *Globally coupled oscillator networks*, in Perspectives and Problems in Nolinear Science, Springer, 2003, pp. 183–215.

[27] B. W. Brunton, L. A. Johnson, J. G. Ojemann, and J. N. Kutz, *Extracting spatial–temporal coherent patterns in large-scale neural recordings using dynamic mode decomposition*, Journal of neuroscience methods, 258 (2016), pp. 1–15.

[28] S. L. Brunton, J. L. Proctor, and J. N. Kutz, *Discovering governing equations from data by sparse identification of nonlinear dynamical systems*, Proceedings of the National Academy of Sciences, (2016), p. 201517384.

[29] M. Budišić, R. Mohr, and I. Mezić, *Applied Koopmanism*, Chaos: An Interdisciplinary Journal of Nonlinear Science, 22 (2012), p. 047510.

[30] T. Carletti, D. Fanelli, and S. Nicoletti, *Dynamical systems on hypergraphs*, Journal of Physics: Complexity, 1 (2020), p. 035006.

[31] Y. S. Cho, T. Nishikawa, and A. E. Motter, *Stable chimeras and independently synchronizable clusters*, Physical Review Letters, 119 (2017), p. 084101.

[32] J. J. Collins and I. N. Stewart, *Coupled nonlinear oscillators and the symmetries of animal gaits*, Journal of Nonlinear Science, 3 (1993), pp. 349–392.

[33] J. F. Cornwell, *Group theory in physics: An introduction*, vol. 1, Academic press, 1997.

[34] C. Curto and K. Morrison, *Relating network connectivity to dynamics: opportunities and challenges for theoretical neuroscience*, Current opinion in neurobiology, 58 (2019), pp. 11–20.

[35] L. Danon, A. P. Ford, T. House, C. P. Jewell, M. J. Keeling, G. O. Roberts, J. V. Ross, and M. C. Vernon, *Networks and the epidemiology of infectious disease*, Interdisciplinary perspectives on infectious diseases, 2011 (2011).

[36] S. T. Dawson, M. S. Hemati, M. O. Williams, and C. W. Rowley, *Characterizing and correcting for the effect of sensor noise in the dynamic mode decomposition*, Experiments in Fluids, 57 (2016), p. 42.

[37] G. F. de Arruda, M. Tizzani, and Y. Moreno, *Phase transitions and stability of dynamical processes on hypergraphs*, Communications Physics, 4 (2021), pp. 1–9.

[38] F. Della Rossa, L. Pecora, K. Blaha, A. Shirin, I. Klickstein, and F. Sorrentino, *Symmetries and cluster synchronization in multilayer networks*, Nature Communications, 11 (2020), pp. 1–17.

[39] M. Dellnitz and S. Klus, *Sensing and control in symmetric networks*, Dynamical Systems, 32 (2016), p. 61–79.

[40] ———, *Sensing and control in symmetric networks*, Dynamical Systems, 32 (2017), pp. 61–79.

[41] L. DeVille, *Consensus on simplicial complexes: Results on stability and synchronization*, Chaos: An Interdisciplinary Journal of Nonlinear Science, 31 (2021), p. 023137.

[42] J. Emenheiser, A. Chapman, M. Pósfai, J. P. Crutchfield, M. Mesbahi, and R. M. D'Souza, *Patterns of patterns of synchronization: Noise induced attractor switching in rings of coupled nonlinear oscillators*, Chaos: An Interdisciplinary Journal of Nonlinear Science, 26 (2016), p. 094816.

[43] J. Emenheiser, A. Salova, J. Snyder, J. P. Crutchfield, and R. M. D'Souza, *Network and phase symmetries reveal that amplitude dynamics stabilize decoupled oscillator clusters*, arXiv preprint arXiv:2010.09131, (2020).

[44] B. Ermentrout, *An adaptive model for synchrony in the firefly pteroptyx malaccae*, Journal of Mathematical Biology, 29 (1991), pp. 571–585.

[45] L. Gambuzza, F. Di Patti, L. Gallo, S. Lepri, M. Romance, R. Criado, M. Frasca, V. Latora, and S. Boccaletti, *Stability of synchronization in simplicial complexes*, Nature Communications, 12 (2021), pp. 1–13.

[46] L. V. Gambuzza, A. Cardillo, A. Fiasconaro, L. Fortuna, J. Gómez-Gardenes, and M. Frasca, *Analysis of remote synchronization in complex networks*, Chaos: An Interdisciplinary Journal of Nonlinear Science, 23 (2013), p. 043103.

[47] R. Ghorbanchian, J. G. Restrepo, J. J. Torres, and G. Bianconi, *Higher-order simplicial synchronization of coupled topological signals*, Communications Physics, 4 (2021), pp. 1–13.

[48] M. Golubitsky, D. Romano, and Y. Wang, *Network periodic solutions: full oscillation and rigid synchrony*, Nonlinearity, 23 (2010), p. 3227.

[49] ——, *Network periodic solutions: patterns of phase-shift synchrony*, Nonlinearity, 25 (2012), p. 1045.

[50] M. Golubitsky and I. Stewart, *The symmetry perspective: from equilibrium to chaos in phase space and physical space*, vol. 200, Springer Science & Business Media, 2003.

[51] ——, *Synchrony versus symmetry in coupled cells*, in EQUADIFF 2003, World Scientific, 2005, pp. 13–24.

[52] ——, *Recent advances in symmetric and network dynamics*, Chaos: An Interdisciplinary Journal of Nonlinear Science, 25 (2015), p. 097612.

[53] ——, *Rigid patterns of synchrony for equilibria and periodic cycles in network dynamics*, Chaos: An Interdisciplinary Journal of Nonlinear Science, 26 (2016), p. 094803.

[54] M. Golubitsky, I. Stewart, and D. G. Schaeffer, *Singularities and groups in bifurcation theory*, vol. 2, Springer Science & Business Media, 2012.

[55] R. Guevara Erra, J. L. Perez Velazquez, and M. Rosenblum, *Neural synchronization from the perspective of non-linear dynamics*, Frontiers in computational neuroscience, 11 (2017), p. 98.

[56] A. Hagberg, P. Swart, and D. S Chult, *Exploring network structure, dynamics, and function using networkx*, tech. rep., Los Alamos National Lab.(LANL), Los Alamos, NM (United States), 2008.

[57] A. Hagerstrom, *Network symmetries and synchronization*, https://sourceforge.net/projects/networksym/, 112 (2014), p. 154101.

[58] V. Hakim and W.-J. Rappel, *Dynamics of the globally coupled complex Ginzburg-Landau equation*, Physical Review A, 46 (1992), p. R7347.

[59] Y. Han, B. Zhou, J. Pei, and Y. Jia, *Understanding importance of collaborations in co-authorship networks: A supportiveness analysis approach*, in Proceedings of the 2009 SIAM international conference on data mining, SIAM, 2009, pp. 1112–1123.

[60] K. M. Hannay, D. B. Forger, and V. Booth, *Macroscopic models for networks of coupled biological oscillators*, Science advances, 4 (2018), p. e1701047.

[61] J. D. Hart, D. C. Schmadel, T. E. Murphy, and R. Roy, *Experiments with arbitrary networks in time-multiplexed delay systems*, Chaos: An Interdisciplinary Journal of Nonlinear Science, 27 (2017), p. 121103.

[62] J. D. Hart, Y. Zhang, R. Roy, and A. E. Motter, *Topological control of synchronization patterns: Trading symmetry for stability.*

[63] I. Iacopini, G. Petri, A. Barrat, and V. Latora, *Simplicial models of social contagion*, Nature Communications, 10 (2019), pp. 1–9.

[64] D. Irving and F. Sorrentino, *Synchronization of dynamical hypernetworks: Dimensionality reduction through simultaneous block-diagonalization of matrices*, Physical Review E, 86 (2012), p. 056102.

[65] S. Jalan and R. Amritkar, *Self-organized and driven phase synchronization in coupled maps*, Physical Review Letters, 90 (2003), p. 014101.

[66] S. Jalan, R. Amritkar, and C.-K. Hu, *Synchronized clusters in coupled map networks. i. numerical studies*, Physical Review E, 72 (2005), p. 016211.

[67] J. Jost and R. Mulas, *Hypergraph Laplace operators for chemical reaction networks*, Advances in Mathematics, 351 (2019), pp. 870–896.

[68] E. Kaiser, J. N. Kutz, and S. L. Brunton, *Discovering conservation laws from data for control*, in 2018 IEEE Conference on Decision and Control (CDC), IEEE, 2018, pp. 6415–6421.

[69] H. Kamei and P. J. Cock, *Computation of balanced equivalence relations and their lattice for a coupled cell network*, SIAM Journal on Applied Dynamical Systems, 12 (2013), pp. 352–382.

[70] B. Karakaya, L. Minati, L. V. Gambuzza, and M. Frasca, *Fading of remote synchronization in tree networks of Stuart-Landau oscillators*, Physical Review E, 99 (2019), p. 052301.

[71] S. Kirkland, *Two-mode networks exhibiting data loss*, Journal of Complex Networks, 6 (2018), pp. 297–316.

[72] S. Klamt, U.-U. Haus, and F. Theis, *Hypergraphs and cellular networks*, PLoS Comput Biol, 5 (2009), p. e1000385.

[73] S. Klus, P. Koltai, and C. Schütte, *On the numerical approximation of the Perron-Frobenius and Koopman operator*, arXiv preprint arXiv:1512.05997, (2015).

[74] D. E. Knuth, *The art of computer programming*, vol. 3, Pearson Education, 1997.

[75] R. Kondor and S. Trivedi, *On the generalization of equivariance and convolution in neural networks to the action of compact groups*, in International Conference on Machine Learning, PMLR, 2018, pp. 2747–2755.

[76] B. Koopman and J. v. Neumann, *Dynamical systems of continuous spectra*, Proceedings of the National Academy of Sciences, 18 (1932), pp. 255–263.

[77] B. O. Koopman, *Hamiltonian systems and transformation in Hilbert space*, Proceedings of the National Academy of Sciences, 17 (1931), pp. 315–318.

[78] M. Korda and I. Mezić, *On convergence of extended dynamic mode decomposition to the Koopman operator*, Journal of Nonlinear Science, 28 (2018), pp. 687–710.

[79] M. Korda, M. Putinar, and I. Mezić, *Data-driven spectral analysis of the Koopman operator*, Applied and Computational Harmonic Analysis, (2018).

[80] A. Krawiecki, *Chaotic synchronization on complex hypergraphs*, Chaos, Solitons & Fractals, 65 (2014), pp. 44–50.

[81] S. Krishnagopal, J. Lehnert, W. Poel, A. Zakharova, and E. Schöll, *Synchronization patterns: from network motifs to hierarchical networks*, Philosophical Transactions of the Royal Society A: Mathematical, Physical and Engineering Sciences, 375 (2017), p. 20160216.

[82] W. L. Ku, M. Girvan, and E. Ott, *Dynamical transitions in large systems of mean field-coupled Landau-Stuart oscillators: Extensive chaos and cluster states*, Chaos: An Interdisciplinary Journal of Nonlinear Science, 25 (2015), p. 123122.

[83] Y. Kuramoto, *Chemical oscillations, waves, and turbulence*, Courier Corporation, 2003.

[84] J. N. Kutz, S. L. Brunton, B. W. Brunton, and J. L. Proctor, *Dynamic mode decomposition: data-driven modeling of complex systems*, SIAM, 2016.

[85] N. W. Landry and J. G. Restrepo, *The effect of heterogeneity on hypergraph contagion models*, Chaos: An Interdisciplinary Journal of Nonlinear Science, 30 (2020), p. 103117.

[86] A. Lasota and M. C. Mackey, *Probabilistic properties of deterministic systems*, Cambridge University Press, 1985.

[87] S. Lee, Y. S. Cho, and H. Hong, *Twisted states in low-dimensional hypercubic lattices*, Physical Review E, 98 (2018), p. 062221.

[88] C. Letellier and L. A. Aguirre, *Investigating nonlinear dynamics from time series: the influence of symmetries and the choice of observables*, Chaos: An Interdisciplinary Journal of Nonlinear Science, 12 (2002), pp. 549–558.

[89] Q. Li, F. Dietrich, E. M. Bollt, and I. G. Kevrekidis, *Extended dynamic mode decomposition with dictionary learning: A data-driven adaptive spectral decomposition of the Koopman operator*, Chaos: An Interdisciplinary Journal of Nonlinear Science, 27 (2017), p. 103111.

[90] R. Lifshitz and M. Cross, *Nonlinear dynamics of nanomechanical and micromechanical resonators*, Review of nonlinear dynamics and complexity, 1 (2008), pp. 1–52.

[91] M. Lodi, F. Della Rossa, F. Sorrentino, and M. Storace, *Analyzing synchronized clusters in neuron networks*, Scientific Reports, 10 (2020), pp. 1–14.

[92] M. Lodi, F. Sorrentino, and M. Storace, *One-way dependent clusters and stability of cluster synchronization in directed networks*, arXiv preprint arXiv:2106.06611, (2021).

[93] M. Lucas, G. Cencetti, and F. Battiston, *Multiorder laplacian for synchronization in higher-order networks*, Phys. Rev. Research, 2 (2020), p. 033410.

[94] R. I. Lung, N. Gaskó, and M. A. Suciu, *A hypergraph model for representing scientific output*, Scientometrics, 117 (2018), pp. 1361–1379.

[95] B. Lusch, J. N. Kutz, and S. L. Brunton, *Deep learning for universal linear embeddings of nonlinear dynamics*, Nature communications, 9 (2018), p. 4950.

[96] B. D. MacArthur, R. J. Sánchez-García, and J. W. Anderson, *Symmetry in complex networks*, Discrete Applied Mathematics, 156 (2008), pp. 3525–3531.

[97] M. H. Matheny, J. Emenheiser, W. Fon, A. Chapman, A. Salova, M. Rohden, J. Li, M. H. de Badyn, M. Pósfai, L. Duenas-Osorio, et al., *Exotic states in a simple network of nanoelectromechanical oscillators*, Science, 363 (2019), p. eaav7932.

[98] P. G. Mehta, M. Hessel-von Molo, and M. Dellnitz, *Symmetry of attractors and the Perron-Frobenius operator*, Journal of Difference Equations and Applications, 12 (2006), pp. 1147–1178.

[99] T. Menara, G. Baggio, D. S. Bassett, and F. Pasqualetti, *Stability conditions for cluster synchronization in networks of heterogeneous Kuramoto oscillators*, IEEE Transactions on Control of Network Systems, 7 (2019), pp. 302–314.

[100] A. Mesbahi, J. Bu, and M. Mesbahi, *Nonlinear observability via Koopman analysis: Characterizing the role of symmetry*, arXiv preprint arXiv:1904.08449, (2019).

[101] A. P. Millán, J. J. Torres, and G. Bianconi, *Explosive higher-order Kuramoto dynamics on simplicial complexes*, Physical Review Letters, 124 (2020), p. 218301.

[102] R. E. Mirollo and S. H. Strogatz, *Amplitude death in an array of limit-cycle oscillators*, Journal of Statistical Physics, 60 (1990), pp. 245–262.

[103] ———, *Synchronization of pulse-coupled biological oscillators*, SIAM Journal on Applied Mathematics, 50 (1990), pp. 1645–1662.

[104] A. E. Motter, S. A. Myers, M. Anghel, and T. Nishikawa, *Spontaneous synchrony in power-grid networks*, Nature Physics, 9 (2013), pp. 191–197.

[105] R. Mulas, C. Kuehn, and J. Jost, *Coupled dynamics on hypergraphs: Master stability of steady states and synchronization*, arXiv preprint arXiv:2003.13775, (2020).

[106] R. Mulas, C. Kuehn, and J. Jost, *Coupled dynamics on hypergraphs: Master stability of steady states and synchronization*, Phys. Rev. E, 101 (2020), p. 062313.

[107] R. Mulas, R. J. Sánchez-García, and B. D. MacArthur, *Hypergraph automorphisms*, arXiv preprint arXiv:2010.01049, (2020).

[108] L. Neuhäuser, A. Mellor, and R. Lambiotte, *Multibody interactions and nonlinear consensus dynamics on networked systems*, Physical Review E, 101 (2020), p. 032310.

[109] L. Neuhäuser, M. T. Schaub, A. Mellor, and R. Lambiotte, *Opinion dynamics with multi-body interactions*, arXiv preprint arXiv:2004.00901, (2020).

[110] M. Newman, *Networks*, Oxford University Press, 2018.

[111] V. Nicosia, M. Valencia, M. Chavez, A. Díaz-Guilera, and V. Latora, *Remote synchronization reveals network symmetries and functional modules*, Physical Review Letters, 110 (2013), p. 174102.

[112] T. Nishikawa and A. E. Motter, *Comparative analysis of existing models for power-grid synchronization*, New Journal of Physics, 17 (2015), p. 015012.

[113] N. O'Clery, Y. Yuan, G.-B. Stan, and M. Barahona, *Observability and coarse graining of consensus dynamics through the external equitable partition*, Physical Review E, 88 (2013), p. 042805.

[114] L. M. Pecora, F. Sorrentino, A. M. Hagerstrom, T. E. Murphy, and R. Roy, *Cluster synchronization and isolated desynchronization in complex networks with symmetries*, Nature communications, 5 (2014), p. 4079.

[115] ———, *Discovering, constructing, and analyzing synchronous clusters of oscillators in a complex network using symmetries*, in Advances in Dynamics, Patterns, Cognition, Springer, 2017, pp. 145–160.

[116] R. Penrose, *A generalized inverse for matrices*, in Mathematical proceedings of the Cambridge philosophical society, vol. 51, Cambridge University Press, 1955, pp. 406–413.

[117] A. Pikovsky, M. Rosenblum, and J. Kurths, *Synchronization: a universal concept in nonlinear science*, 2002.

[118] W. Poel, A. Zakharova, and E. Schöll, *Partial synchronization and partial amplitude death in mesoscale network motifs*, Physical Review E, 91 (2015), p. 022915.

[119] M. A. Porter, *Nonlinearity+ networks: A 2020 vision*, in Emerging Frontiers in Nonlinear Science, Springer, 2020, pp. 131–159.

[120] C. Pozrikidis, *An introduction to grids, graphs, and networks*, Oxford University Press, 2014.

[121] Y. Qin, M. Cao, B. Anderson, D. S. Bassett, and F. Pasqualetti, *Mediated remote synchronization: the number of mediators matters*, arXiv preprint arXiv:2003.07405, (2020).

[122] M. Rohden, A. Sorge, M. Timme, and D. Witthaut, *Self-organized synchronization in decentralized power grids*, Physical Review Letters, 109 (2012), p. 064101.

[123] ———, *Self-organized synchronization in decentralized power grids*, Phys. Rev. Lett., 109 (2012), p. 064101.

[124] C. W. Rowley and S. T. Dawson, *Model reduction for flow analysis and control*, Annual Review of Fluid Mechanics, 49 (2017), pp. 387–417.

[125] H. Rubin and H. Meadows, *Controllability and observability in linear time-variable networks with arbitrary symmetry groups*, Bell System Technical Journal, 51 (1972), pp. 507–542.

[126] A. Salova, *Admissibility and stability of cluster synchronization patterns on hypergraphs*. `https://github.com/asalova/hypergraph-cluster-sync`.

[127] A. Salova and R. M. D'Souza, *Decoupled synchronized states in networks of linearly coupled limit cycle oscillators*, Physical Review Research, 2 (2020), p. 043261.

[128] A. Salova and R. M. D'Souza, *Analyzing states beyond full synchronization on hypergraphs requires methods beyond projected networks*, arXiv:2107.13712, (2021).

[129] ———, *Cluster synchronization on hypergraphs*, arXiv preprint arXiv:2101.05464, (2021).

[130] A. Salova, J. Emenheiser, A. Rupe, J. P. Crutchfield, and R. M. D'Souza, *Koopman operator and its approximations for systems with symmetries*, Chaos: An Interdisciplinary Journal of Nonlinear Science, 29 (2019), p. 093128.

[131] M. T. Schaub, N. O'Clery, Y. N. Billeh, J.-C. Delvenne, R. Lambiotte, and M. Barahona, *Graph partitions and cluster synchronization in networks of oscillators*, Chaos: An Interdisciplinary Journal of Nonlinear Science, 26 (2016), p. 094821.

[132] P. J. Schmid, *Dynamic mode decomposition of numerical and experimental data*, Journal of fluid mechanics, 656 (2010), pp. 5–28.

[133] A. S. Sharma, I. Mezić, and B. J. McKeon, *Correspondence between Koopman mode decomposition, resolvent mode decomposition, and invariant solutions of the Navier-Stokes equations*, Physical Review Fluids, 1 (2016), p. 032402.

[134] A. B. Siddique, L. Pecora, J. D. Hart, and F. Sorrentino, *Symmetry-and input-cluster synchronization in networks*, Physical Review E, 97 (2018), p. 042217.

[135] S. Sinha, B. Huang, and U. Vaidya, *Robust approximation of Koopman operator and prediction in random dynamical systems*, in 2018 Annual American Control Conference (ACC), IEEE, 2018, pp. 5491–5496.

[136] P. S. Skardal and A. Arenas, *Abrupt desynchronization and extensive multistability in globally coupled oscillator simplexes*, Physical Review Letters, 122 (2019), p. 248301.

[137] ———, *Higher order interactions in complex networks of phase oscillators promote abrupt synchronization switching*, Communications Physics, 3 (2020), pp. 1–6.

[138] ———, *Memory selection and information switching in oscillator networks with higher-order interactions*, Journal of Physics: Complexity, (2020).

[139] F. Sorrentino, L. M. Pecora, A. M. Hagerstrom, T. E. Murphy, and R. Roy, *Complete characterization of the stability of cluster synchronization in complex dynamical networks*, Science advances, 2 (2016), p. e1501737.

[140] F. Sorrentino, L. M. Pecora, and L. Trajkovic, *Group consensus in multilayer networks*, IEEE Transactions on Network Science and Engineering, (2020).

[141] I. Stewart and D. Gökaydin, *Symmetries of quotient networks for doubly periodic patterns on the square lattice*, International Journal of Bifurcation and Chaos, 29 (2019), p. 1930026.

[142] I. Stewart, M. Golubitsky, and M. Pivato, *Symmetry groupoids and patterns of synchrony in coupled cell networks*, SIAM Journal on Applied Dynamical Systems, 2 (2003), pp. 609–646.

[143] E. Stiefel and A. Fässler, *Group theoretical methods and their applications*, Springer Science & Business Media, 2012.

[144] S. H. Strogatz, *From Kuramoto to Crawford: exploring the onset of synchronization in populations of coupled oscillators*, Physica D: Nonlinear Phenomena, 143 (2000), pp. 1–20.

[145] S. H. Strogatz and R. E. Mirollo, *Splay states in globally coupled Josephson arrays: Analytical prediction of Floquet multipliers*, Physical Review E, 47 (1993), p. 220.

[146] S. H. Strogatz and I. Stewart, *Coupled oscillators and biological synchronization*, Scientific American, 269 (1993), pp. 102–109.

[147] Y. Susuki and I. Mezic, *Nonlinear Koopman modes and coherency identification of coupled swing dynamics*, IEEE Transactions on Power Systems, 26 (2011), pp. 1894–1904.

[148] Y. Susuki, I. Mezic, F. Raak, and T. Hikihara, *Applied Koopman operator theory for power systems technology*, Nonlinear Theory and Its Applications, IEICE, 7 (2016), pp. 430–459.

[149] A. Tantet, V. Lucarini, F. Lunkeit, and H. A. Dijkstra, *Crisis of the chaotic attractor of a climate model: a transfer operator approach*, Nonlinearity, 31 (2018), p. 2221.

[150] N. Thomas, T. Smidt, S. Kearnes, L. Yang, L. Li, K. Kohlhoff, and P. Riley, *Tensor field networks: Rotation-and translation-equivariant neural networks for 3d point clouds*, arXiv preprint arXiv:1802.08219, (2018).

[151] L. Tumash, E. Panteley, A. Zakharova, and E. Schöll, *Synchronization patterns in stuart–landau networks: a reduced system approach*, The European Physical Journal B, 92 (2019), p. 100.

[152] S. M. Ulam, *A collection of mathematical problems*, vol. 8, Interscience Publishers, 1960.

[153] Y. Wang and M. Golubitsky, *Two-colour patterns of synchrony in lattice dynamical systems*, Nonlinearity, 18 (2004), p. 631.

[154] X. Wei, J. Emenheiser, X. Wu, J.-a. Lu, and R. M. D'Souza, *Maximizing synchronizability of duplex networks*, Chaos: An Interdisciplinary Journal of Nonlinear Science, 28 (2018), p. 013110.

[155] A. J. Whalen, S. N. Brennan, T. D. Sauer, and S. J. Schiff, *Observability and controllability of nonlinear networks: The role of symmetry*, Physical Review X, 5 (2015), p. 011005.

[156] D. A. Wiley, S. H. Strogatz, and M. Girvan, *The size of the sync basin*, Chaos: An Interdisciplinary Journal of Nonlinear Science, 16 (2006), p. 015103.

[157] M. O. Williams, I. G. Kevrekidis, and C. W. Rowley, *A data–driven approximation of the Koopman operator: Extending dynamic mode decomposition*, Journal of Nonlinear Science, 25 (2015), pp. 1307–1346.

[158] M. O. Williams, C. W. Rowley, and I. G. Kevrekidis, *A kernel-based approach to data-driven Koopman spectral analysis*, arXiv preprint arXiv:1411.2260, (2014).

[159] C. Xu, X. Wang, and P. S. Skardal, *Bifurcation analysis and structural stability of simplicial oscillator populations*, Physical Review Research, 2 (2020), p. 023281.

[160] ——, *Bifurcation analysis and structural stability of simplicial oscillator populations*, Phys. Rev. Research, 2 (2020), p. 023281.

[161] A. Zakharova, M. Kapeller, and E. Schöll, *Chimera death: Symmetry breaking in dynamical networks*, Physical Review Letters, 112 (2014), p. 154101.

[162] Y. Zhang, V. Latora, and A. E. Motter, *Unified treatment of dynamical processes on generalized networks: Higher-order, multilayer, and temporal interactions*, arXiv preprint arXiv:2010.00613, (2020).

[163] Y. Zhang and A. E. Motter, *Symmetry-independent stability analysis of synchronization patterns*, arXiv preprint arXiv:2003.05461, (2020).

[164] W. Zou and M. Zhan, *Splay states in a ring of coupled oscillators: From local to global coupling*, SIAM Journal on Applied Dynamical Systems, 8 (2009), pp. 1324–1340.